TREND

Trapped Radiation Environment Model Development

Technical Note 2

Atmospheric Cut-Off

ESTEC Contract No. 9828/92/NL/FM[1]

D. Heynderickx (BIRA)
V. Pierrard (IASB)
J. Lemaire (IASB)

March 1995

[1]ESA Technical Management: E.J. Daly (WMA)

Contents

List of Figures

List of Tables

Introduction

In this technical note we describe a coordinate that can be used instead of B/B_0 to map trapped radiation fluxes in combination with L. This alternative coordinate is the atmospheric density averaged over a drift shell (B, L).

In Chapter 1 we review different coordinate systems that may be used to map trapped radiation fluxes. These coordinates work well over most of the region covered by the Van Allen belts, but are less suitable in the low altitude region where the Earth's upper atmosphere interacts with the trapped particle population. The concept of atmospheric cut-off also is introduced in this chapter.

An average density along the bounce motion of particles between their mirror points and along their drift shells can be determined by means of a computer code designed by Hassitt (1964) and kindly provided to J. Lemaire by C.E. McIlwain. This code has been updated and improved. The implementation of the code for this project is described in Chapter 2. Section 2.1 contains the definition of the drift shell averaged density and a description of the calculation method.

In order to calculate drift shell averaged densities, one needs models of the density distribution in the neutral atmosphere and in the ionosphere. We describe the models used in this study in Chapter 2. For the neutral atmospheric density distribution, we make use of MSIS, described in Sect. 2.2. A model developed by McDonnell Douglas Astronautics Co. also is implemented and described in Sect. 2.3. Since charge exchange and Coulomb interaction contribute to remove and scatter protons and electrons, even at very high altitude, we need ionospheric and plasmaspheric density models besides a neutral atmosphere model. For the ionospheric model we used IRI, which is described in Sect. 2.4.1. We used the model of Carpenter & Anderson (1992) for the plasmaspheric density distribution which gives the electron density distribution in the equatorial plane, inside and outside the plasmasphere. In Sect. 2.4.2 we describe this model and its extension along magnetic field lines.

Finally, in order to determine the penetration depths and the trapping life time of protons and electrons we need estimates of the collision cross sections for these particles as a function of energy. A compilation of the relevant collision processes and the associated cross sections is given in Sect. 2.5.

The software is applied to the proton flux distribution given by the AP-8 model in Chapter 3. It will be used to map DMSP and AZUR data in the future. Greyscale plots of the averaged density over the Earth's surface are presented as well.

Acknowledgments

We thank C.E. McIlwain for sending a revised copy of Hassitt's (1946) software. We thank D. Bilitza for providing us with the MSIS and IRI codes.

Chapter 1

Coordinate systems for low-altitude modelling

Trapped particle fluxes usually are mapped in the (B, L) coordinate system (McIlwain 1961). While these coordinates have proved very suitable for most of the region covered by the Van Allen belts, they are not very well suited for the low-altitude regions where the Earth's atmosphere interacts with the trapped particle population. The concept of atmospheric cut-off is defined in Sect. 1.1. An alternative coordinate has been proposed by Daly & Evans (1993) to take into account the steep flux gradients in the region of the upper atmosphere. This coordinate is discussed in Sect. 1.2.

It is well known from previous studies that the cosmic ray intensity observed within the atmosphere depends on the quantity of absorbing material traversed before observation. Besides the magnetic rigidity effect, the barometric pressure has an appreciable effect on the measured cosmic ray intensity. This is why cosmic ray fluxes usually are reported in terms of atmospheric depth, i.e. the mass of air per unit area above the point of observation, or air pressure at the point of observation.

The same concept should also be applied to identify an equivalent atmospheric penetration depth of Van Allen belt particles. Evidence that the flux of Van Allen belt particles depends on the atmospheric density distribution has been forwarded by Pfitzer (1990), who found that the atmospheric density at space station altitudes is a better variable than B/B_0 to organise the AP-8 MIN and AP-8 MAX fluxes.

In order to estimate the influence of the Earth's atmosphere on the distribution of trapped particles, the effects of the atmosphere have to be averaged over the particle's orbit. Ray (1960) and Lenchek & Singer (1962) have derived expressions for the atmospheric density averaged over the orbit of a particle trapped in a dipole field. Newkirk & Walt (1964) have determined the average density for a realistic representation of the geomagnetic field. Hassitt (1965b) has simplified considerably

the procedure of Newkirk & Walt (1964), while maintaining the same accuracy. In Chapter 2, we describe Hassitt's (1965b) method and its application to the study of low-altitude coordinate systems.

1.1 Definition of atmospheric cut-off

Trapped ions and electrons whose pitch angle is scattered in the loss cone, either by wave-particle interaction at high altitude or Coulomb collisions with ions and electrons in the ionosphere, are dumped in the atmosphere where they lose their energy.

Some of these energetic particles are backscattered and re-enter the magnetosphere with a different energy. The penetration depth of the primaries into the atmosphere depends on their energy. Calculations of penetration depths have been given by Bailey (1959), Rees (1963) and Kamiyama (1966).

Electrons of 2 keV, vertically incident, penetrate down to 120 km altitude. When their energy is 1 MeV, they can penetrate down to 60 km altitude. Protons of 20 keV and 20 MeV penetrate down to 120 km and 60 km, respectively. Of course, particles with pitch angles not equal to zero penetrate with a larger angle of incidence in the atmosphere and dissipate their energy at higher altitudes.

The range of cut-off altitudes over which primary Van Allen belt particles are interacting most strongly with the neutral atmosphere is rather narrow (from 50 to 200 km) compared to the length of their drift path within the magnetosphere. Over this small altitude range the magnetic field intensity varies only slightly: an altitude variation corresponding to one atmospheric scale height of 50 km corresponds to a change of only a few percent in the value of B but of orders of magnitude in the energetic particle flux. This indicates how sensitive flux values provided by environment models are to even small inaccuracies and imprecisions in the value of B or B/B_0 (where B_0 is defined as $B_0 = 0.311653/L^3$) at low altitudes[1].

Table 1 gives the equatorial pitch angles α_0 of particles mirroring at a series of altitudes and latitudes in the meridian plane passing through the South Atlantic Anomaly (SAA). It can be seen that the equatorial loss cone is very narrow at medium and high latitudes. As a direct consequence, the distribution of atmospheric density between 60 km and 200 km will mostly influence the equatorial pitch angle distribution of particles in only the very narrow loss cone angle around $\alpha_0 = 0°$ and $\alpha_0 = 180°$. At $L = 3$, the loss cone angle $\alpha_0 = 5.83°$ for $h = 60$ km and $\alpha_0 = 8.66°$ for $h = 120$ km: the difference in α_0 is smaller than the angular resolution of current directional measurements of energetic trapped ions and electrons.

[1] Note that with the above definition, B_0 is an invariant of motion.

Table 1. Equatorial pitch angles α_0 corresponding to mirror altitudes between 60 and 1000 km for different latitudes in the meridian plane passing through the SAA

$h\backslash\lambda$	30°	35°	40°	45°	50°	55°	60°
60	36.01	27.92	20.77	14.99	10.61	7.04	4.33
100	35.86	27.81	20.69	14.97	10.59	7.02	4.32
200	35.51	27.55	20.53	14.93	10.53	6.98	4.29
300	35.18	27.31	20.36	14.88	10.48	6.94	4.26
400	34.86	27.08	20.29	14.82	10.43	6.91	4.24
500	34.56	26.87	20.19	14.76	10.37	6.87	4.21
750	33.89	26.40	19.94	14.59	10.23	6.77	4.15
1000	33.30	26.00	19.68	14.41	10.11	6.69	4.09

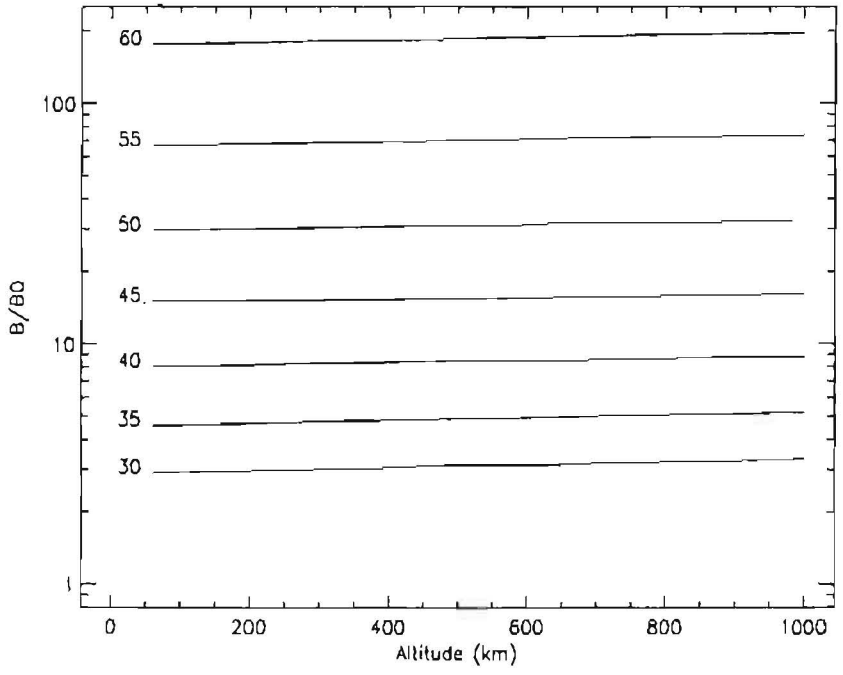

Figure 1. Relative magnetic field intensity B/B_0 as a function of altitude in the meridian plane passing through the SAA, for the latitudes in Table 1

Figure 1 shows the relative magnetic field intensity B/B_0 as a function of altitude in the meridian plane through the heart of the SAA, for different latitudes. An altitude variation corresponding to one atmospheric scale height of 50 km corresponds to a change of only 2.3% in the value of B/B_0. This indicates again how sensitive flux values provided by environment models may be to small inaccuracies in the value of B or B/B_0 at low altitudes in the atmosphere.

The locus of points of deepest penetration for trapped particles can be described by the magnetic cut-off field intensity $B_c(L)$. Among the family of drift shells (B, L), for a given L, B_c is the highest B value for which all particles on the drift shell (B, L) are trapped. Particles on drift shells (B, L) with $B > B_c$ are precipitating or quasi-trapped particles. Since the separation between trapped and quasi-trapped particles is determined by the neutral atmosphere, B_c must be a function of the parameters influencing the density distribution of the atmosphere, such as A_p or K_p and mainly the solar radio flux $F_{10.7}$, which controls the heating of the upper atmosphere. In addition, B_c also depends on the particle energy E.

The thin atmospheric layer where the precipitated particles lose their energy can be considered as a rather abrupt absorbing wall. In the AP-8 (Sawyer & Vette 1976) and AE-8 (Vette 1991) trapped particle models, the omnidirectional integral flux $J(E, L, B/B_0)$ drops to zero for $B_c/B_0 = 0.6572\,L^{3.452}$, an empirical formula derived by Vette (1991) (note that with this definition B_c/B_0 also is an adiabatic invariant since it only depends on L). In the family of drift shells (B, L), the drift shell (B_c, L) is the one where the lowest altitude reached by a particle moving on this shell is 100 km. Whether the atmospheric cut-off is located at 100 km or 200 km altitude will not change significantly the equatorial loss cone angle $\alpha_{0c} = \arcsin\sqrt{B_0/B_c}$. Similarly, the equatorial pitch angle distribution $J(E, L, \alpha_0)$ will only depend significantly on B_c near $\alpha_0 = \alpha_{0c}$ and not at all near $\alpha_0 = 90°$.

Because of the very small variation of the magnetic field over the limited altitude range where the trapped particle flux decreases by several orders of magnitude, neither B, B/B_0, nor α_0 are appropriate coordinates to map omnidirectional or directional particle fluxes at low altitudes. Indeed, small inaccuracies in the determination of B or α_0 will result in large errors on the atmospheric cut-off altitude. To illustrate this point, we show in Fig. 2 the integral proton flux $J(> 10\,\mathrm{MeV})$ in the AP-8 models (Sawyer & Vette 1976) as a function of B/B_0, for five values of L. The solid lines correspond to proton fluxes for minimum solar activity, the symbols to fluxes for solar maximum. For L values below 3 the flux decreases almost vertically when B/B_0 approaches B_c/B_0. This steep gradient of J clearly makes an accurate determination of the particle flux by interpolation in B/B_0 difficult and coarse near the atmospheric cut-off. The dependence of the particle flux J on the equatorial pitch angle α_0 is equally steep near the loss cone angle α_{0c} and equally difficult to interpolate.

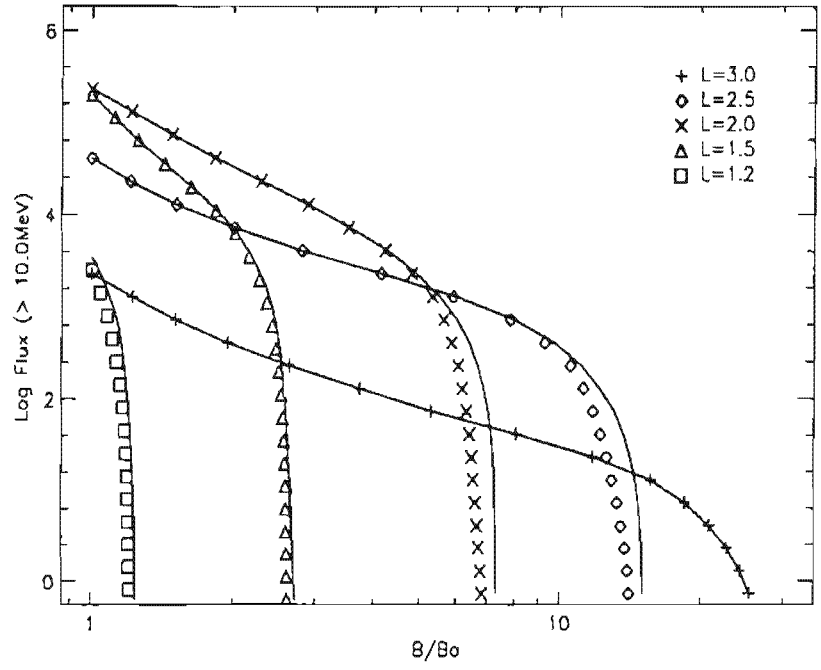

Figure 2. Integral AP-8 MIN/MAX proton flux above 10 MeV as a function of B/B_0 for selected L-values. The symbols denote AP-8 MAX values, the AP-8 MIN values are represented by the solid lines.

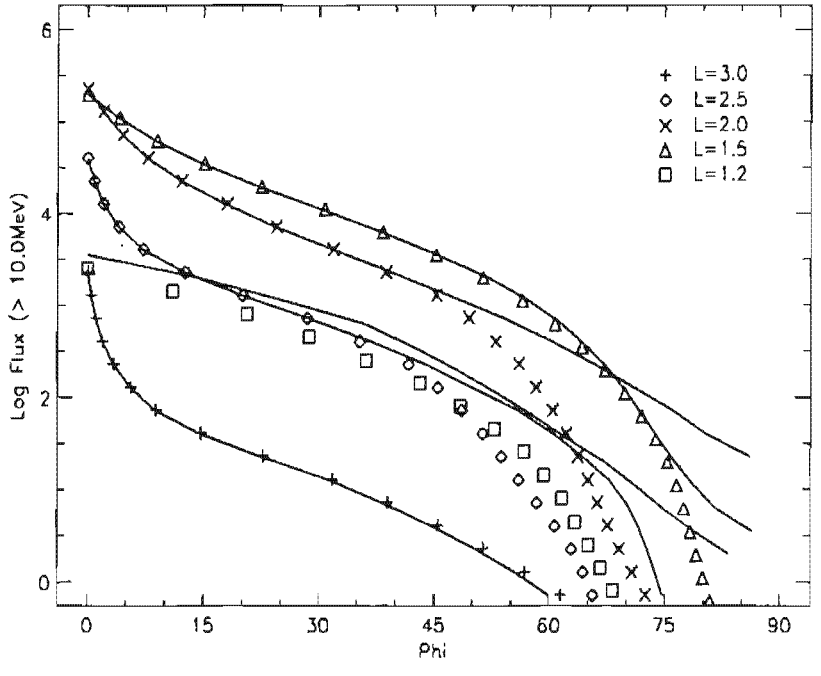

Figure 3. Integral AP-8 MIN/MAX proton flux above 10 MeV as a function of φ for selected L-values. The symbols and lines have the same meaning as in Fig. 2.

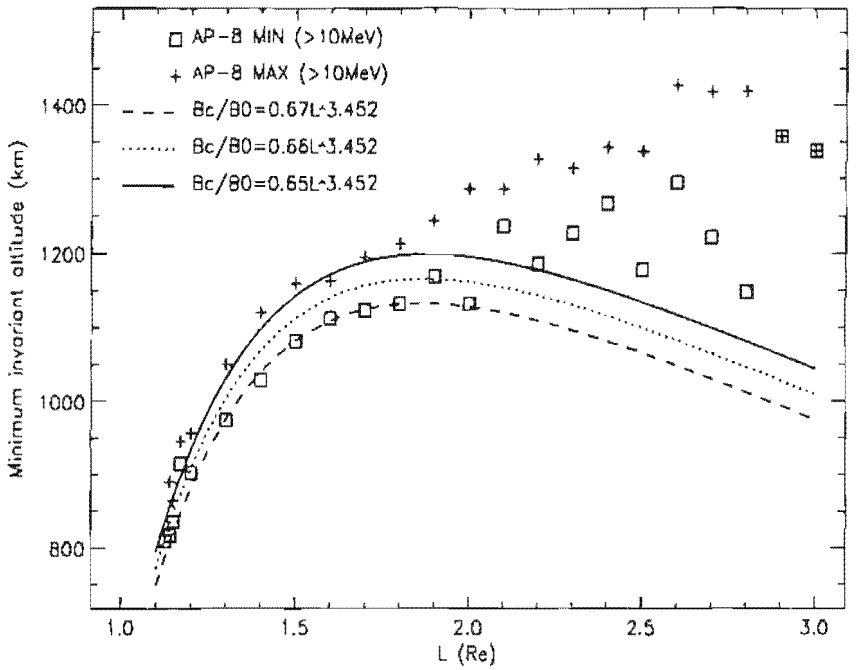

Figure 4. Invariant altitudes corresponding to the last B/B_0 value of the L blocks in AP-8 MAX (+) and AP-8 MIN (□), for $E > 10$ MeV. The lines show the invariant altitude corresponding to three fits of B_c/B_0.

1.2 Alternative coordinates

A useful alternative to B/B_0 has been proposed by Daly & Evans (1993). While B/B_0 varies from a value close to 1 at the geomagnetic equator to a large value near the Earth's surface, the angle φ defined as

$$\varphi = \arcsin\left(\frac{B - B_0}{B_c - B_0}\right) \tag{1.1}$$

varies from a value close to 0° at the equator to 90° at the atmospheric cut-off where $B = B_c$. The advantage of φ is that low-altitude variations in flux are spread over a larger range of variation of φ, so that interpolation between flux values becomes less difficult. This effect is illustrated in Fig. 3, which shows the dependence of the AP-8 MIN (solid line) and AP-8 MAX (symbols) fluxes on φ, for the same values of E and L as in Fig. 2.

However, it remains that the determination of the coordinate φ by means of Eq. (1.1) requires a magnetic field model with a very high accuracy and precision. In particular, near the cut-off region the coordinate φ becomes very sensitive to the value chosen for B_c. It should be emphasized that the altitude corresponding to B_c depends on the energy of the particle and ranges between 50 and 200 km.

Daly & Evans (1993) used the following values for B_c/B_0:

$$\frac{B_c}{B_0} = \begin{cases} 0.66\,L^{3.452} & \text{for AP-8 MIN} \\ 0.65\,L^{3.452} & \text{for AP-8 MAX}, \end{cases} \tag{1.2}$$

which they obtained by fitting the maximum B/B_0 values in AP-8. Figure 4 shows the invariant altitude corresponding to the last value of B/B_0 of the L-blocks in the AP-8 models, for $E > 10\,\mathrm{MeV}$, as a function of L. The dotted and solid lines in this figure represent the invariant altitude for B_c as given by Eqs. (1.2). It can be seen that for $L \leq 2$ the invariant altitude corresponding to B_c for the solar minimum model lies above the minimum invariant altitudes of the model points, which means that the B_c values are too low. A better agreement is found by raising the coefficient in the fit function from 0.66 to 0.67 (we have used the coefficient 0.67 for Fig. 3). The corresponding invariant altitude is shown by the dashed line in Fig. 4. Below $L \simeq 2$ the field line segments in AP-8 terminate very close to or on the fitted B_c values. Above $L \simeq 2$ the proton flux in the models drops to zero before the cut-off region is reached.

1.3 Drift shell average of atmospheric density

Although the use of the coordinate φ makes the interpolation of low altitude fluxes more accurate, Def. (1.1) is a functional dependence chosen solely for its benefit of improving the numerical accuracy of the interpolation and has no physical grounds. Similarly, Def. (1.2) is an empirical relation that was found to fit the AP-8 model data.

It has already been pointed out by Pfitzer (1990) that the atmospheric density is a better coordinate to organise AP-8 proton fluxes at Space Station altitudes. He found that the AP-8 MIN and AP-8 MAX proton fluxes for Space Station altitudes (350–500 km), shown in Fig. 5, fall on almost the same curve when plotted as a function of the atmospheric densities for minimum and maximum solar activity conditions, respectively. Pfitzer's (1990) study confirms that at low altitudes the atmospheric density distribution governs the flux distribution of trapped protons. Note that the limited altitude range considered by Pfitzer corresponds to a restricted range of atmospheric density of 10^{-16}–$10^{-14}\,\mathrm{g\,cm^{-3}}$. Our study covers the full range of atmospheric densities and altitudes.

The atmospheric density $\rho(h_1)$ at a given altitude h_1 does not determine, however, the total mass of material traversed by a particle detected at the altitude h_1. In an atmosphere where the density decreases exponentially with a constant scale

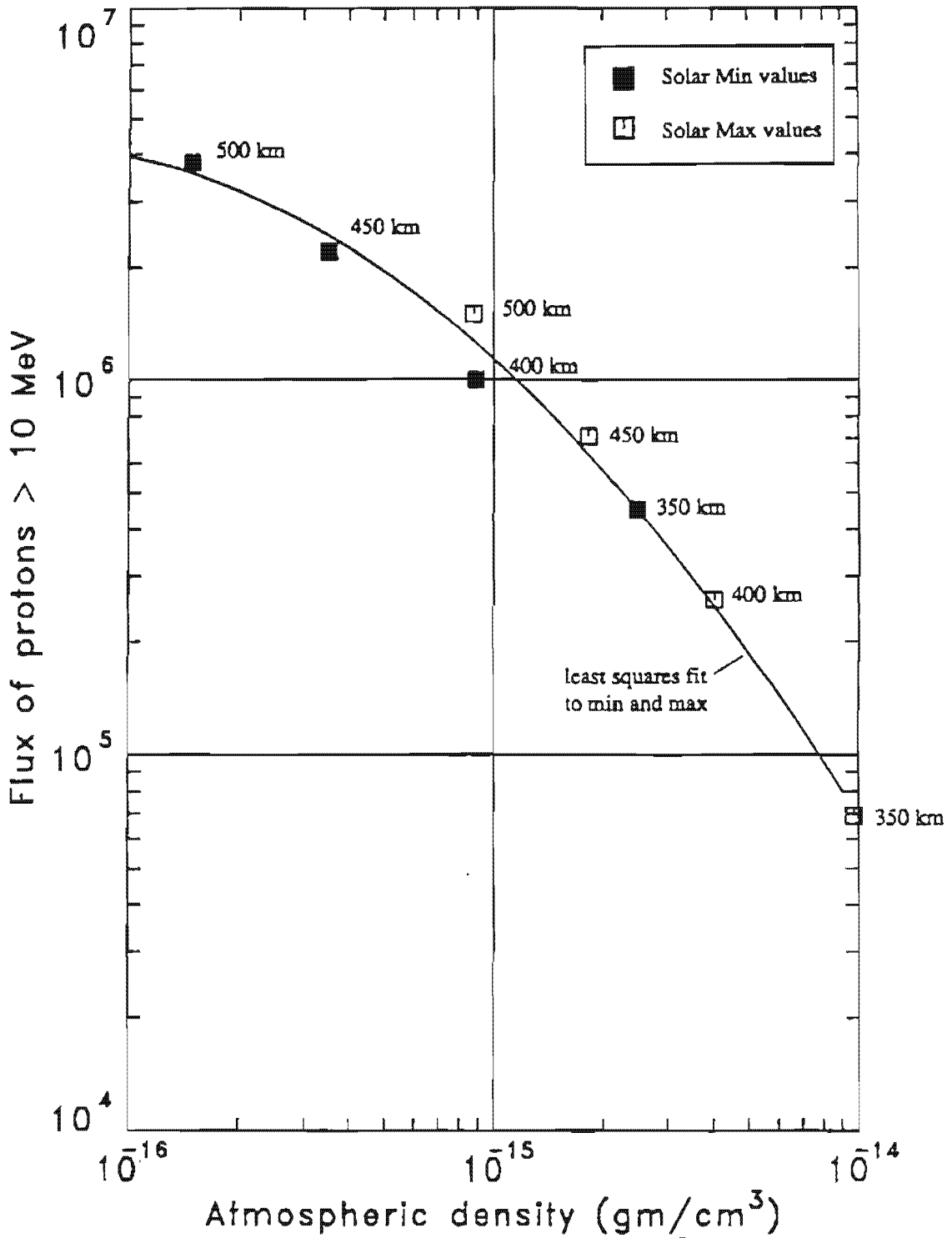

Figure 5. A-8 MIN and AP-8 MAX integral proton fluxes above 10 MeV for different altitudes, as a function of mean atmospheric density. [from Pfitzer (1990)]

height H, i.e.

$$\rho(h) = \rho(h_0)\,\exp\left(-\frac{h-h_0}{H}\right)\,, \tag{1.3}$$

the total mass of material per unit area above the point of observation at altitude h_1 is given by

$$\begin{aligned} M(h_1) &= \int_{h_1}^{\infty} \rho(h)\,dh \\ &= \rho(h_1)\,H\,. \end{aligned} \tag{1.4}$$

The atmospheric pressure scale height H is defined as

$$H = \frac{kT}{\overline{m}g}\,. \tag{1.5}$$

H is proportional to the thermospheric temperature T which is larger during solar maximum conditions than during solar minimum conditions. Therefore, the total mass $M(h_1)$ encountered by a precipitated particle is not only proportional to $\rho(h_1)$, but to $\rho(h_1)\,H$, where both $\rho(h_1)$ and H depend on solar activity conditions. Consequently, it is expected that the low altitude observations of precipitated fluxes should be better organized in terms of $M(h_1)$ than in $\rho(h_1)$.

Instead, one should consider an average of the atmospheric density over an azimuthal drift path of particles of a given species and with a given energy. Hassitt (1965b) has developed a computer code at UCSD Physics Department which calculates the number density of atoms, ions, and molecules given by appropriate atmospheric and ionospheric models over a drift shell (B, L). A weighted average density $n_s(B, L)$ is then determined by multiplying the resulting number densities with the collision cross section σ_i of the trapped particles with the constituents i, summing over i and integrating the sum over the drift shell (B, L). C.E. McIlwain has kindly provided J. Lemaire with a revised version of Hassitt's original program, which we have modified further. A detailed description of the software package is given by Hassitt (1964).

The final output of Hassitt's code is the shell height $H_s(B, L)$, the altitude where the drift shell mean density is equal to the density in a conventional one-dimensional atmospheric model. In order to obtain a meaningful correspondence between H_s and real altitudes, it is useful (but not necessary) to adopt a reasonable density profile of the upper atmosphere.

Hassitt's code also provides the minimum altitude reached while tracing the drift shell and the atmospheric density averaged over the mirror points.

In Chapter 2 we describe the algorithm developed by Hassitt (1964) and the improvements we made to it.

Chapter 2

The drift shell averaged density

2.1 Definition and calculation method

In order to estimate the influence of the Earth's atmosphere on the distribution of trapped particles, the effects of the atmosphere have to be averaged over the particle's orbit. Ray (1960) and Lenchek & Singer (1962) have derived expressions for the atmospheric density averaged over the orbit of a particle trapped in a dipole field. Newkirk & Walt (1964) have determined the average density for a realistic representation of the geomagnetic field. Hassitt (1965b) has simplified considerably the procedure of Newkirk & Walt (1964), while maintaining the same accuracy. In the following sections, we will describe Hassitt's (1965b) method and it's application to the study of low-altitude coordinate systems.

2.1.1 Definition of the average

The guiding centre of a trapped particle moves along a field line with velocity

$$v_{\mathrm{p}} = v\sqrt{1 - \frac{B}{B_{\mathrm{m}}}}, \tag{2.1}$$

where v is the total velocity of the particle, B is the local magnetic field intensity, and B_{m} is the magnetic field intensity in the mirror points. The guiding centre also follows a longitudinal drift motion perpendicular to the field line. The average perpendicular drift velocity is

$$v_{\mathrm{d}} = \frac{c}{qB^2T}\nabla J \times \nabla B, \tag{2.2}$$

where c is the velocity of light and q is the charge of the particle (Roederer 1970). T is the bounce time for one oscillation between the conjugate mirror points M and

M':

$$T = \int_{M'}^{M} \frac{ds}{v_p}, \tag{2.3}$$

where ds denotes an element of length along the field line. J is the second adiabatic invariant

$$J = \int_{M'}^{M} v_p \, ds \,. \tag{2.4}$$

In the absence of external forces v is constant and

$$I \equiv \frac{J}{v} \tag{2.5}$$

also is an invariant of the motion.

The adiabatic motion of a trapped particle is determined by the invariants B_m and L_m [McIlwain's (1961) L obtained by tracing to the conjugate mirror points; from here on, we will drop the index "m"]. During the drift motion of a trapped particle, its guiding centre moves on a surface formed by segments of field lines determined by the conditions B=cst and L=cst. This surface is called a drift shell and is defined by the coordinate pair (B, L) (not just by L). The average atmospheric density—or the average of any quantity $f(\boldsymbol{r})$—encountered by a trapped particle is obtained by averaging $f(\boldsymbol{r})$ over the particle's drift shell.

Consider particles of energy E trapped on a drift shell (B, L). At a point P on the drift shell with geocentric coordinate vector $\boldsymbol{r}$, the number density $n_i(\boldsymbol{r})$ of atmospheric or ionospheric constituent i can be determined from suitable atmospheric and ionospheric models. We define a local weighted average density $n(\boldsymbol{r})$ as

$$n(\boldsymbol{r}) = \frac{\sum_i \sigma_i(E)\, n_i(\boldsymbol{r})}{\sigma_0}, \tag{2.6}$$

where $\sigma_0 = 10^{-15}\mathrm{cm}^2$ is a normalization factor of the order of magnitude of the collision cross sections for trapped protons with atmospheric particles. The summation in Eq. (2.6) extends over all atmospheric, ionospheric and plasmaspheric constituents that interact with trapped particles. Note that originally Hassitt's (1964) code used constant values for the cross sections, while we implemented energy dependent cross sections.

The field aligned velocity component v_p of the trapped particles depends on their local pitch angle, being zero at the mirror points and reaching its maximum on the geomagnetic equator. Consequently, the particles spend more time in the high density region around their mirror points than closer to the equator. To account for this effect when integrating the local average density n over the drift shell, we apply as a weight factor the time needed for the particles to move to a neighbouring point on the same field line during their bounce motion. The azimuthal drift velocity also

is position dependent, so that a second weight factor, namely the time needed to drift to a neighbouring field line on the azimuthal drift motion, has to be used.

Let dx and dy denote elements of length along a field line and along the direction of azimuthal drift, respectively, and v_p and v_d the corresponding local drift velocities. A drift shell averaged atmospheric density n_s then can be defined as

$$n_s(B,L) = \frac{S(n,B,L)}{S(1,B,L)}, \tag{2.7}$$

with

$$S(n,B,L) = \iint n(r)\,\frac{dx}{v_p}\,\frac{dy}{v_d}, \tag{2.8}$$

where the denominator in Eq. (2.7) serves as a normalisation factor and the integration in Eq. (2.8) extends over the whole drift shell.

Equation (2.8) can be written in an alternative way. Let $\dot{\phi}$ be the projection of v_d along the ϕ axis in polar coordinates (r,θ,ϕ). One then has that

$$\frac{dy}{v_d} = \frac{d\phi}{\dot{\phi}}, \tag{2.9}$$

so that S can be defined in terms of $d\phi/\dot{\phi}$ rather than dy/v_d.

2.1.2 Calculation of the average

The calculation of $\dot{\phi}$ is a difficult and time consuming numerical process. Hassitt (1965a) has shown that $d\phi/\dot{\phi}$ is independent of s, s being the distance along the field line measured from the equator. The distance between two neighbouring field lines varies with s, as does $\dot{\phi}$, but $d\phi/\dot{\phi}$—which represents the time needed to drift from one field line to the other—is independent of s, as a first approximation. Consequently, Eq. (2.8) can be written as

$$S(n,L,B) = \int U(n,L,B,\phi_0)\,\frac{d\phi}{\dot{\phi}}, \tag{2.10}$$

where

$$U(n,L,B,\phi_0) = \int n(r)\,\frac{ds}{v_p}, \tag{2.11}$$

and ϕ_0 is the azimuth of the point where the field line intersects the equator. The quantity $d\phi/\dot{\phi}$ can be evaluated at any point on the field line, but the simplest way is to choose the point of intersection with the magnetic equator plane. By using Eqs. (2.10) and (2.11), the two-dimensional integration over the drift shell is decomposed into two one-dimensional integrations. In addition, $\dot{\phi}$ has to be evaluated in one point only for each field line. Note that it follows from Eq. (2.3) that $U(1,L,B,\phi_0) = T$, where T is the bounce time between mirror points.

2.1.3 The computer program

Hassitt (1964) has written a computer code to evaluate n_s. It uses the Jensen & Cain (1962) geomagnetic field model and the now obsolete atmosphere model of Anderson & Francis (1964). In Hassitt's program, $n = n(r)$ is a function of the geodetic altitude only and does not depend on latitude or longitude, which is a severe limitation.

Hassitt's (1964) program makes use of two additional approximations, which could have been avoided at the expense of (significantly) increased computing time. The first approximation is that $\dot{\phi}$ is approximated by the value of $\dot{\phi}$ for a particle mirroring at the equator. In this case, the following expression can be used:

$$v_d = mcv^2 \frac{|\nabla B|}{2qB^2} \tag{2.12}$$

(see, for instance, Lew 1961). $\dot{\phi}$ is a function of B_m, but Hassitt (1965a) has shown that for two mirror points on the same field line the ratio $\dot{\phi}(B_1)/\dot{\phi}(B_2)$ depends only weakly on ϕ.

The second approximation in the program is that a drift shell is defined as a shell of constant B_0. In other words, L is assumed to be constant along field lines, which is—although only true for a dipole field—a reasonable approximation in the near-Earth geomagnetic field where the dipole is the dominant term. Hassitt (1965b) argues that by averaging over the longitudinal drift, the resulting errors are virtually cancelled out. The major advantage of identifying a shell by B_0 is that it is much easier to locate it than if one has to calculate L in a series of points along the field line. In addition, for a given value of ϕ_0 and a series of values of B, it is sufficient to trace one field line, while otherwise it would be necessary to retrace the field line for each value of B.

2.1.4 Definition of a shell height

The drift shell averaging program provides the weighted average density of a number of atmospheric and ionospheric constituents encountered by a trapped particle during one full drift motion around the Earth. In order to visualize better the result of the calculations, Hassitt (1965b) introduced an average height related to the average density.

Hassitt's definition

Originally, Hassitt (1965b) made use of a simple exponential atmosphere model to relate a shell height to the average density. In this model, the density of the neutral

constituents of the atmosphere varies as

$$n(h) = A\,\mathrm{e}^{-\mu h^*}\,, \tag{2.13}$$

where

$$h^* = \frac{h}{R_\mathrm{E} + h} \tag{2.14}$$

is the reduced height and $R_\mathrm{E} = 6371.2\,\mathrm{km}$ is the radius of the Earth. Given an average density $n_\mathrm{s}(L, B_\mathrm{m})$, the corresponding reduced average height is defined as

$$h^*_\mathrm{av} = -\frac{\ln\left(\frac{n_\mathrm{s}}{A}\right)}{\mu}\,, \tag{2.15}$$

and the average height as

$$h_\mathrm{av} = \frac{h^*_\mathrm{av}}{1 - h^*_\mathrm{av}}\,R_\mathrm{E}\,. \tag{2.16}$$

Hassitt (1965b) has fitted the Anderson & Francis (1964) model with Expression (2.13) and determined A and μ for the various atmospheric constituents.

McIlwain's definition

In the software BIRA/IASB received from C. McIlwain, the shell height is computed in a different way. For a given value of the shell-averaged density, the subroutine EQAT determines the altitude at which the average density is equal to the density given by the Anderson & Francis (1964) model. This approach has the disadvantage that the shell height depends on the choice of the atmosphere model used to calculate the average density, so that solar cycle effects and other influences are largely cancelled out.

New approach

We opted for a simpler approach, in which we make use of a very basic average atmosphere model. Allen (1985) provides a table with average atmosphere and ionosphere number densities as a function of altitude. We fitted this distribution with an exponential distribution below 100 km and with two linear functions between 100 and 1000 km and above 1000 km. The tabulated points and the fit functions are shown in Fig. 6. Depending on the input density, the appropriate fit function is inverted to yield the shell height.

The advantage of this approach is that the shell height does not depend on the atmosphere model used to calculate the shell-averaged density. In addition, the inversion procedure is very simple and does not involve a numerical procedure for location of zero points.

Table 2. NAMELIST parameters for the shell height program

Parameter	Data Type	Default	Function
		SHELL	
MODEL	INTEGER	0	Chooses the geomagnetic model: 0: DGRF/IGRF 1: Jensen & Cain (1962) 2: GSFC 12/66 (Cain et al. 1967)
BLTIME	REAL*8	1990.0	Epoch for geomagnetic field model
		ATMOS	
ATMMOD	CHARACTER*2	MI	Chooses the atmosphere model: AF: Anderson & Francis (1964) MI: MSISE-90, IRI-90, Carpenter & Anderson (1992) MD: MDAC (Pfitzer 1990) NO: No atmosphere model
DAY	INTEGER	1	Day of year
UT	REAL*8	0.0	Universal time (hrs)
TL	REAL*8	0.0	Local time (hrs)
F107	REAL*8	100.0	Daily $F_{10.7}$ flux for previous day
F107M	REAL*8	100.0	3 Month average of $F_{10.7}$ flux
AP	REAL*8(7)	7*0.0	Magnetic index A_p: AP(1): daily A_p AP(2): 3 hr A_p index for current time AP(3): 3 hr A_p index for 3 hrs. before current time AP(4): 3 hr A_p index for 6 hrs. before current time AP(5): 3 hr A_p index for 9 hrs. before current time AP(6): average of eight 3 hr A_p indices from 12 to 33 hrs. prior to current time AP(7): average of eight 3 hr A_p indices from 36 to 59 hrs. prior to current time SWI(9) $\neq -1$: only daily A_p is used.
SWI	REAL*8(25)	25*1.0	Selects variation on 25 parameters: 0: main effects off, cross terms off 1: main effects on, cross terms on 2: main effects on, cross terms off

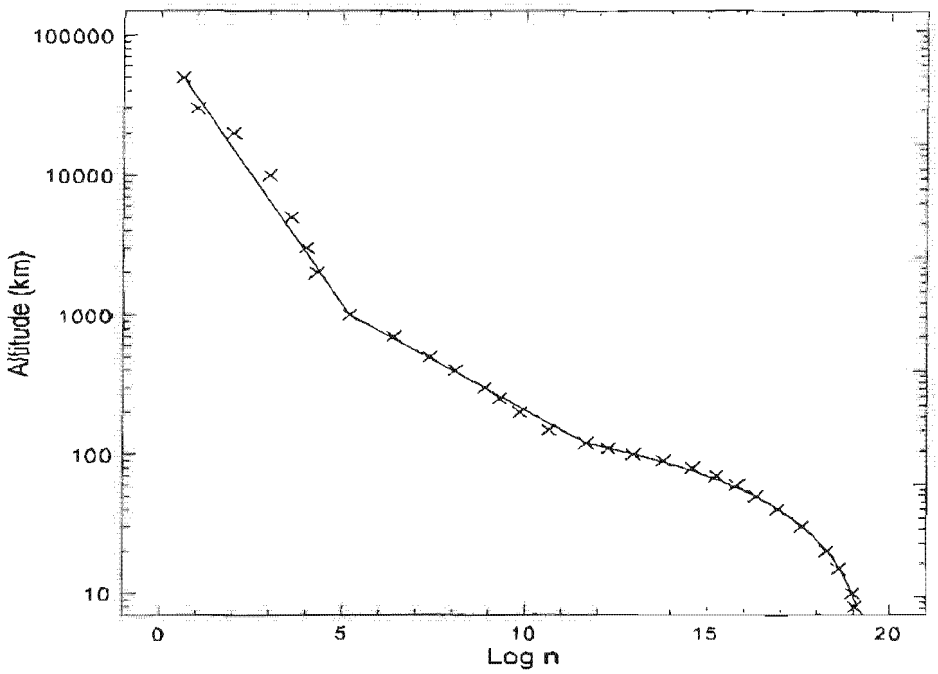

Figure 6. Density distribution (from Allen [1985]) used in the new definition of the shell height. The solid line represents the fit functions used for different altitude ranges.

Table 2. (continued)

Parameter	Data Type	Default	Function
		ATMOS	
RZ	REAL*8	100.0	Zürich solar sunspot number
KPMAX	REAL*8	1.0	Maximum K_p value for Carpenter & Anderson (1992) model
CROSS	INTEGER	1	0: Hassitt's cross sections $\neq$ 0: cross section obtained with CROSS

Table 3. NAMELIST parameters for the shell height program, for conditions of solar minimum and solar maximum

Parameter	Solar minimum	Solar maximum
F107	50.0	300
F107M	60.0	200.0
AP	7*0.0	300.0, 6*0.0
SWI	25*1.0	25*1.0
RZ	50.0	250.0
KPMAX	1.0	6.0

2.1.5 Modifications of Hassitt's software

This section gives an overview of the modifications that were made to Hassitt's (1964) original software:

1. The DGRF/IGRF and GSFC 12/66 (Cain et al. 1967) geomagnetic field models were added.

2. The MSIS and IRI models and the model of Carpenter & Anderson (1992) were added for a better description of the upper atmosphere, the ionosphere, and the plasmasphere. The atmosphere model developed by McDonnell Douglas Astronautics Co. (MDAC), used by Pfitzer (1990), also was included. The subroutine ATMO was added to calculate or set up appropriate parameters depending on the choice of atmosphere model. It is also possible to run the code without an atmospheric model.

3. The input parameters are read from two NAMELISTs, SHELL and ATMOS. The parameters are listed in Table 2. The values of the NAMELIST parameters we adopted for solar minimum and solar maximum conditions in the next sections are listed in Table 3.

4. The subroutine that calculates the shell height was replaced.

In addition, the structure of the original program was modified and simplified. The old Fortran code was updated to the FORTRAN-77 standard. Comments have been inserted where significant modifications were made.

The implementation of MSIS, MDAC, IRI and the plasmaspheric extension are discussed in the following sections.

2.2 The MSIS atmosphere models

The Mass-Spectrometer-Incoherent-Scatter (MSIS) neutral atmosphere model describes the neutral temperature and the densities of He, O, N_2, O_2, Ar, H, and N. The MSIS model is based on the extensive data compilation and analysis of A.E. Hedin and his collaborators (Hedin et al. 1977ab, Hedin 1983, Hedin 1987). The model version used for TREND is MSISE-90 (Hedin 1991).

Data sources for the model MSISE-90 include temperature and density measurements from several rockets, satellites (OGO 6, San Marco 3, Aeros-A, AE-C, AE-D, AE-E, ESRO 4, DE 2) and incoherent scatter radars (Millstone Hill, St. Santin, Arecibo, Jicamarca, Malvern). Since the MSIS-83 model, terms were added or changed to better represent seasonal variations in the polar regions under both quiet and magnetically disturbed conditions and local time variations in the magnetic activity effect. In addition, a new species, atomic N, was added to the list of species covered by the model.

The model expects as input: year, day of year, universal time, geodetic altitude, latitude and longitude, local apparent solar time, solar $F_{10.7}$ flux (for previous day and three-month average), and magnetic A_p index (daily A_p or A_p history for last 59 hours). For these conditions, the following output parameters are calculated: number density of He, O, N_2, O_2, Ar, H and N, total mass density, neutral temperature, and exospheric temperature. The source code is equipped with 25 flags `SWI` to turn on or off variations due to seasonal, diurnal, semidiurnal, terdiurnal, ... changes.

The software package available at NSSDC contains an interactive driver program developed at NSSDC. The driver program produces tables of temperature and densities. Any model input parameter can be chosen as the variable for the table output. It has been verified that the output densities obtained with the MSISE-90 copy installed at BIRA/IASB are identical to the densities in the log file in the NSSDC distribution.

2.2.1 Implementation of MSISE-90

The input parameters for MSISE-90 are supplied in the `NAMELIST ATMOS`. Table 2 lists the `NAMELIST` parameters, together with their data type, default values, and a brief description. The main MSIS routine is called from the subroutine `ATMO` with the appropriate input parameters. The values returned are the neutral and the exospheric temperature, the number density of all constituents, and the total mass density.

The `NAMELIST` parameters for MSISE-90 are: `DAYNR`, `UT`, `F107`, `F107M`, `AP`, `SWI`. The 25 flags `SWI` allow one to disable all longitudinal and temporal variations in the calculation of the MSIS densities. We set the default `SWI` values to one.

2.2.2 Distribution of atmospheric densities

In this section, we present a series of graphs with the distribution of MSISE-90 atmospheric densities for fixed altitudes as well as a function of altitude, for values for the input parameters representative of solar minimum and solar maximum conditions.

Figure 7 represents the MSISE-90 total mass density at 200 km altitude, for the summer solstice, at midnight U.T., with the MSISE-90 NAMELIST parameters for solar minimum conditions, i.e. $A_p = 0$, $F_{10.7} = 50$, $F_{10.7M} = 60$. The same distribution, but for the winter solstice, is shown in Fig. 8. The seasonal shift of the regions of minimum and maximum density is clearly seen.

Figures 9 and 10 are the analogs of Figs. 7 and 8 for noon U.T. Comparison of this set of four graphs illustrates the diurnal density shifts over the Earth's surface. The contour lines as a function of L.T. change very little from midnight to noon U.T.

The series of two graphs for midnight U.T. formed by Figs. 7–8 is repeated three times in Figs. 11–16, each series with one of the parameters changed to the values $A_p = 300$, $F_{10.7} = 300$, $F_{10.7M} = 200$, which represent conditions of high solar activity. In this way, the influence of each parameter can be evaluated individually.

Clearly, the A_p index has a very strong effect on the density distributions. Off the equator, the density isocontours are almost independent of L.T. for $A_p = 300$, and the densities are much higher than with $A_p = 0$. Increasing the solar radio flux only influences the density levels and does not greatly change the shapes of the contour lines. As expected, the densities increase with increasing solar flux, and much more so with the 13 month average than with the one day average.

The dependence of the MSISE-90 mean mass density on altitude is shown in Figs. 17–20 for the region of the centre of the SAA, for summer and winter solstice, for midnight L.T. Each figure shows the mass density profile obtained with the values for A_p and $F_{10.7}$ valid for low solar activity, and the two profiles obtained by increasing one parameter to solar maximum conditions. For Figs. 17–18 the 13 month average of the solar radio flux was kept equal to 60, while it was set to 200 for Figs. 19–20. In order to facilitate the comparison between different graphs, the profiles for $F_{10.7M} = 60$ are repeated in Figs. 19–20.

When comparing the density profiles, it appears that the density below about 120 km is only very little affected by diurnal, seasonal, or solar cycle effects. Also, only the combined increase in $F_{10.7}$ and $F_{10.7M}$ raises the densities above the levels obtained with $A_p = 300$.

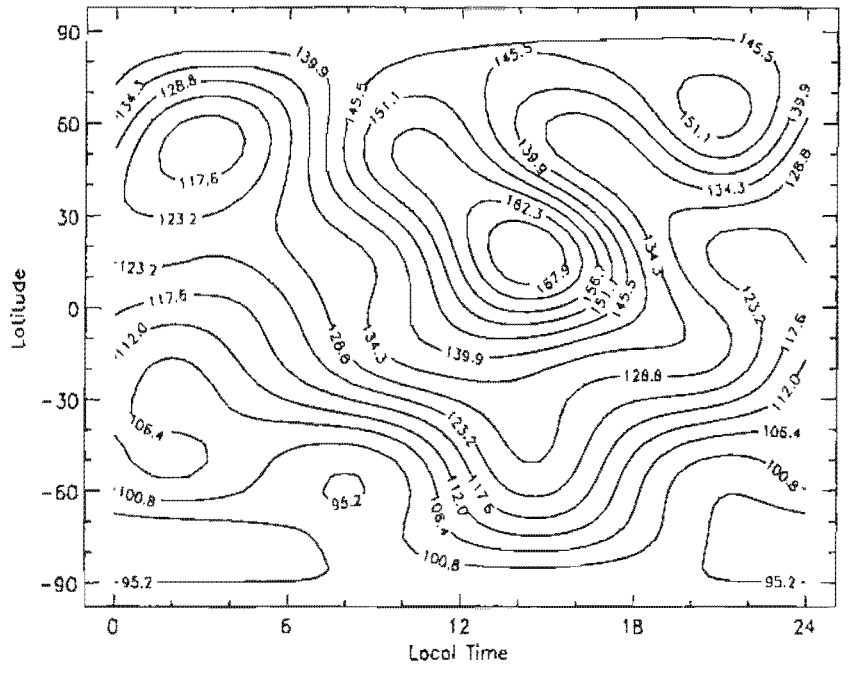

Figure 7. Distribution of MSISE-90 total mass density (10^{15}g cm^{-3}) at 200 km altitude for the summer solstice, midnight U.T., $A_p = 0$, $F_{10.7} = 50$, $F_{10.7M} = 60$

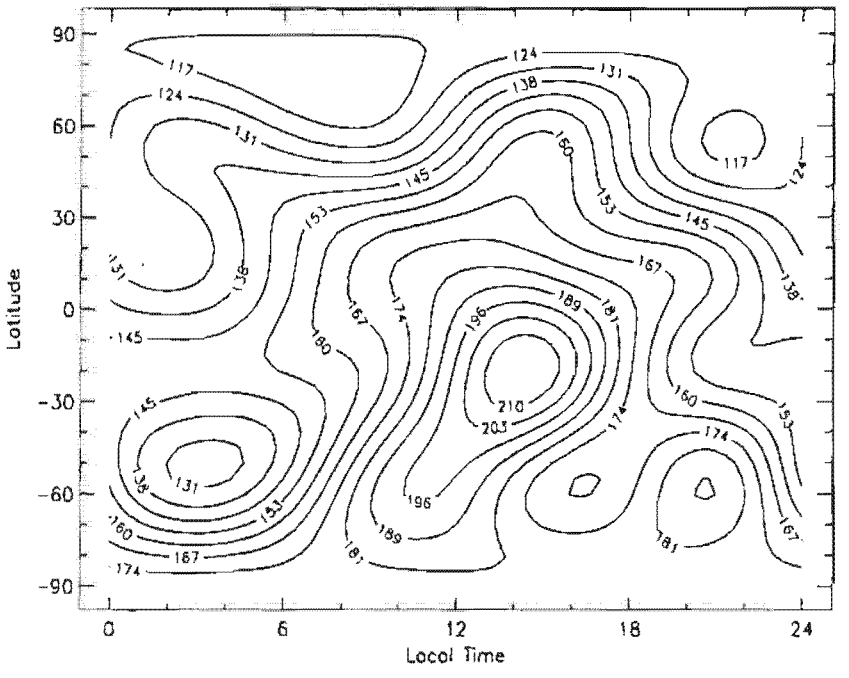

Figure 8. Distribution of MSISE-90 total mass density (10^{15}g cm^{-3}) at 200 km altitude for the winter solstice, midnight U.T., $A_p = 0$, $F_{10.7} = 50$, $F_{10.7M} = 60$

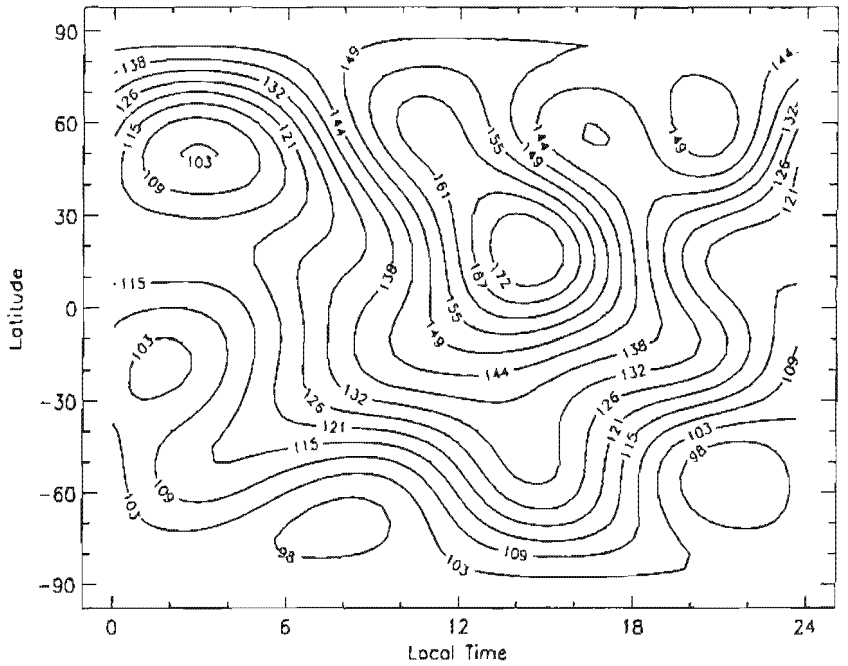

Figure 9. Distribution of MSISE-90 total mass density (10^{15}g cm^{-3}) at 200 km altitude for the summer solstice, noon U.T., $A_p = 0$, $F_{10.7} = 50$, $F_{10.7M} = 60$

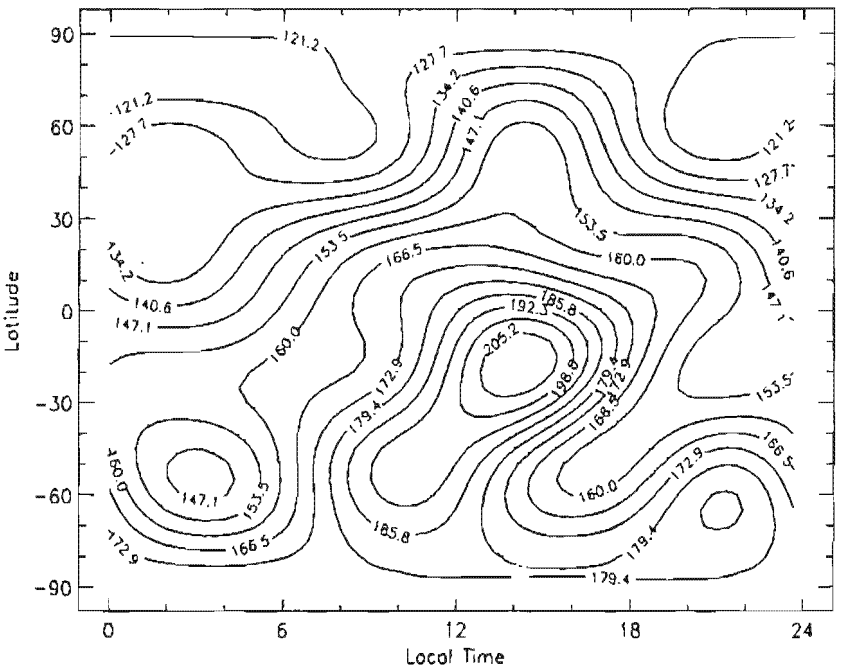

Figure 10. Distribution of MSISE-90 total mass density (10^{15}g cm^{-3}) at 200 km altitude for the winter solstice, noon U.T., $A_p = 0$, $F_{10.7} = 50$, $F_{10.7M} = 60$

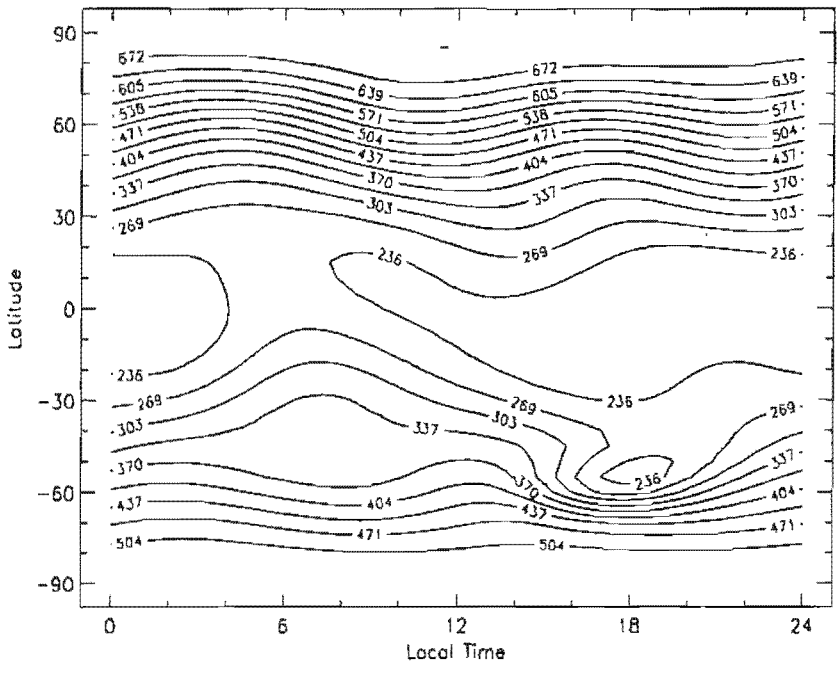

Figure 11. Distribution of MSISE-90 total mass density (10^{15}g cm^{-3}) at 200 km altitude for the summer solstice, midnight U.T., $A_p = 300$, $F_{10.7} = 50$, $F_{10.7M} = 60$

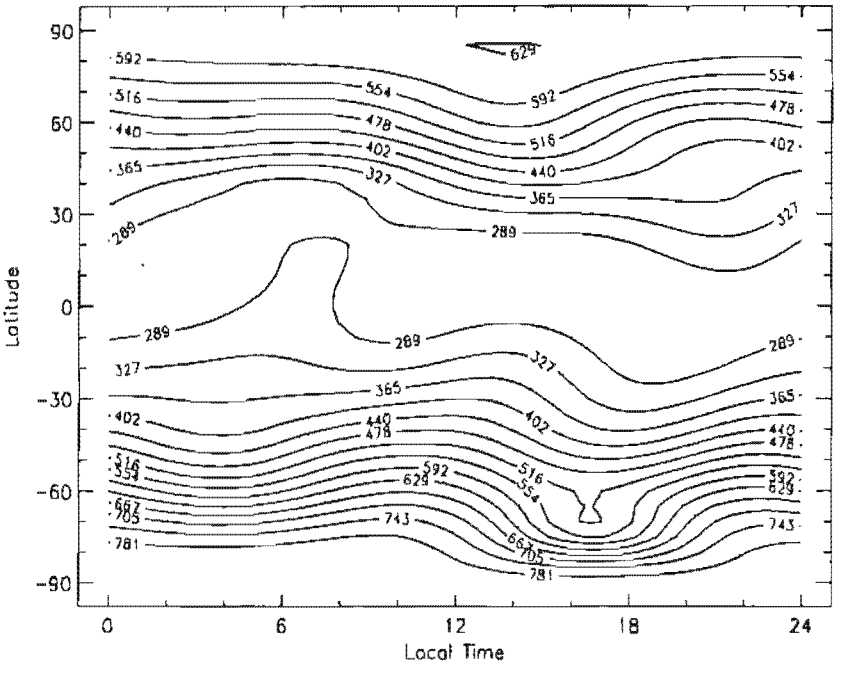

Figure 12. Distribution of MSISE-90 total mass density (10^{15}g cm^{-3}) at 200 km altitude for the winter solstice, midnight U.T., $A_p = 300$, $F_{10.7} = 50$, $F_{10.7M} = 60$

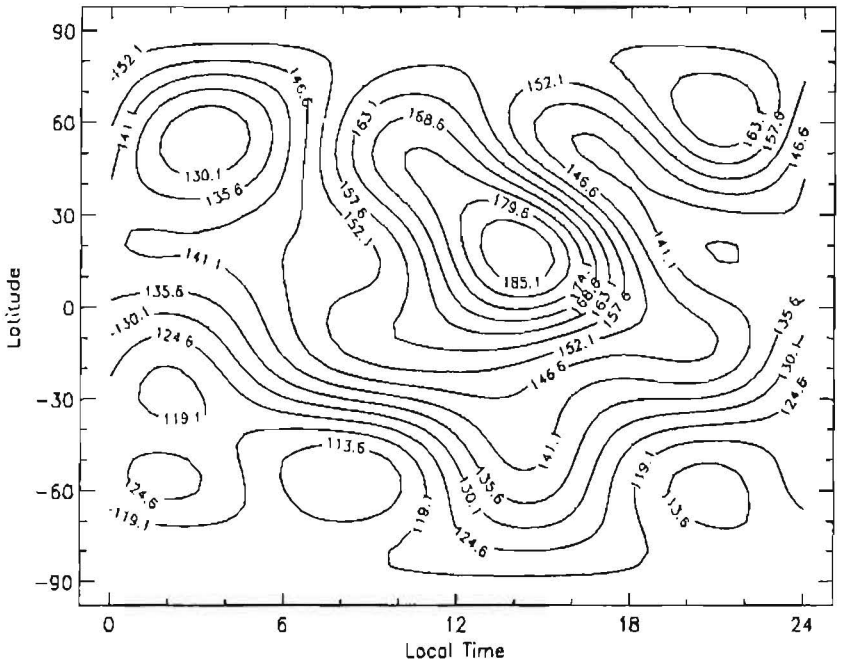

Figure 13. Distribution of MSISE-90 total mass density (10^{15}g cm^{-3}) at 200 km altitude for the summer solstice, midnight U.T., $A_p = 0$, $F_{10.7} = 300$, $F_{10.7M} = 60$

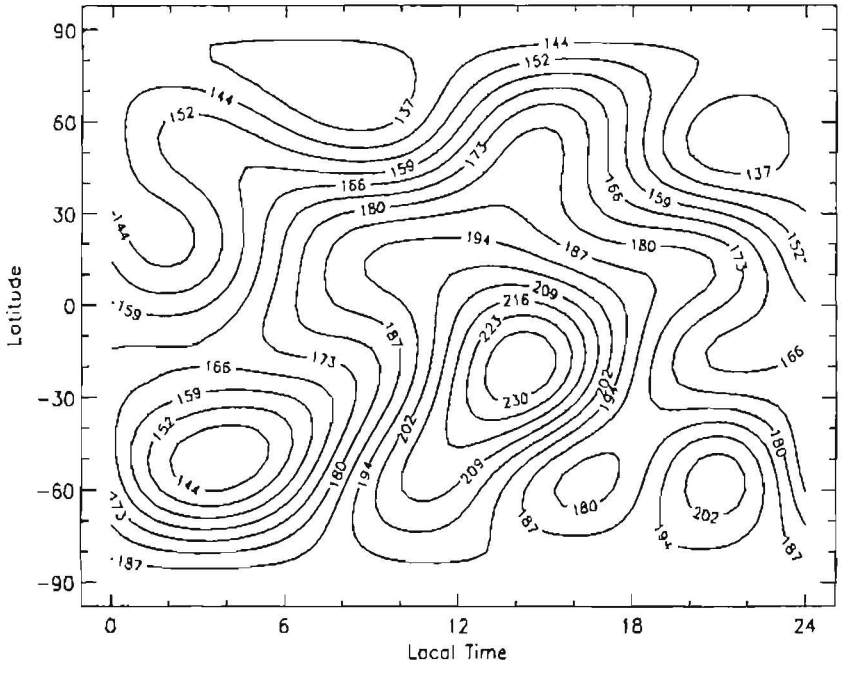

Figure 14. Distribution of MSISE-90 total mass density (10^{15}g cm^{-3}) at 200 km altitude for the winter solstice, midnight U.T., $A_p = 0$, $F_{10.7} = 300$, $F_{10.7M} = 60$

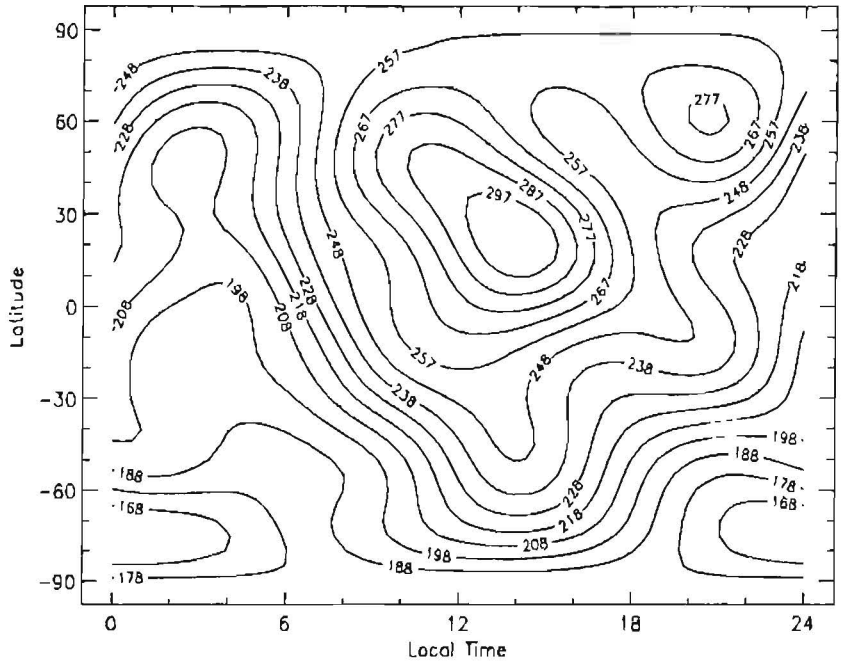

Figure 15. Distribution of MSISE-90 total mass density (10^{15}g cm^{-3}) at 200 km altitude for the summer solstice, midnight U.T., $A_p = 0$, $F_{10.7} = 50$, $F_{10.7M} = 200$

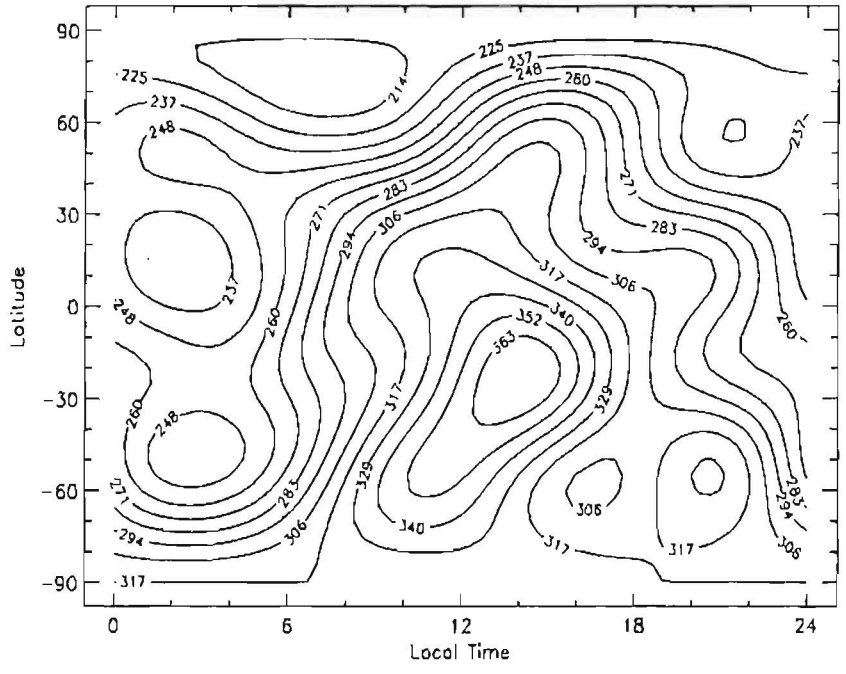

Figure 16. Distribution of MSISE-90 total mass density (10^{15}g cm^{-3}) at 200 km altitude for the winter solstice, midnight U.T., $A_p = 0$, $F_{10.7} = 50$, $F_{10.7M} = 200$

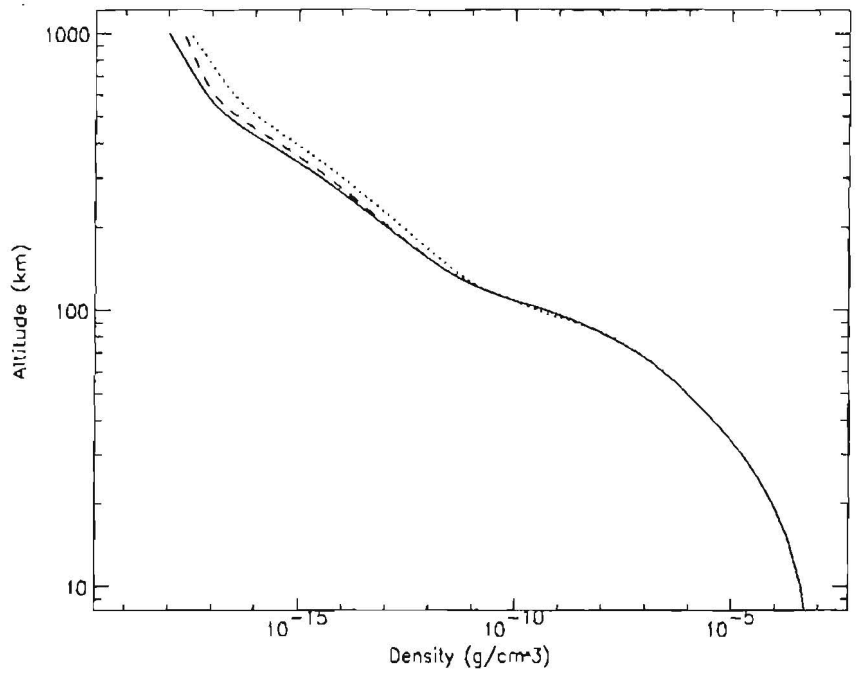

Figure 17. MSISE-90 total mass density profile in the SAA for the summer solstice, midnight L.T. The solid curve is for the default values of the parameters in Table 2, the dotted curve for $A_p = 300$, and the dashed curve for $F_{10.7} = 300$.

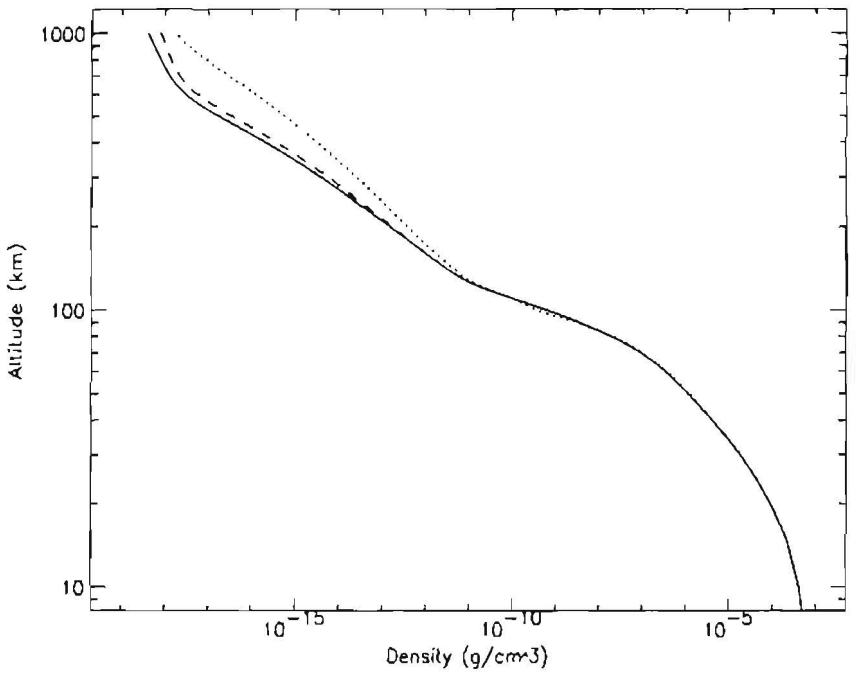

Figure 18. MSISE-90 total mass density profile in the SAA for the winter solstice, midnight L.T. The solid curve is for the default values of the parameters in Table 2, the dotted curve for $A_p = 300$, and the dashed curve for $F_{10.7} = 300$.

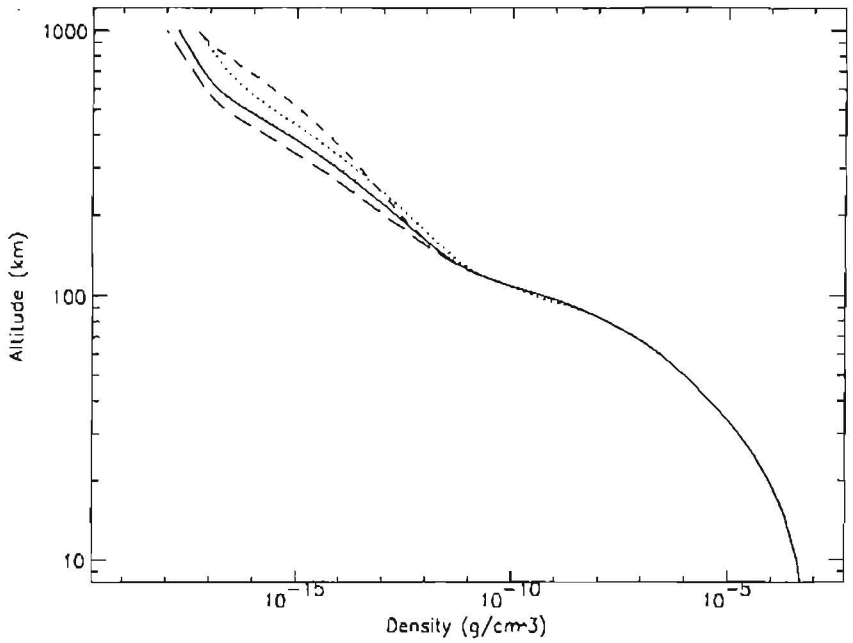

Figure 19. MSISE-90 total mass density profile in the SAA for the summer solstice, midnight L.T. The long-dashed curve is for the default values of the parameters in Table 2. For the solid curve and the other curves $F_{10.7M} = 200$: the dotted curve is for $A_p = 300$, and the dashed curve for $F_{10.7} = 300$.

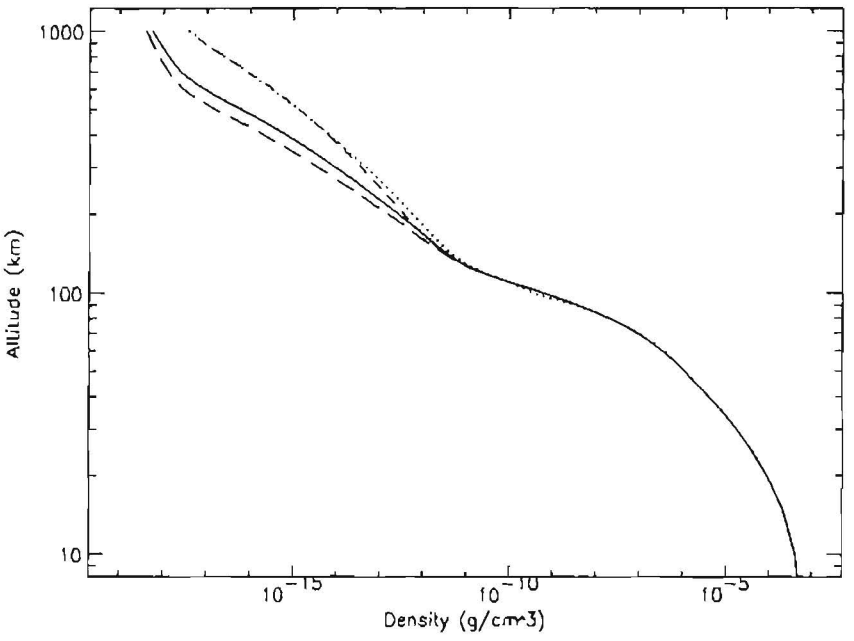

Figure 20. MSISE-90 total mass density profile in the SAA for the winter solstice, midnight L.T. The long-dashed curve is for the default values of the parameters in Table 2. For the solid curve and the other curves $F_{10.7M} = 200$: the dotted curve is for $A_p = 300$, and the dashed curve for $F_{10.7} = 300$.

2.3 The MDAC atmosphere model

McDonnell Douglas Astronautics Co. under contract to the Air Force Office of Scientific Research developed an atmospheric density model (*Response of the Magnetosphere and Atmosphere to the Solar Wind*, Final MDAC Scientific Report for Contract F44620-72-C-0084 for the Air Force Office of Scientific Research, December 1975).

This model has the advantage of simplicity. The altitude dependent term is a global average term and thus can be used directly in this study. The average atmospheric density d is given as

$$d = d_0 \exp\left(-\frac{z-120}{A\sqrt{z-103}}\right), \tag{2.17}$$

where d is the density in $\mathrm{g\,cm^{-3}}$, $d_0 = 2.7 \times 10^{-11}\mathrm{g\,cm^{-3}}$, z is the altitude in km, and A is the solar cycle term:

$$A = 0.99 + 0.518\sqrt{\frac{F_{10.7} + F_{10.7M}}{110}}. \tag{2.18}$$

Figures 21 and 22 show the MDAC total mass density profile in the SAA for three values of $F_{10.7}$, with $F_{10.7M}$ set to 60 and 200, respectively.

2.4 Ionospheric and plasmaspheric models

2.4.1 The IRI ionosphere models

The International Refererence Ionosphere (IRI) is the standard ionospheric model established and updated by a joint working group of URSI and COSPAR. Based on a large volume of ground and space data, IRI describes monthly averages of electron density, electron temperature, ion temperature, ion composition and ion drift in the altitude range from 50 km to 1000 km for magnetically quiet conditions in the non-auroral ionosphere. The auroral region is beyond the L values corresponding to the trapped radiation belts.

The latest version of IRI is IRI-90 (Bilitza 1990). The most recent version of the IRI computer program (No. 12) was released in November 1991. It includes the most recent COSPAR International Reference Atmosphere (CIRA) for the neutral temperature. We obtained this version from NSSDC and implemented it in Hassitt's software. The input parameters for IRI-90 are day of year, U.T., and the Zürich solar sunspot number R_Z. The data types and default values for these parameters are given in Table 2. The limiting values for the altitude and for R_Z are listed in Table 4.

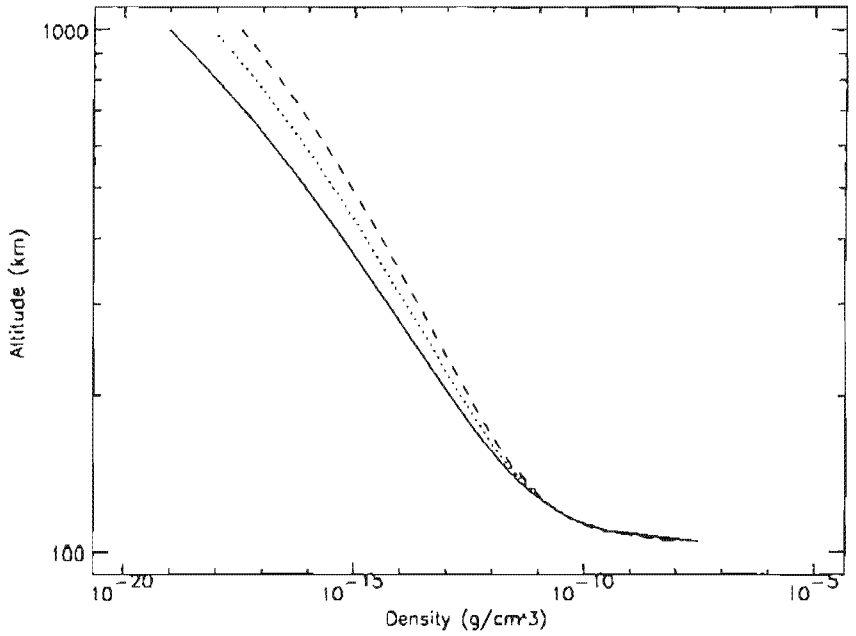

Figure 21. MDAC total mass density profile in the SAA for three values of $F_{10.7}$: 50 (solid), 150 (dotted), 250 (dashed), with $F_{10.7M} = 60$

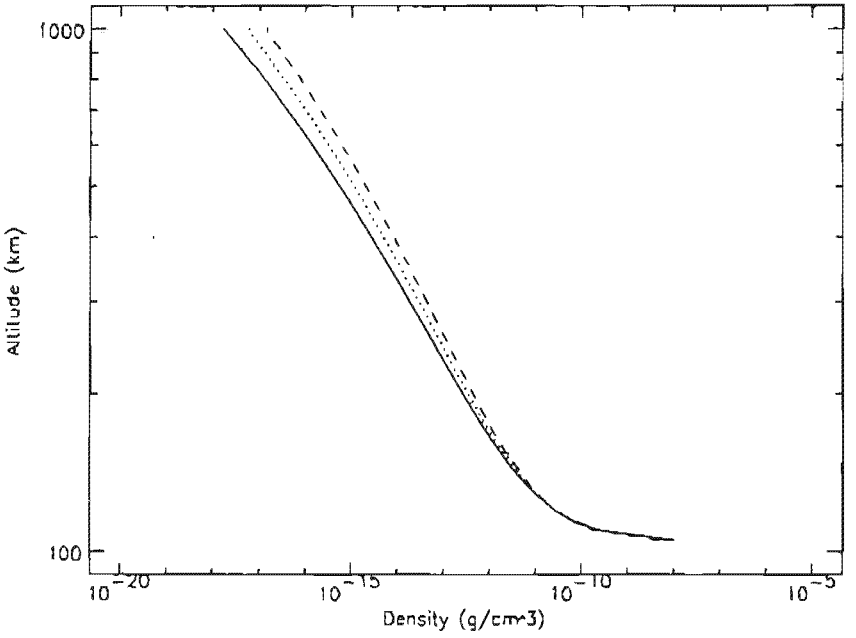

Figure 22. MDAC total mass density profile in the SAA for three values of $F_{10.7}$: 50 (solid), 150 (dotted), 250 (dashed), with $F_{10.7M} = 200$

Table 4. Limiting values for the input parameters in IRI-90

Parameter	Lower (Day/Night)	Upper
Altitude for electron density	60/80 km	1000 km
Altitude for temperatures	120 km	3000 km
Altitude for ion densities	100 km	1000 km
Solar sunspot number	0	250

2.4.2 Plasmaspheric extensions

Since the IRI-90 model is limited to the altitudes given in Table 4, an extension of the ionization density in the magnetosphere is required to account for the small loss from pitch angle scattering experienced by the trapped ions and electrons forming the radiation belts. It is usually held that pitch angle scattering of trapped particles is due to wave-particle interactions. In this study, we will only consider the effects of collisions.

Several three dimensional models have been proposed to describe the equatorial and field-aligned ionization density in the plasmasphere and plasmatrough. In the following sections, we describe two such models which are based on extensive sets of observations.

The Carpenter-Anderson model

The model of Carpenter & Anderson (1992) of the equatorial density is based on

1. electron density profiles derived from sweep frequency receiver radio measurements made along near-equatorial ISEE 1 satellite orbits,
2. results from whistlers.

The model describes, in piecewise fashion, the "saturated plasmasphere", i.e. the region of steep plasmapause gradients, and the plasmatrough (Carpenter & Anderson 1992). Figure 23 shows the equatorial density profiles corresponding to day- and nighttime conditions.

The plasmapause inner limit L_{ppi} is a function of the magnetic activity index K_{pmax}:

$$L_{\mathrm{ppi}} = 5.6 - 0.46\, K_{\mathrm{pmax}}\,, \tag{2.19}$$

where K_{pmax} is the maximum K_{p} value of the preceding 24 hours. There are three exceptions: for L_{ppi} in the magnetic local time (MLT) intervals 06–09, 09–12, and

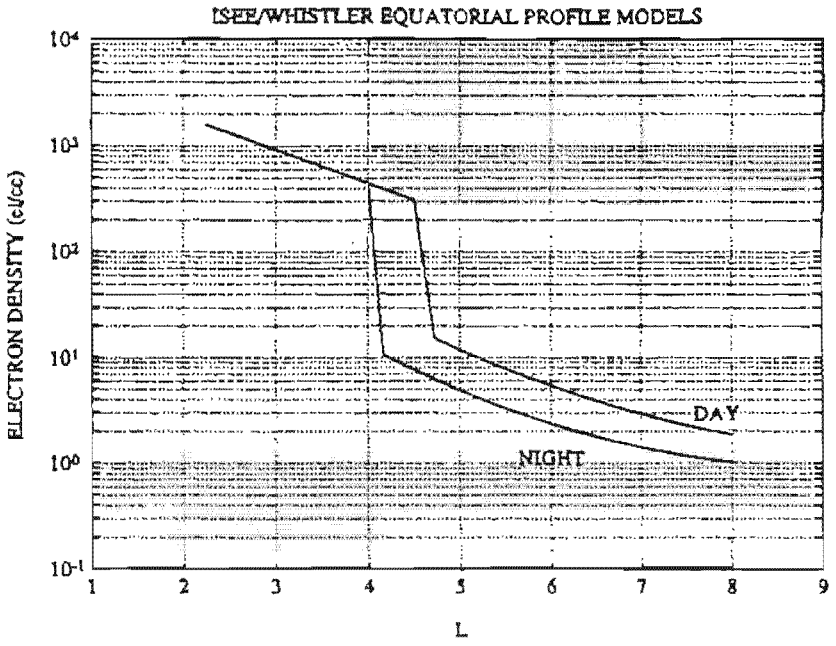

Figure 23. Equatorial density profiles obtained with the model of Carpenter & Anderson (1992).

12–15, omit the one, two, or three immediately preceding K_p values, respectively, in the determination of $K_{p_{max}}$.

The model can be summarized as follows.

1. The density of the saturated plasmasphere element for $2.25 \leq L \leq L_{ppi}$:

$$\log n_e = (-0.3145\,L + 3.9043) + \left\{0.15\left[\cos\frac{2\pi(d+9)}{365} - 0.5\cos\frac{4\pi(d+9)}{365}\right] + 0.00127R_Z - 0.0635\right\} e^{-(L-2)/1.5}, \quad (2.20)$$

where R_Z is the 13 month average sunspot number and d the day number.

2. The plasmapause segment $L_{ppi} \leq L \leq L_{ppo}$:

$$\left.\begin{aligned} n_e &= n_e(L_{ppi}) \times 10^{-(L-L_{ppi})/0.1} && 00 \leq t < 06 \text{ MLT}, \\ n_e &= n_e(L_{ppi}) \times 10^{-(L-L_{ppi})/[0.1+0.011(t-6)]} && 06 \leq t \leq 15 \text{ MLT}. \end{aligned}\right\} \quad (2.21)$$

3. The extended plasmatrough $2.25 \leq L \leq 8$:

$$\left.\begin{aligned} n_e &= (5800 + 300\,t)\,L^{-4.5} + \left[1 - e^{(L-2)/10}\right] \qquad 00 \leq t < 06 \text{ MLT}\,, \\ n_e &= (-800 + 1400\,t)\,L^{-4.5} + \left[1 - e^{-(L-2)/10}\right] \qquad 06 \leq t \leq 15 \text{ MLT}\,. \end{aligned}\right\} \tag{2.22}$$

4. The plasmasphere outer limit L_{ppo}, determined by solving simultaneously for the plasmapause segment and the extended plasmatrough.

5. The plasmatrough segment $L_{\text{ppo}} \leq L \leq 8$:

$$n_e = n_e(L_{\text{ppo}}) \times \left(\frac{L}{L_{\text{ppo}}}\right)^{-4.5} + \left[1 - e^{-(L-2)/10}\right]\,. \tag{2.23}$$

The above expressions give the electron density in the equatorial plane. In this study, we only use Eq. (2.20) for the plasmasphere density.

In order to determine the thermal plasma densities at non-equatorial latitudes along magnetic flux tubes, the hydrostatic equations should in principle be integrated as in Angerami & Thomas (1964), or a more complex kinetic (exospheric) model should be used as in Lemaire (1989), Chiu et al. (1978), or Rycroft & Jones (1985, 1987). Even more sophisticated dynamical models are now developed by using Monte Carlo simulation methods (Wilson 1992).

In this study, we used the following procedure. For points beyond the plasmapause, i.e. when the geocentric distance $r > L_{\text{ppi}}$, we set $n_e = n_{H^+} = 10\,\text{cm}^{-3}$ and $T_e = T_{H^+} = 4000\,\text{K}$. The densities of the other ions are neglected and set to zero.

The field-aligned electron density in a point P below the plasmapause, with geodetic coordinates (r, λ, ϕ), is approximated by

$$n_e(r, \lambda, \phi) = n_{\text{CA}}(L)\,e^{-CR_E/r}\,, \tag{2.24}$$

where n_{CA} is the Carpenter & Anderson (1992) equatorial electron density on the dipole field line passing through P. For a centred dipole geomagnetic field model, the corresponding L value is given by

$$LR_E = \frac{r}{\cos^2\lambda_1}\,, \tag{2.25}$$

where λ_1 is the geomagnetic latitude of P. C is determined by the IRI-90 electron density at the point Q on the same field line (and thus with the same geomagnetic

longitude ϕ_1 in the centred dipole model) at altitude 1000 km (the limiting altitude of IRI-90). The geomagnetic latitude of Q is

$$\lambda_m \equiv \arccos\sqrt{\frac{R_E + 1000}{LR_E}}\,. \tag{2.26}$$

Applying the coordinate transformation from geomagnetic to geocentric coordinates yields the geocentric latitude and longitude λ_c, ϕ_c of Q, which are used as input to IRI-90 to determine n_{1000}, the electron density at 1000 km altitude. From Eq. (2.24) it then follows that

$$C = -\left(1 + \frac{1000}{R_E}\right) \ln \frac{n_e(R_E + 1000, \lambda_c, \phi_c)}{n_{CA}(L)}\,. \tag{2.27}$$

In order to determine the ion densities, we assume that the plasmaspheric density of a plasma constituent i can be approximated by using the condition of isothermal diffusive equilibrium, i.e.

$$n_i(r, \lambda, \phi) = n_i(R_E + 1000, \lambda, \phi) \exp\left[-\frac{1}{H_i}\,\frac{(R_E + 1000)(r - R_E - 1000)}{r}\right]\,, \tag{2.28}$$

where $n_i(R_E + 1000, \lambda, \phi)$ is determined with IRI-90 and H_i is a shell height. H_i can be derived from the condition of hydrostatic equilibrium for a plasma consisting of electrons and N ion species in an electric field E:

$$\frac{dp_e}{dr} = -n_e m_e g - n_e e E \tag{2.29}$$

for electrons and

$$\frac{dp_i}{dr} = -n_i m_i g + n_i Z_i e E \tag{2.30}$$

for ion species i, where p is the pressure, m the atomic mass, and Ze the charge of the particles. In the ideal gas approximation $p = nkT$, so that

$$\frac{dn_e}{dr} = -\frac{n_e m_e}{kT_e}\,g - \frac{n_e}{kT_e}\,eE \tag{2.31}$$

and

$$\frac{dn_i}{dr} = -\frac{n_i m_i}{kT_i}\,g + \frac{n_i Z_i}{kT_i}\,eE\,. \tag{2.32}$$

Multiplying both members by Z and summing over electrons and all ions gives

$$-\frac{dn_e}{dr} + \sum_{i=1}^{N} \frac{dn_i}{dr}\,Z_i = \frac{n_e m_e}{kT_e}\,g + \frac{n_e}{kT_e}\,eE - \sum_{i=1}^{N} \frac{n_i m_i Z_i}{kT_i}\,g + \sum_{i=1}^{N} \frac{n_i Z_i^2}{kT_i}\,eE\,. \tag{2.33}$$

Since the plasma is neutral $-n_e + \sum_{i=1}^{N} n_i Z_i = 0$, and consequently the left-hand side of Eq. (2.33) is zero, so that

$$eE = \frac{-\frac{n_e m_e}{T_e} + \sum_{i=1}^{N} \frac{n_i m_i Z_i}{T_i}}{\frac{n_e}{T_e} + \sum_{i=1}^{N} \frac{n_i Z_i^2}{T_i}} g \,. \tag{2.34}$$

Substituting in Eq. (2.32) and dividing both sides by n_i yields

$$-\frac{d \ln n_i}{dr} = \frac{1}{H_i} = \left(m_i - Z_i \frac{-\frac{n_e m_e}{T_e} + \sum_{j=1}^{N} \frac{n_j m_j Z_j}{T_j}}{\frac{n_e}{T_e} + \sum_{j=1}^{N} \frac{n_j Z_j^2}{T_j}} \right) \frac{g}{kT_i} \,. \tag{2.35}$$

The electron and ion temperatures are provided by IRI-90. The ion temperature is the same for each species. With Eqs. (2.28) and (2.35) the plasmaspheric density for four of the ion species in IRI-90 (O^+, He^+, O_2^+, NO^+) can be determined. The H^+ density is obtained as

$$n_{H^+} = n_e - (n_{O^+} + n_{He^+} + n_{O_2^+} + n_{NO^+}) \,, \tag{2.36}$$

in order to ensure the neutrality of the plasma. However, this approach causes a problem for the He^+ density, which has a negative scale height at 1000 km (i.e. the density is still rising). Therefore, we make one more approximation in that we artificially keep the ratio of the He^+ to the H^+ densities constant at its value at 1000 km. Equation (2.36) then becomes

$$n_{H^+} = \frac{n_e - (n_{O^+} + n_{O_2^+} + n_{NO^+})}{1 + \frac{n_{He^+1000}}{n_{H^+1000}}} \,. \tag{2.37}$$

The He^+ density is then obtained as

$$n_{He^+} = \frac{n_{He^+1000}}{n_{H^+1000}} n_{H^+} \,. \tag{2.38}$$

The Rycroft-Jones model

Rycroft & Jones (1985, 1987) have developed a plasmaspheric extension for the IRI electron density model. Their diffusive equilibrium model describes the field-aligned distribution of plasma out to $L = 6$. A merging procedure with the IRI topside profile is suggested at a reference level near 650 km. This plasmaspheric extension is not yet included in IRI-90 and will not be used here.

2.4.3 Software implementation

The input parameters for the main subroutine IRIS12.FOR in IRI-90 are geodetic or geomagnetic latitude and longitude, geodetic altitude, Zürich sunspot number (twelve-month running mean), day of year, local or universal time, and a series of logical variables. The output consists of: electron density, normalised electron density (to F2 peak density), neutral temperature (CIRA-86), electron and ion temperature, electron to ion temperature ratio, and relative percentage densities of O^+, H^+, He^+, NO^+, and O_2^+. The altitude limits are given in Table 4.

The plasmaspheric extension of the electron and ion densities, described in Sect. 2.4.2, has been implemented in a subroutine called DCA.FOR. This subroutine takes one input parameter, KPMAX, corresponding to the maximum K_p over the preceding day. This parameter was added to the NAMELIST ATMOS (see Table 2).

2.4.4 Distribution of ionospheric and plasmaspheric densities

Figure 24 shows the electron and ion density profiles between 100 and 10 000 km in the heart of the SAA, for the summer solstice and local midnight, in the case of low solar activity (i.e. $R_Z = 50$ and $K_{p_{max}} = 1$). Figure 25 contains the corresponding graph for high solar activity (i.e. $R_Z = 250$ and $K_{p_{max}} = 6$). Figures 24 and 25 are repeated in Figs. 26–27 for local noon. These four figures are repeated in Figs. 28–31 for the winter solstice.

The transition from local midnight to local noon leads to changes in the number densities of a factor ten and more at low altitudes. The seasonal changes are smaller, but still important. The main effect of raising R_Z and $K_{p_{max}}$ is the appearance of a discontinuity in the density profile near 10 000 km.

2.5 Calculation of atmospheric cross sections

The collisional cross section of trapped particles interacting with the neutral atmosphere and the ionosphere serves as a measure for the relative scattering efficiency of the various constituents and processes involved.

In this section, the different collision processes relevant for electrons and protons impacting on atmospheric constituents are discussed. The main processes to consider are: excitation and ionization of the target, dissociation for target molecules, charge exchange for protons on atoms and Coulomb interaction for charged particles. The relative importance of the different processes depends on the type of particles and the energy range. For each interaction, analytic expressions for the collision cross

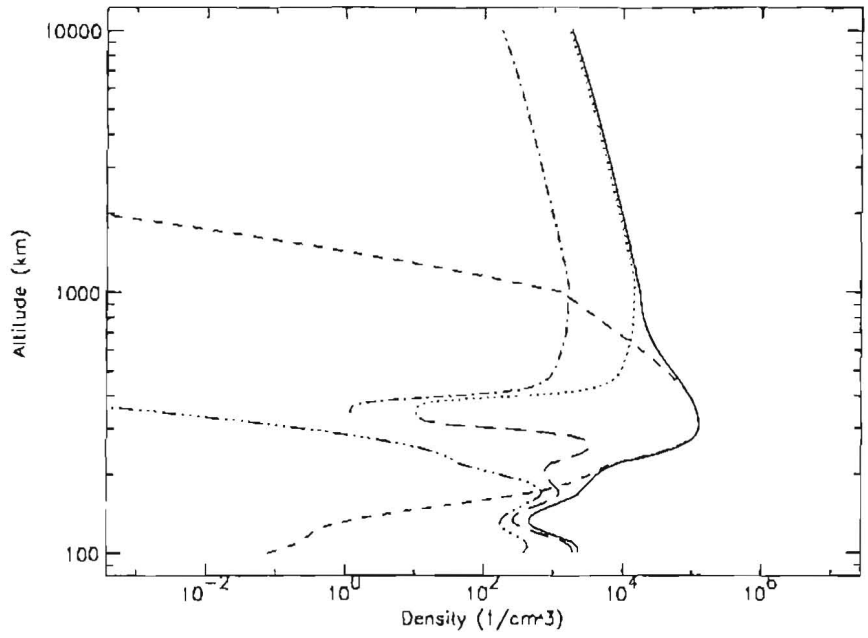

Figure 24. Electron and ion number density profiles obtained with IRI-90 and the plasmasphere extension in the SAA for the summer solstice, midnight L.T., with $R_Z = 50$ and $K_{p_{max}} = 1$. The line styles represent the constituents as: solid: electrons, short-dashed: O^+, dotted: H^+, dot-dashed: He^+, triple-dot-dashed: O_2^+, long-dashed: NO^+.

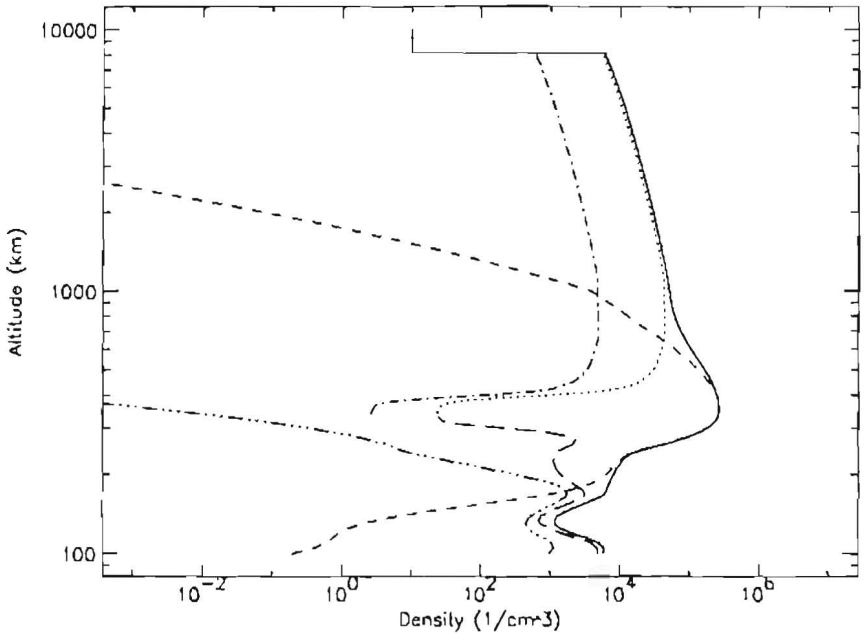

Figure 25. Electron and ion number density profiles obtained with IRI-90 and the plasmasphere extension in the SAA for the summer solstice, midnight L.T., with $R_Z = 250$ and $K_{p_{max}} = 6$. The line styles have the same meaning as in Fig. 24.

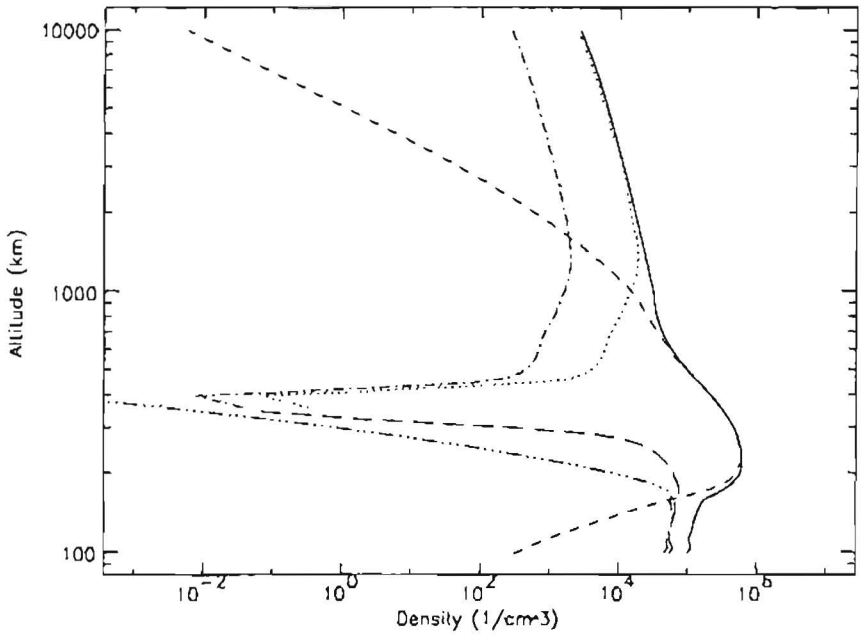

Figure 26. Electron and ion number density profiles obtained with IRI-90 and the plasmasphere extension in the SAA for the summer solstice, noon L.T., with $R_Z = 50$ and $K_{p_{max}} = 1$. The line styles have the same meaning as in Fig. 24.

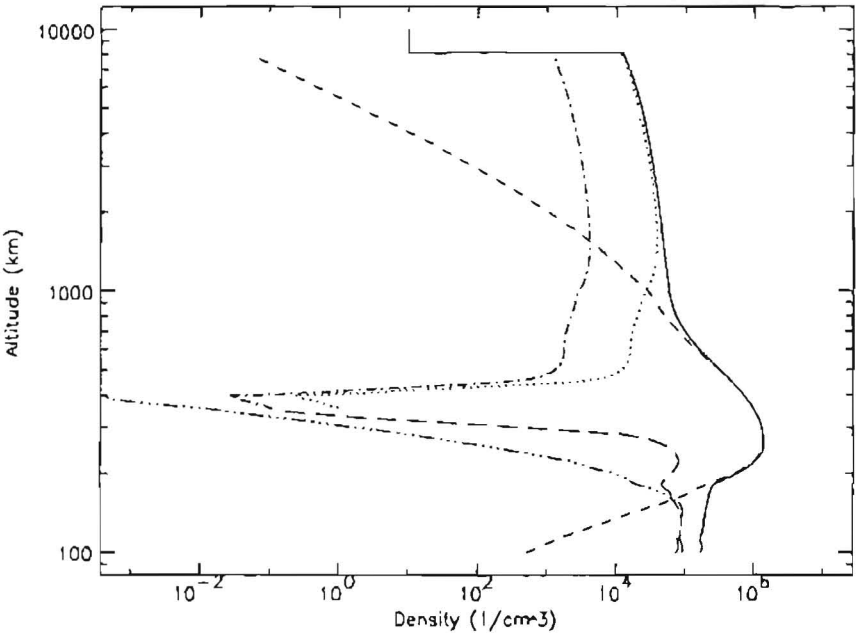

Figure 27. Electron and ion number density profiles obtained with IRI-90 and the plasmasphere extension in the SAA for the summer solstice, noon L.T., with $R_Z = 250$ and $K_{p_{max}} = 6$. The line styles have the same meaning as in Fig. 24.

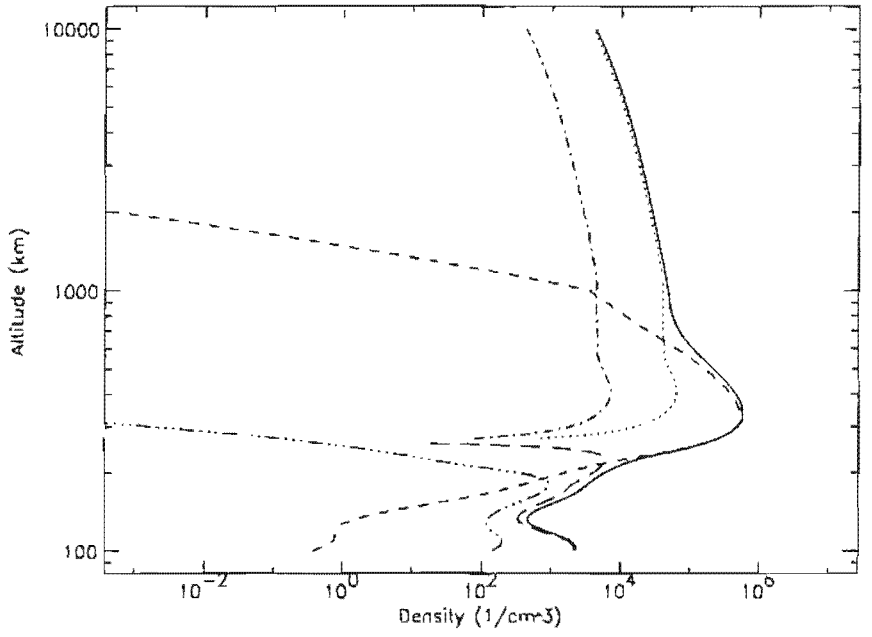

Figure 28. Electron and ion number density profiles obtained with IRI-90 and the plasmasphere extension in the SAA for the winter solstice, midnight L.T., with $R_Z = 50$ and $K_{p_{max}} = 1$. The line styles have the same meaning as in Fig. 24.

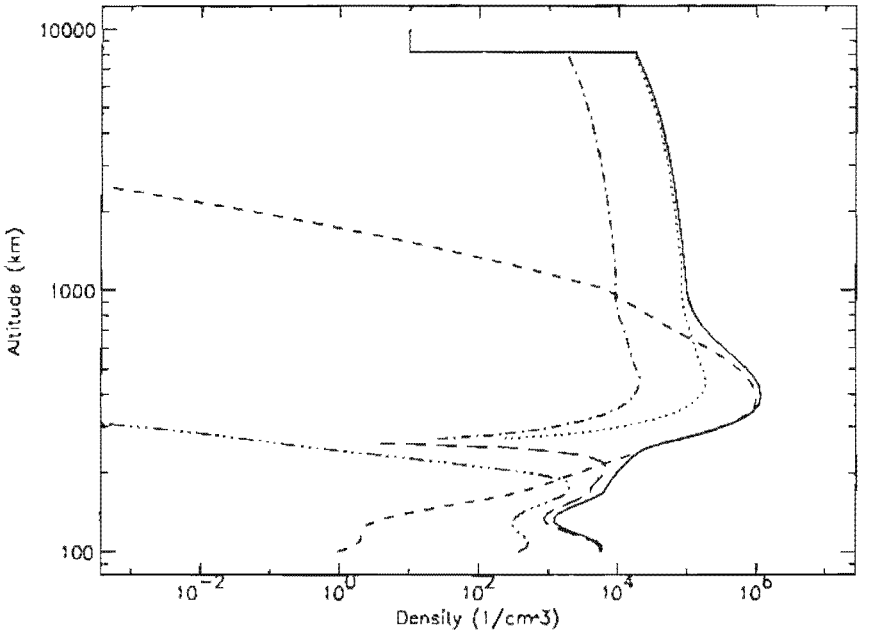

Figure 29. Electron and ion number density profiles obtained with IRI-90 and the plasmasphere extension in the SAA for the winter solstice, midnight L.T., with $R_Z = 250$ and $K_{p_{max}} = 6$. The line styles have the same meaning as in Fig. 24.

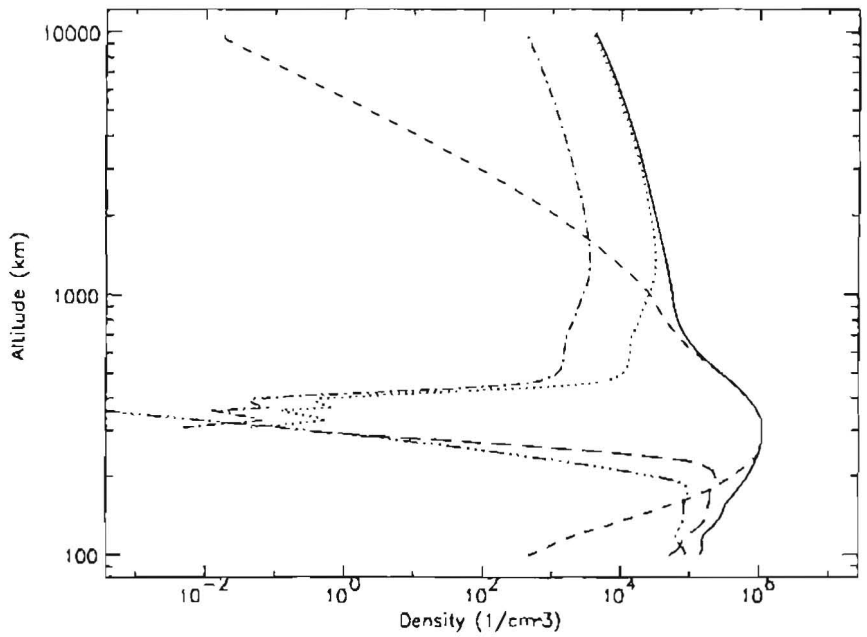

Figure 30. Electron and ion number density profiles obtained with IRI-90 and the plasmasphere extension in the SAA for the winter solstice, noon L.T., with $R_Z = 50$ and $K_{p_{max}} = 1$. The line styles have the same meaning as in Fig. 24.

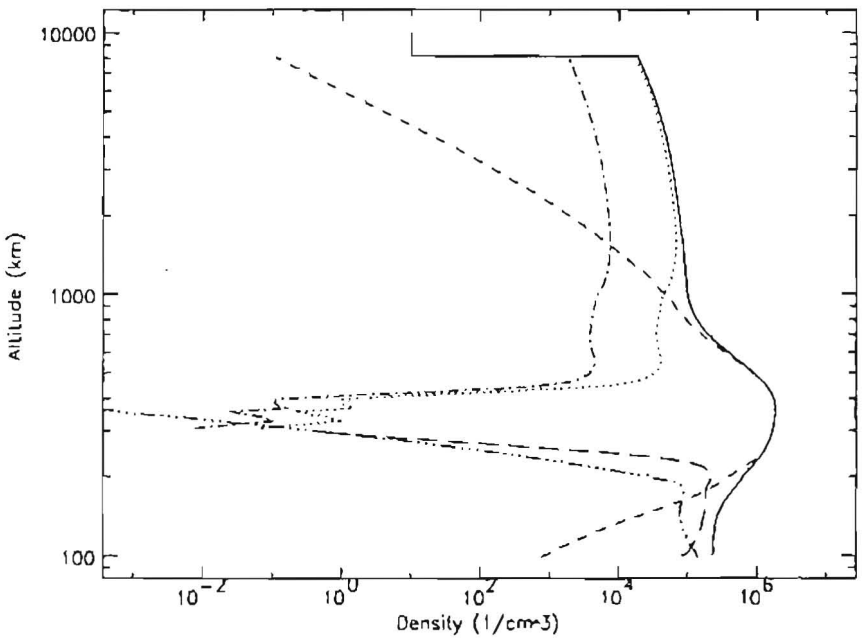

Figure 31. Electron and ion number density profiles obtained with IRI-90 and the plasmasphere extension in the SAA for the winter solstice, noon L.T., with $R_Z = 250$ and $K_{p_{max}} = 6$. The line styles have the same meaning as in Fig. 24.

section as a function of the kinetic energy of the incident particle have been derived in the literature. The expressions have been implemented in a computer program, CROSS, that takes as input the kinetic energy of the incident particle, the type of particle, both incident and target, and returns the total cross section for all relevant collision processes.

2.5.1 Definitions

Consider a target consisting of particles of a given kind, randomly distributed within a layer of infinitesimal thickness δx, with a mean density of n particles per unit volume. Consider a large flux $N(E)$ of particles of the same or of a different kind impinging perpendiculary upon this layer with kinetic energy E. We can assume that the product $n\delta x$ is so small that only a minute fraction of the incident particles undergoes a collision in the layer. Then $\delta N(E)$, the total number of particles that collide per unit of time on a unit surface is proportional to $N(E)$, δx, and n (Rossi & Olbert 1981):

$$\delta N = -N\sigma(E)\, n\, \delta x, \tag{2.39}$$

The proportionality factor $\sigma(E)$ is called the *cross section* for collision between the two kinds of particles. σ has the dimensions of an area.

Now, consider a target of finite thickness dx. As Eq. (2.39) holds for all the infinitesimal layers into which the finite layer can be subdivided, it may be written as a differential equation:

$$-\frac{dN(E)}{N(E)} = \sigma(E)\, n\, dx. \tag{2.40}$$

In the case of the atmosphere, n is not constant but depends on altitude. Integration yields

$$N(E,x) = N_0(E,x_0)\, \exp\left[-\sigma(E)\int_{x_0}^{x} n(x')\, dx'\right], \tag{2.41}$$

where $N_0(E,x_0)$ is the number of incident particles and $N(x)$ the number of particles that have escaped collisions while travelling a distance $x - x_0$. The quantity

$$\lambda_1 \equiv \frac{1}{\sigma(E)n} \tag{2.42}$$

has the dimensions of a length and is called the *mean free path*. It corresponds to the mean distance covered by the particles before they undergo their first collision.

Hassitt's (1964) software does not take into account the dependence of the cross section on the kinetic energy of the incident particles. The program CROSS, described below, determines the total cross sections as a function of energy, for collisions

between high energy electrons or protons and the main atmospheric constituents. The type of incident particle (electron or proton), the target particles (i.e. H, He, O, N, O_2, N_2, H_2 and their ions) and the kinetic energy of the incident particle (in eV) are given as inputs. The program computes the cross section in mbarns (1 mbarn=10^{-27} cm^2) and is based on analytical functions described in the following sections.

2.5.2 Electrons as incident particles

For high energy electrons ($E > 200$ eV) the major interactions are ionizing collisions with atoms and molecules. Excitation is also an important collisional process. When electrons collide with ions, ionization is important for high energy but elastic Coulomb interaction prevails for energies lower than 500 eV.

Elastic collisions of electrons with neutral particles

If the energy of the incident electron is lower than the energy threshold of the first excitation level, the collision is necessarily elastic. Elastic collisons result mainly in very small deflections and very small fractional losses of energy. The excitation level is of the order of 10 eV, i.e. a very low energy. Nevertheless, the elastic cross section remains important up to 500 eV. Since we are interested in much higher energies, we will neglect the elastic cross section. Thus, the program CROSS only gives cross sections for energies above 500 eV.

Inelastic collisions of electrons with neutral particles

For inelastic collisions, the Bethe-Born approximation (Bethe 1930) is taken as the starting point. This theory, which is valid for energies higher than 500 eV, leads to analytic expressions for the excitation and ionization cross sections as a function of the incident kinetic energy and adjustable parameters (Green & Barth 1965). These functions can be fitted to experimental data to determine the free parameters. The resulting function can be used above the energies of the experimental data.

Excitation of the target by electrons In the framework of the Bethe-Born semi-analytical approximation (Green & Dutta 1967), the electron collision cross section for the excitation of atmospheric gases is given by the equation:

$$\sigma(E) = \frac{q_0 c_0 f_0}{W^2} \left[1 - \left(\frac{W}{E}\right)^{\gamma}\right]^{\nu} \left(\frac{W}{E}\right)^{\Omega}, \qquad (2.43)$$

where $q_0 = 6.51 \times 10^{-14}\,\mathrm{eV^2\,cm^2}$ and W is the threshold energy for a particular excitation state measured in eV. The free parameters $c_0 f_0$, γ, ν and Ω can be adjusted to fit the experimental data. Their values are given in Table 5 for the main excitation states of N_2, O_2, O (Banks & Kockarts 1973), and He (Jusick et al. 1967). To obtain the total excitation cross section, the program computes the sum over all possible excitation states. Equation (2.43) has been found to represent accurately a large number of experimental data.

Ionization of the target by electrons For the ionization cross section, one has to consider the integral

$$\sigma(E) = \int_I^{(E+I)/2} \frac{d\sigma}{dW}\, dW\,, \tag{2.44}$$

where I is the ionization threshold for a particular target state. The same analytic form is used for σ as for discrete transitions [Eq. (2.43)], but $c_0 f_0$ is replaced by $c_0 f_0\,(I/W)^p$ (Jusick et al. 1967).

$$\sigma(E) = \int_I^{(E+I)/2} \frac{q_0 c_0 f_0}{W^2} \left(\frac{I}{W}\right)^p \left[1 - \left(\frac{W}{E}\right)^\gamma\right]^\nu \left(\frac{W}{E}\right)^\Omega dW\,, \tag{2.45}$$

where $c_0 f_0$, p, γ, ν and Ω are parameters obtained from the best fit of this analytic function to experimental results. Table 5 lists values of the parameters for impact ionization of N_2, O_2, O (Banks & Kockarts 1973), and He (Jusick et al. 1967). For molecules, the different dissociation states are considered as well. The ionization and dissociation states need to be added to obtain the total ionization cross section.

Figure 32 shows an example of the excitation and ionization cross sections as a function of the kinetic energy of impacting electrons on O_2. The two curves have similar shapes and have a maximum around 100 eV. For $E > 100\,\mathrm{eV}$, $\sigma(E)$ decreases as the electron energy increases and the ionization cross section is always greater than the excitation cross section.

For ionization of H, Lotz (1966) proposes an analytic function based on Bethe (1930). For high energy, the Lotz cross section has a functional dependence of the form

$$\sigma(E) = \xi\, a\, \frac{\ln(E/I_\mathrm{H})}{I_\mathrm{H} E}\,, \tag{2.46}$$

where $a = 4.0 \times 10^{-14}$ is a constant, $I_\mathrm{H} = 13.6\,\mathrm{eV}$ is the H ionization potential, and ξ is a free parameter called the effective number ($\xi = 1$ for H).

Electron-ion collisions

Ionization of ions by electrons The Lotz analytic function can be adapted to compute the ionization cross section of different atoms and ions. To describe the

Table 5. Values of the free parameters in Eq. (2.43) (excitation) and Eq. (2.45) (ionization and dissociation) for the inelastic collision cross section between electrons and atmospheric constituents. W is the threshold energy (in eV) for each excitation level and I is the ionization energy (in eV) for different molecules and atoms found in the Earth's atmosphere (Banks & Kockarts 1973, Jusick et al. 1967).

Gas	Final state	W or I (eV)	$c_0 f_0$	Ω	ν	γ	p
N_2	$A^3\Sigma_u^+$	6.14	0.226	3.0	1.0	1.0	
N_2	$B^3\Pi_g$	7.30	0.178	3.0	1.0	3.0	
N_2	$C^3\Pi_u$	11.03	0.28	3.0	1.0	3.0	
N_2	$a^1\Pi_g$	9.10	0.136	1.0	1.0	1.0	
N_2	$b^1\Pi_u$	12.85	0.67	0.75	3.0	1.0	
N_2	$b'^1\Sigma_u^+$	14.0	0.33	0.75	3.0	1.0	
N_2	$\Sigma_{Rydberg}$	13.75	2.66	0.75	3.0	1.0	
N_2	$N_2^+(X^2\Sigma_g^+)$	15.58	0.370	0.80	3.0	1.0	1.2
N_2	$N_2^+(A^2\Pi_u)$	16.73	0.160	0.83	1.0	1.0	1.2
N_2	$N_2^+(B^2\Sigma_u^+)$	18.75	0.073	0.83	2.0	1.0	1.2
N_2	$N_2^+(D^2\Pi_g)$	22.0	0.056	0.83	2.0	1.0	1.2
N_2	$N_2^+(C^2\Sigma_u^+)$	23.6	0.60	0.83	2.0	1.0	1.2
N_2	Dissociative	25.0	0.380	0.96	2.0	1.0	1.2
O_2	$a^1\Delta_g$	0.98	0.0005	3.0	1.0	3.0	
O_2	$b^1\Sigma_g$	1.64	0.0005	3.0	1.0	3.0	
O_2	$A^3\Sigma_u^+$	4.5	0.021	0.9	1.0	3.0	
O_2	$B^3\Sigma_u^-$	8.4	0.23	0.75	2.0	1.0	
O_2	9.9 eV allowed	9.9	0.08	0.75	3.0	1.0	
O_2	$\Sigma_{Rydberg}$	13.5	2.77	0.75	3.0	1.0	
O_2	$O_2^+(X^2\Pi_g)$	12.1	0.058	0.80	2.0	1.0	1.1
O_2	$O_2^+(a^4\Pi_u)$	16.1	0.150	0.80	2.0	1.0	1.1
O_2	$O_2^+(A^2\Pi_u)$	16.9	0.150	0.80	2.0	1.0	1.1
O_2	$O_2^+(b^4\Sigma_g^-)$	18.2	0.130	0.80	2.0	1.0	1.1
O_2	$O_2^+(B)$	23.0	0.064	0.80	2.0	1.0	1.1
O_2	Dissociative $O^+(^4S)$	18.0	0.400	0.93	3.0	1.0	1.1
O_2	Dissociative $O^+(^2D)$	22.0	0.250	0.93	3.0	1.0	1.1
O	^1D	1.96	0.01	1.0	2.0	1.0	
O	^1S	4.17	0.0042	1.0	1.0	0.5	
O	^3S	9.53	0.0465	0.75	3.0	1.0	
O	^5S	9.15	0.023	2.0	1.0	1.0	
O	$\Sigma(\delta l = 1, \delta s = 0)$	14.2	0.367	0.75	3.0	1.0	
O	$\Sigma(\delta s = 1)$	14.7	0.694	2.0	1.0	1.0	
O	$\Sigma(\delta l = 0, \delta s = 0)$	13.5	0.043	0.75	1.0	2.0	
O	$O^+(^4S)$	13.6	0.290	0.85	1.0	0.3	1.2
O	$O^+(^2D)$	16.9	0.360	0.85	1.0	0.3	1.2
O	$O^+(^2P)$	18.5	0.190	0.85	1.0	0.3	1.2

Table 5. (continued)

Gas	Final state	W or I (eV)	$c_0 f_0$	Ω	ν	γ	p
He	He(2^1P)	21.17	0.338	0.7	2.5	1.0	
He	He(3^1P)	23.08	0.1	0.7	2.5	1.0	
He	He(4^1P)	23.75	0.042	0.7	2.5	1.0	
He	He(3^1S)	22.93	0.0054	0.7	0.5	1.0	
He	He(4^1S)	23.68	0.0022	0.7	0.5	1.0	
He	He(5^1S)	24.02	0.0011	0.7	0.5	1.0	
He	He(6^1S)	24.20	0.0006	1.0	0.5	1.0	
He	He(3^1D)	23.08	0.0067	1.0	1.0	1.0	
He	He(4^1D)	23.75	0.0028	1.0	1.0	1.0	
He	He(5^1D)	24.05	0.0014	1.0	1.0	1.0	
He	He(6^1D)	24.22	0.0008	2.0	1.0	1.0	
He	He(3^2P)	22.93	0.030	2.0	1.0	1.0	
He	He(3^3S)	22.63	0.0294	2.0	1.0	1.0	
He	He(4^3S)	23.57	0.0112	2.0	1.0	1.0	
He	He(5^1S)	23.97	0.0054	2.0	1.0	1.0	
He	He(3^3D)	23.00	0.010	2.0	1.0	1.0	
He	He(3^3D)	23.71	0.0041	2.0	1.0	1.0	
He	He(3^3D)	24.04	0.0021	2.0	1.0	1.0	
He	He(3^3D)	24.21	0.0012	2.0	1.0	1.0	
He	He^+	24.6	0.140	0.75	1.0	1.0	1.5

ionization of ions by impacting electrons, the Lotz function becomes

$$\sigma(E) = \xi a \frac{\ln(E/\bar{I})}{\bar{I}E} . \tag{2.47}$$

For large E, the electrons of the next inner sub-shell also contribute appreciably to the cross section. $\bar{I}$ is a weighted mean of I_1, the ionization potential for outer shell electrons, and I_2, the ionization potential for electrons of the next inner sub-shell[1]. The values of ξ and $\bar{I}$ are given in Table 6 (Lotz 1966) for He, C, N, O, Ne atoms and ions in different states of ionization.

[1]For elements with higher Z-number (for intance Kr or Xe), a third sub-shell gives a better approximation.

Table 6. Values of the ionization potential $\overline{I}$ (in eV) and of the effective number $\overline{\xi}$, to be used in Eq. (2.47) to obtain the ionization cross section for collisions between energetic electrons and different atmospheric atoms and ions (Lotz 1966)

Species	Ionization state	$\overline{I}$ (eV)	$\overline{\xi}$
H	H^+	13.6	1.0
He^+	He^{2+}	54.4	1.1
C^+	C^{2+}	28.2	3.0
C^{2+}	C^{3+}	61.3	2.9
C^{3+}	C^{4+}	102	2.2
C^{4+}	C^{5+}	392	2.0
C^{5+}	C^{6+}	490	1.0
N^+	N^{2+}	32.6	4.1
N^{2+}	N^{3+}	52.5	3.0
N^{3+}	N^{4+}	100	3.0
N^{4+}	N^{5+}	155	2.2
N^{5+}	N^{6+}	552	2.0
N^{6+}	N^{7+}	667	1.0
O^+	O^{2+}	37.6	5.0
O^{2+}	O^{3+}	58.8	4.0
O^{3+}	O^{4+}	83.7	3.0
O^{4+}	O^{5+}	148	3.1
O^{5+}	O^{6+}	219	2.2
O^{6+}	O^{7+}	739	2.0
O^{7+}	O^{8+}	871	1.0
Ne^+	Ne^{2+}	45.2	5.5
Ne^{2+}	Ne^{3+}	68.9	6.0
Ne^{3+}	Ne^{4+}	101	5.0
Ne^{4+}	Ne^{5+}	132	4.0
Ne^{5+}	Ne^{6+}	167	3.0
Ne^{6+}	Ne^{7+}	270	3.1
Ne^{7+}	Ne^{8+}	380	2.3
Ne^{8+}	Ne^{9+}	1186	2.0
Ne^{9+}	Ne^{10+}	1362	1.0

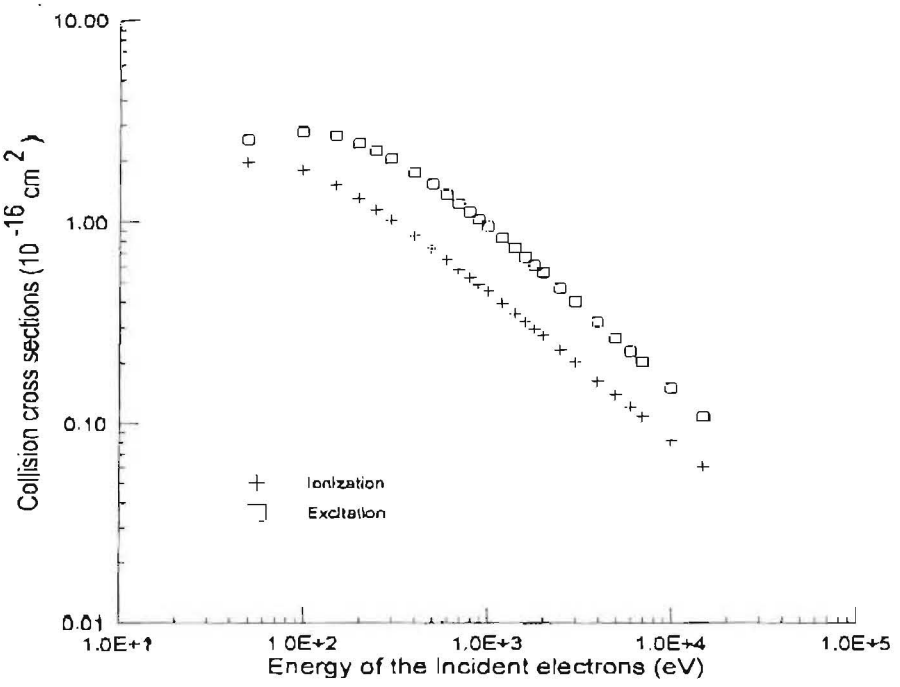

Figure 32. Ionization (taking into account dissociation) and excitation (taking into account atom production dissociation) cross sections computed by the computer code CROSS for collisions between energetic electrons and O_2. Both cross sections reach a maximum ($3 \times 10^{-16}\,\mathrm{cm}^2$) around 100 eV and decrease with the kinetic energy of the electron.

Coulomb interaction The force between charged particles obeys the Coulomb law

$$F_{12} = \frac{1}{4\pi\epsilon_0}\frac{Z_1 Z_2 e^2}{r^2}\,, \tag{2.48}$$

where Z_j is the charge state of each particle ($Z_1 = -1$ for electrons), e the electric charge of the electron, r the distance between both charges, and ϵ_0 the permittivity of vacuum ($\epsilon_0 = 8.854 \times 10^{-12}\,\mathrm{F\,m^{-1}}$). As the cross section diverges for small scattering angles as a result of the infinite range of the Coulomb force, a minimum scattering angle has to be chosen consistent with the concept of the plasma Debye length:

$$\lambda_D = \left(\sum_j \frac{n_j |Z_j| e^2}{\epsilon_0 k T_j}\right)^{-1/2}\,, \tag{2.49}$$

where the densities n_j are taken into account. The summation is taken over all particle species present, including electrons. The Coulomb interaction leads to the Coulomb cross section which is very important at low energy (Banks & Kockarts

1973):

$$\sigma(E) = \frac{2\pi}{(4\pi\epsilon_0)^2}\left[\frac{m_1+m_2}{m_1 m_2}\frac{Z_1 Z_2 e^2}{g^2}\right]^2 \ln\Lambda\,, \tag{2.50}$$

where m_i is the rest mass of the particles and g is their relative speed. Λ is defined as a function of λ_D:

$$\Lambda = 4\pi\epsilon_0 \frac{m_1 m_2}{m_1+m_2} g^2 \frac{1}{|Z_1 Z_2| e^2}\lambda_D\,. \tag{2.51}$$

When the energy of the incident particle is much larger than the energy of the atmospheric target particle (but not relativistic), $E = m_1 g^2/2$ and

$$\sigma(E) = 3.25\times 10^{-14}\left[\frac{m_1+m_2}{m_2}\frac{Z_1 Z_2}{E}\right]^2 \ln\Lambda\,\mathrm{cm}^2\,, \tag{2.52}$$

where E is given in eV. Since the mass of the electron is very small compared to the mass of any ion, we can neglect it, in which case Eq. (2.52) becomes:

$$\sigma(E) = 3.25\times 10^{-14}\left(\frac{Z_1 Z_2}{E}\right)^2 \ln\Lambda\,\mathrm{cm}^2\,. \tag{2.53}$$

Coulomb collisions are very important at low energies. Below 100 eV, the ion cross section is much greater than the cross section of the corresponding neutral atom. At higher energies, the Coulomb interaction becomes less important since it decreases as E^{-2}.

The program CROSS gives the total cross section for the main ions of the atmosphere, i.e. He^+, C^+, N^+, O^+, Ne^+, O_2^+, N_2^+, and for other ionization states of these constituents.

2.5.3 Protons as incident particles

Two important processes must be considered for the collisions between energetic protons and neutral particles: charge exchange, which prevails below 100 keV, and electron production, which is important for higher energies. Coulomb interaction is a very important process. For collisions with ions, the ionization cross section prevails. At high energy, the ionization cross section by protons is equal to the electron ionization cross section at the same kinetic velocity.

Electron production by protons impacting on atoms and molecules

When a proton with kinetic energy E_p encounters an atom or a molecule, one or more electrons can be emitted. The equation used to fit the ionization and dissociation with the electron production cross section for the whole energy range is a simple

Table 7. Values of the free parameters in Eq. (2.54) for the electron production cross section for collisions between energetic protons and different atoms and molecules of the Earth's atmosphere (Rudd et al. 1985)

Target	A	B	C	D	Reliability[a] Low E	Near max	High E
H	0.28	1.15	0.44	0.907	*c*	*b*	*a*
He	0.49	0.62	0.13	1.52	*c*	*b*	*a*
Ne	1.63	0.73	0.31	1.14	*c*	*b*	*a*
Ar	3.85	1.98	1.89	0.89	*c*	*c*	*b*
Kr	5.67	5.50	2.42	0.65	*c*	*c*	*b*
Xe	7.33	11.1	4.12	0.41	*c*	*b*	*b*
H_2	0.71	1.63	0.51	1.24	*c*	*b*	*b*
N_2	3.82	2.78	1.80	0.70	*b*	*b*	*a*
O_2	4.77	0.00	1.76	0.93	*c*	*c*	*a*
CO	3.67	2.79	2.08	1.05	*b*	*b*	*a*
CO_2	6.55	0.00	3.74	1.16	*b*	*b*	*a*
NH_3	4.01	0.00	1.73	1.02	*c*	*b*	*b*
CH_4	4.55	2.07	2.54	1.08	*c*	*c*	*b*

[a] *a*: < 10 %. *b*: 10–25 %. *c*: > 25 %.

combination of the cross sections appropriate for the high and low energy regions (Rudd et al. 1985):

$$\sigma(E_\mathrm{p}) = 4\pi a_0^2 \left[\frac{U}{A\ln(1+U)+B} + \frac{1}{CU^D}\right]^{-1}, \tag{2.54}$$

where $U = E/I_\mathrm{H}$, $E = E_\mathrm{p}/1836$, and $a_0 = 0.529 \times 10^{-8}\,\mathrm{cm}$. A, B, C and D are free parameters. Their values are given in Table 7 (taken from Rudd et al. 1985) for 13 elements present in the Earth's atmosphere: H, He, Ne, Ar, Kr, Xe, H_2, N_2, O_2, CO, CO_2, NH_3, CH_4.

Equation (2.54) has a correct behaviour at low energy where a power-law is a good fit to the experimental results:

$$\sigma(E_\mathrm{p}) = 4\pi a_0^2 C U^D . \tag{2.55}$$

At high energy, $\sigma(E_\mathrm{p})$ is assumed to have the energy dependence predicted by the Bethe approximation:

$$\sigma(E_\mathrm{p}) = 4\pi a_0^2 \frac{A\ln(1+U)+B}{U} . \tag{2.56}$$

At high energy, $\sigma(E_\mathrm{p})$ becomes proportional to $\ln U/U$.

Bethe's treatment shows that for protons the cross sections should be exactly the same as for electrons in the asymptotic energy region, provided that the comparison

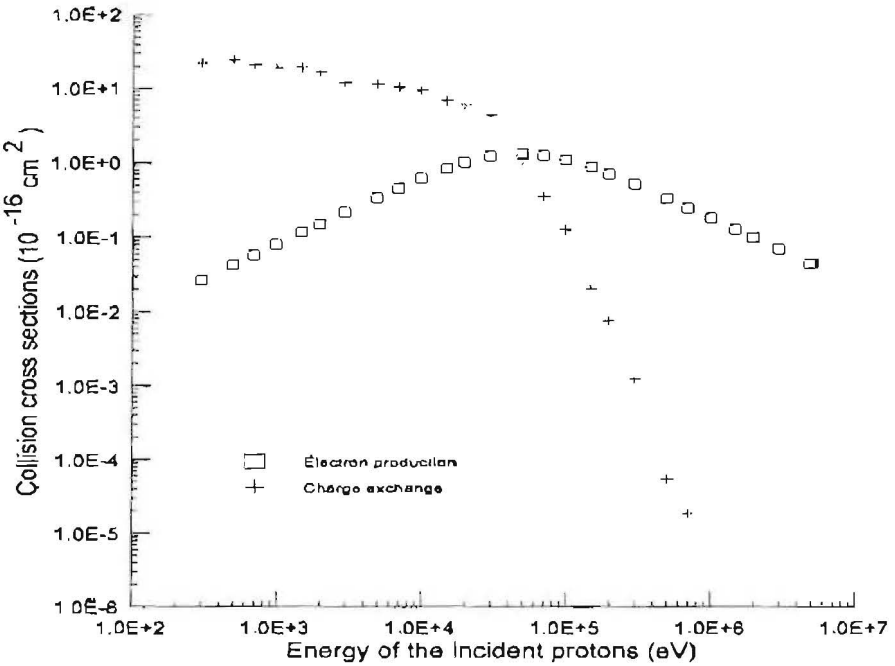

Figure 33. Charge exchange and electron production cross sections for collisions between protons and H. Charge transfer prevails up to around 100 keV but quickly becomes negligible for higher energy in comparison with ionization.

is made at the same velocity. Both cases can be compared by defining $E = m_e v^2/2 = m_p v^2/2/1836 = E_p/1836$ where the indices "e" and "p" represent the electron and the proton, respectively. For N and O, which are not presented in Table 7, we can evaluate the cross section at high energy ($E_p > 500$ keV) by taking into account that the proton and electron cross sections are the same for equal incident velocities. The program then uses the simple analytic function given by Lotz [Eq. (2.47)] with the appropriate parameters.

Charge exchange between protons and neutral atoms

The charge exchange process is characterized by a transfer of an electric charge between two particles, where each retains its original kinetic energy. In general, calculating the charge exchange cross section is very difficult. It is preferable to resort to experimental results since analytical functions are not available for the whole energy range and for all types of particles.

For H, a resonance effect appears because the proton is the parent ion of H. The computer code uses the complete set of measurements collected since 1958 by Tawara et al. (1985) for collisions between protons and H (atomic H and molecular H_2) (cf.

Table 8. Values of measured charge exchange cross sections between energetic protons and atomic and molecular H (Tawara et al. 1985)

Electron Capture in Collisions with Atomic Hydrogen

$H^+ + H \rightarrow H$					$H^+ + H \rightarrow H$ (cont.)				
E(eV/amu)	ϕ(cm^2)	Error	Author	Year	E(eV/amu)	ϕ(cm^2)	Error	Author	Year
1.70E-01	5.94E-15	1.66E-15	Newman	(1982)	1.80E+03	1.70E-15	2.50E-16	Fite	(1960)
5.19E-01	4.87E-15	9.10E-16	"		1.92E+03	1.33E-15	6.70E-17	McClure	(1966)
1.02E+00	4.62E-15	7.70E-16	"		1.95E+03	1.70E-15		Fite	(1962)
1.28E+00	4.42E-15	6.60E-16	"		2.01E+03	1.73E-15		Fite	(1958)
1.99E+00	4.09E-15	7.40E-16	"		2.41E+03	1.36E-15	6.80E-17	McClure	(1966)
3.10E+00	5.60E-15	7.00E-16	Belyaev	(1967)	2.50E+03	1.59E-15		Fite	(1958)
3.37E+00	3.71E-15	5.60E-16	Newman	(1982)	3.00E+03	1.20E-15	1.80E-16	Bayfield	(1969)
4.13E+00	3.50E-15	4.30E-16	"		3.03E+03	1.50E-15		Fite	(1958)
5.00E+00	5.10E-15	6.00E-16	Belyaev	(1967)	3.04E+03	1.21E-15	6.10E-17	McClure	(1966)
5.50E+00	5.50E-15	6.00E-16	"		3.50E+03	1.20E-15	1.80E-16	Bayfield	(1969)
5.68E+00	3.67E-15	5.80E-16	Newman	(1982)	3.60E+03	1.45E-15		Fite	(1958)
9.00E+00	4.70E-15	7.00E-16	Belyaev	(1967)	3.60E+03	1.40E-15	2.00E-16	Fite	(1960)
9.51E+00	3.91E-15	6.10E-16	Newman	(1982)	3.82E+03	1.11E-15	5.60E-17	McClure	(1966)
9.68E+00	3.70E-15	5.70E-16	"		4.00E+03	1.20E-15	1.80E-16	Bayfield	(1969)
1.00E+01	5.00E-15	4.00E-16	Belyaev	(1967)	4.00E+03	1.43E-15		Fite	(1958)
1.50E+01	4.60E-15	4.00E-16	"		4.50E+03	1.25E-15	1.90E-16	Bayfield	(1969)
1.90E+01	4.30E-15	4.00E-16	Fite	(1962)	4.80E+03	1.05E-15	5.30E-17	McClure	(1966)
2.00E+01	4.80E-15	4.00E-16	Belyaev	(1967)	5.00E+03	1.15E-15	1.70E-16	Bayfield	(1969)
2.20E+01	3.60E-15	3.00E-16	Fite	(1962)	5.50E+03	1.00E-15	1.50E-16	"	
2.21E+01	3.28E-15	4.80E-16	Newman	(1982)	5.78E+03	1.27E-15		Fite	(1958)
2.30E+01	4.00E-15		Fite	(1962)	6.00E+03	1.05E-15	1.60E-16	Bayfield	(1969)
2.48E+01	2.91E-15	4.10E-16	Newman	(1982)	6.05E+03	9.85E-16	4.90E-17	McClure	(1966)
2.50E+01	4.40E-15	4.00E-16	Belyaev	(1967)	7.00E+03	1.01E-15	1.50E-16	Bayfield	(1969)
3.00E+01	3.60E-15	3.00E-16	Fite	(1962)	7.00E+03	1.05E-15	1.50E-16	Fite	(1960)
3.00E+01	4.20E-15	3.60E-16	Belyaev	(1967)	7.06E+03	1.22E-15		Fite	(1958)
3.05E+01	3.24E-15	5.70E-16	Newman	(1982)	7.62E+03	8.80E-16	4.40E-17	McClure	(1966)
3.60E+01	3.60E-15		Fite	(1962)	8.00E+03	9.50E-16	1.40E-16	Bayfield	(1969)
3.80E+01	3.20E-15	2.00E-16	"		9.00E+03	8.30E-16	1.20E-16	"	
4.00E+01	4.10E-15	2.00E-16	Belyaev	(1967)	9.01E+03	1.04E-15		Fite	(1958)
4.01E+01	3.00E-15	4.90E-16	Newman	(1982)	9.60E+03	8.60E-16	4.30E-17	McClure	(1966)
4.60E+01	3.30E-15		Fite	(1962)	1.00E+04	9.40E-16	1.40E-16	Bayfield	(1969)
5.00E+01	3.90E-15	3.00E-16	Belyaev	(1967)	1.00E+04	9.00E-16	1.50E-16	Fite	(1960)
5.01E+01	2.83E-15	4.30E-16	Newman	(1982)	1.05E+04	9.00E-16	1.40E-16	Bayfield	(1969)
5.50E+01	3.50E-15		Fite	(1962)	1.20E+04	7.90E-16	1.20E-16	"	
6.00E+01	3.20E-15	1.00E-16	"		1.21E+04	7.50E-16	3.80E-17	McClure	(1966)
6.98E+01	2.69E-15	5.20E-16	Newman	(1982)	1.32E+04	8.00E-16		Fite	(1958)
7.60E+01	2.70E-15		Fite	(1962)	1.40E+04	6.90E-16	1.00E-16	Bayfield	(1969)
1.00E+02	3.40E-15	2.00E-16	Belyaev	(1967)	1.52E+04	6.50E-16	3.30E-17	McClure	(1966)
1.00E+02	3.10E-15		Fite	(1962)	1.56E+04	5.60E-16		Fite	(1958)
1.07E+02	3.10E-15	1.00E-16	"		1.70E+04	5.90E-16	9.00E-17	Bayfield	(1969)
1.10E+02	2.17E-15	3.50E-16	Newman	(1982)	1.92E+04	5.00E-16	2.50E-17	McClure	(1966)
1.40E+02	2.48E-15	3.60E-16	"		2.00E+04	6.40E-16	1.00E-16	Fite	(1960)
1.43E+02	2.60E-15		Fite	(1962)	2.00E+04	5.00E-16	5.00E-17	Bayfield	(1969)
1.76E+02	1.90E-15	3.10E-16	Newman	(1982)	2.40E+04	4.70E-16	5.00E-17	"	
1.99E+02	2.27E-15	3.50E-16	"		2.41E+04	4.10E-16	2.10E-17	McClure	(1966)
2.00E+02	2.80E-15		Fite	(1962)	2.80E+04	3.40E-16	3.00E-17	Bayfield	(1969)
2.30E+02	2.50E-15	2.00E-16	"		3.00E+04	4.10E-16	7.00E-17	Fite	(1960)
2.40E+02	2.90E-15		Fite	(1958)	3.04E+04	2.97E-16	1.50E-17	McClure	(1966)
2.40E+02	2.08E-15	3.10E-16	Newman	(1982)	3.20E+04	2.70E-16	1.00E-17	Bayfield	(1969)
2.86E+02	2.12E-15	3.10E-16	"		3.70E+04	2.10E-16	2.00E-17	"	
3.00E+02	2.50E-15	2.00E-16	Fite	(1962)	3.80E+04	2.30E-16	4.00E-17	Gilbody	(1966)
3.00E+02	1.98E-15	3.00E-16	Newman	(1982)	3.82E+04	1.86E-16	9.30E-18	McClure	(1966)
3.10E+02	3.04E-15		Fite	(1958)	4.00E+04	1.89E-16		Wittkower	(1966)
4.00E+02	2.81E-15		"		4.00E+04	1.60E-16	1.60E-17	Bayfield	(1969)
4.00E+02	2.60E-15	5.00E-16	Fite	(1960)	4.00E+04	3.10E-16	6.00E-17	Fite	(1960)
4.70E+02	2.20E-15	2.00E-16	Fite	(1962)	4.21E+04	1.58E-16	1.20E-17	Gilbody	(1966)
4.80E+02	2.54E-15		Fite	(1958)	4.50E+04	1.35E-16	1.40E-17	Bayfield	(1969)
6.00E+02	2.29E-15		"		4.80E+04	1.10E-16	5.50E-18	McClure	(1966)
6.10E+02	2.10E-15		Fite	(1962)	4.90E+04	5.90E-17	1.10E-17	Gilbody	(1966)
6.60E+02	2.10E-15	2.00E-16	"		5.00E+04	1.12E-16		Wittkower	(1966)
7.60E+02	2.29E-15		Fite	(1958)	5.00E+04	9.40E-17	9.00E-19	Bayfield	(1969)
8.20E+02	2.10E-15		Fite	(1962)	5.50E+04	7.30E-17	7.00E-18	"	
9.00E+02	2.15E-15		Fite	(1958)	5.89E+04	4.40E-17	5.00E-18	Gilbody	(1966)
1.00E+03	1.90E-15		Fite	(1962)	6.00E+04	7.00E-17		Wittkower	(1966)
1.00E+03	2.00E-15	3.00E-16	Fite	(1960)	6.00E+04	5.80E-17	6.00E-18	Bayfield	(1969)
1.09E+03	2.03E-15		Fite	(1958)	6.05E+04	6.00E-17	3.00E-18	McClure	(1966)
1.16E+03	2.07E-15		"		6.50E+04	4.40E-17	4.00E-18	Bayfield	(1969)
1.45E+03	2.00E-15	4.00E-16	Fite	(1962)	7.00E+04	3.10E-17		Wittkower	(1966)
1.60E+03	1.88E-15		Fite	(1958)	7.00E+04	3.70E-17	4.00E-18	Bayfield	(1969)
								"	

Table 8. (continued)

$H^+ + H \rightarrow H$ (cont.)

E(eV/amu)	Q(cm^2)	Error	Author	Year
7.00E+04	1.00E-17	4.00E-18	Gilbody	(1966)
7.62E+04	1.00E-17	1.50E-18	McClure	(1966)
7.78E+04	2.30E-17	3.00E-18	Gilbody	(1966)
8.00E+04	2.30E-17		Wittkower	(1966)
8.71E+04	1.65E-17	2.00E-18	Gilbody	(1966)
9.80E+04	1.63E-17		Wittkower	(1966)
9.77E+04	1.08E-17	1.80E-18	Gilbody	(1966)
1.00E+05	1.19E-17		Wittkower	(1966)
1.00E+05	1.24E-17	6.20E-19	McClure	(1966)
1.09E+05	7.80E-18	1.60E-18	Gilbody	(1966)
1.18E+05	6.40E-18	3.20E-19	McClure	(1966)
1.19E+05	6.90E-18	1.30E-18	Gilbody	(1966)
1.25E+05	5.00E-18		Wittkower	(1966)
1.29E+05	3.50E-18	2.20E-18	Gilbody	(1966)
1.50E+05	2.10E-18		Wittkower	(1966)
1.75E+05	1.32E-18	"		
2.00E+05	7.80E-19	"		
2.25E+05	4.00E-19	"		
2.50E+05	1.98E-19	"		
2.50E+05	1.65E-19	2.30E-20	Svelplund	(1982)
4.00E+05	1.35E-20	2.80E-21	"	
5.00E+05	5.45E-21	1.00E-21	"	
6.00E+05	1.87E-21	3.60E-22	"	

$H^+ + H \rightarrow H(2s)$

E(eV/amu)	Q(cm^2)	Error	Author	Year
1.50E+03	2.10E-18	6.30E-19	Hill	(1979)
2.00E+03	2.70E-18	8.10E-19	"	
3.00E+03	4.80E-19	3.60E-19	Bayfield	(1969)
3.00E+03	3.20E-18	9.60E-19	Hill	(1979)
3.50E+03	1.35E-18	8.50E-19	Bayfield	(1969)
4.00E+03	4.40E-18	1.30E-18	Hill	(1979)
4.00E+03	1.30E-18	1.20E-18	Bayfield	(1969)
4.00E+03	4.50E-18	1.40E-18	Hill	(1979)
5.00E+03	1.50E-18	5.00E-19	Bayfield	(1969)
5.00E+03	6.30E-18	1.90E-18	Hill	(1979)
5.00E+03	6.30E-18	2.20E-18	Morgan	(1973)
5.50E+03	5.00E-18	1.80E-18	Bayfield	(1969)
5.90E+03	1.48E-17	1.00E-18	Chong	(1977)
6.00E+03	5.00E-18	1.20E-18	Bayfield	(1969)
6.00E+03	7.30E-18	2.20E-18	Hill	(1979)
6.00E+03	7.60E-18	2.50E-18	Morgan	(1973)
6.00E+03	6.90E-18	2.10E-18	Hill	(1979)
7.00E+03	1.19E-17	3.60E-18	"	
7.00E+03	9.90E-18	1.90E-18	Bayfield	(1969)
7.00E+03	9.90E-18	3.00E-18	Morgan	(1973)
8.00E+03	1.58E-17	4.70E-18	Hill	(1979)
8.00E+03	1.75E-17	4.00E-18	Morgan	(1973)
8.00E+03	1.55E-17	3.00E-18	Bayfield	(1969)
8.00E+03	1.70E-17	5.10E-18	Hill	(1979)
8.10E+03	1.61E-17	1.80E-18	Chong	(1977)
9.00E+03	1.85E-17	5.00E-18	Morgan	(1973)
9.00E+03	1.73E-17	1.20E-18	Bayfield	(1969)
9.00E+03	1.93E-17	5.80E-18	Hill	(1979)
1.00E+04	1.78E-17	1.00E-18	Chong	(1977)
1.00E+04	2.10E-17	6.30E-18	Hill	(1979)
1.00E+04	2.40E-17	3.00E-18	Bayfield	(1969)
1.00E+04	2.60E-17	8.00E-18	Morgan	(1973)
1.00E+04	2.19E-17	6.60E-18	Hill	(1979)
1.15E+04	2.40E-17	3.00E-18	Bayfield	(1969)
1.10E+04	2.63E-17	7.90E-18	Hill	(1979)
1.20E+04	2.80E-17	8.00E-18	Morgan	(1973)
1.20E+04	2.71E-17	8.10E-18	Hill	(1979)
1.40E+04	3.43E-17	1.03E-17	"	
1.40E+04	3.20E-17	6.00E-18	Morgan	(1973)
1.40E+04	3.00E-17	2.00E-18	Bayfield	(1969)

$H^+ + H \rightarrow H(2s)$ (cont.)

E(eV/amu)	Q(cm^2)	Error	Author	Year
1.50E+04	2.85E-17	2.20E-18	Chong	(1977)
1.60E+04	3.36E-17	1.01E-17	Hill	(1979)
1.60E+04	3.40E-17	7.00E-18	Morgan	(1973)
1.60E+04	3.20E-17	3.00E-18	Bayfield	(1969)
1.75E+04	3.40E-17	5.00E-18	"	
1.80E+04	3.10E-17	7.00E-18	Morgan	(1973)
1.80E+04	3.44E-17	1.03E-17	Hill	(1979)
2.00E+04	4.30E-17	2.50E-18	Chong	(1977)
2.00E+04	3.60E-17	3.00E-18	Bayfield	(1969)
2.00E+04	3.00E-17	5.00E-18	Morgan	(1973)
2.00E+04	3.26E-17	9.80E-18	Hill	(1979)
2.20E+04	2.98E-17	8.90E-18	"	
2.20E+04	2.90E-17	5.00E-18	Morgan	(1973)
2.20E+04	3.20E-17	2.00E-18	Bayfield	(1969)
2.40E+04	3.00E-17	4.00E-18	Morgan	(1973)
2.40E+04	2.94E-17	8.80E-18	Hill	(1979)
2.50E+04	3.75E-17	3.00E-18	Chong	(1977)
2.50E+04	2.98E-17	8.90E-18	Hill	(1979)
2.60E+04	2.80E-17	6.00E-18	Morgan	(1973)
2.60E+04	3.40E-17	4.00E-18	Bayfield	(1969)
3.00E+04	3.20E-17	4.00E-18	"	
3.70E+04	2.30E-17	5.00E-18	"	
4.00E+04	2.00E-17	3.00E-18	"	
4.30E+04	8.50E-18	2.10E-18	Ryding	(1966)
4.50E+04	1.75E-17	2.50E-18	Bayfield	(1969)
5.00E+04	1.30E-17	2.00E-18	"	
5.00E+04	6.10E-18	1.30E-18	Ryding	(1966)
5.50E+04	9.70E-18	1.30E-18	Bayfield	(1969)
5.00E+04	7.40E-18	8.00E-19	"	
6.00E+04	4.50E-18	9.00E-19	Ryding	(1966)
6.50E+04	5.90E-18	8.00E-19	Bayfield	(1969)
7.00E+04	4.20E-18	7.80E-19	"	
7.00E+04	2.90E-18	7.00E-19	Ryding	(1966)
8.00E+04	2.40E-18	6.00E-19	"	
9.00E+04	1.72E-18	4.00E-19	"	
1.00E+05	1.10E-18	3.00E-19	"	
1.20E+05	5.40E-19	1.60E-19	"	

$H^+ + H \rightarrow H(2p)$

E(eV/amu)	Q(cm^2)	Error	Author	Year
7.50E+02	1.54E-17	3.00E-18	Kondow	(1977)
1.00E+03	2.10E-17	1.10E-17	Stebbings	(1965)
1.00E+03	1.38E-17	1.60E-18	Kondow	(1977)
1.10E+03	2.34E-17	3.00E-18	"	
1.25E+03	2.85E-17	3.80E-18	"	
1.34E+03	2.95E-17	2.80E-18	"	
1.50E+03	2.93E-17	1.40E-18	"	
1.70E+03	3.22E-17	1.90E-18	"	
1.75E+03	3.12E-17	1.70E-18	"	
1.85E+03	3.18E-17	2.60E-18	"	
2.00E+03	2.91E-17	1.10E-18	"	
2.25E+03	2.77E-17	1.50E-18	"	
2.30E+03	2.80E-17	5.00E-18	Morgan	(1973)
2.41E+03	2.70E-17	1.00E-18	Kondow	(1977)
2.50E+03	2.50E-17	1.10E-18	"	
2.75E+03	3.34E-17	2.00E-18	"	
3.00E+03	2.90E-17	4.00E-18	Morgan	(1973)
3.00E+03	2.60E-17	1.30E-17	Stebbings	(1965)
3.00E+03	2.49E-17	1.70E-18	Kondow	(1977)
3.00E+03	2.30E-17	1.80E-18	"	
4.00E+03	3.30E-17	5.00E-18	Morgan	(1973)
4.00E+03	2.49E-17	1.60E-18	Kondow	(1977)
5.00E+03	3.50E-17	1.80E-17	Stebbings	(1965)
5.00E+03	3.40E-17	4.00E-18	Morgan	(1973)
5.00E+03	2.43E-17	1.40E-18	Kondow	(1977)
6.00E+03	3.30E-17	5.00E-18	Morgan	(1973)

Table 8. (continued)

$H^+ + H \rightarrow H(2p)$ (cont.)

E(eV/amu)	$\phi(cm^2)$	Error	Author	Year
6.00E+03	2.45E-17	9.00E-19	Rondow	(1974)
6.00E+03	2.43E-17	9.00E-19	"	
7.00E+03	2.48E-17	2.10E-18	"	
7.00E+03	3.40E-17	5.00E-18	Morgan	(1973)
8.00E+03	2.41E-17	1.80E-18	Rondow	(1974)
8.00E+03	3.30E-17	5.00E-18	Morgan	(1973)
9.00E+03	2.64E-17	2.10E-18	Rondow	(1974)
9.00E+03	3.20E-17	5.00E-18	Morgan	(1973)
1.00E+04	2.64E-17	1.30E-18	Rondow	(1974)
1.00E+04	3.80E-17	1.90E-17	Stebbings	(1965)
1.00E+04	3.10E-17	5.00E-18	Morgan	(1973)
1.10E+04	2.93E-17	2.60E-18	Rondow	(1974)
1.10E+04	3.10E-17	5.00E-18	Morgan	(1973)
1.20E+04	2.83E-17	2.80E-18	Rondow	(1974)
1.20E+04	2.70E-17	3.00E-18	Morgan	(1973)
1.30E+04	2.71E-17	2.70E-18	Rondow	(1974)
1.40E+04	2.69E-17	1.40E-18	"	
1.40E+04	2.60E-17	3.00E-18	Morgan	(1973)
1.50E+04	2.45E-17	1.40E-18	Rondow	(1974)
1.60E+04	2.10E-17	2.20E-18	"	
1.60E+04	2.20E-17	3.00E-18	Morgan	(1973)
1.70E+04	1.96E-17	1.90E-18	Rondow	(1974)
1.80E+04	1.93E-17	1.60E-18	"	
1.80E+04	1.80E-17	3.00E-18	Morgan	(1973)
1.90E+04	1.76E-17	1.50E-18	Rondow	(1974)
2.00E+04	1.87E-17	1.30E-18	"	
2.00E+04	3.10E-17	1.60E-17	Stebbings	(1965)
2.00E+04	1.40E-17	2.00E-18	Morgan	(1973)
2.20E+04	1.68E-17	2.00E-18	Rondow	(1974)
2.20E+04	1.20E-17	1.50E-18	Morgan	(1973)
2.30E+04	1.45E-17	1.20E-18	Rondow	(1974)
2.30E+04	1.20E-17	1.50E-18	Morgan	(1973)
2.40E+04	1.10E-17	1.50E-18	"	
2.50E+04	1.22E-17	1.20E-18	Rondow	(1974)
2.60E+04	1.00E-17	1.50E-18	Morgan	(1973)
2.70E+04	1.48E-17	1.70E-18	Rondow	(1974)
2.90E+04	1.01E-17	1.90E-18	"	
3.00E+04	1.40E-17	7.00E-18	Stebbings	(1965)

$He^+ + H \rightarrow He$

E(eV/amu)	$Q(cm^2)$	Error	Author	Year
2.43E+03	7.10E-17	1.70E-17	Olson	(1977)
3.78E+03	8.70E-17	1.50E-17	"	
4.95E+03	8.90E-17	1.30E-17	"	
7.13E+03	1.77E-16	2.40E-17	"	
1.00E+04	2.03E-16	2.80E-17	"	
1.14E+04	2.71E-16	3.40E-17	"	
1.92E+04	2.72E-16	3.60E-17	"	
2.68E+04	1.92E-16	2.50E-17	"	
3.33E+04	1.48E-16	1.90E-17	"	
5.01E+04	6.10E-17	1.10E-17	"	
7.58E+04	2.60E-17	4.60E-18	"	
1.00E+05	5.90E-18	1.40E-18	Hvelplund	(1982)
1.01E+05	1.75E-17	3.40E-18	Olson	(1977)
1.25E+05	5.70E-18	1.00E-18	Hvelplund	(1982)
1.26E+05	3.00E-18	2.30E-18	Olson	(1977)
1.50E+05	3.22E-18	5.90E-19	Hvelplund	(1982)
1.75E+05	1.10E-18	3.50E-19	"	
2.00E+05	1.70E-18	5.00E-19	"	
2.25E+05	3.30E-19	2.00E-19	"	
2.50E+05	4.10E-19	1.90E-19	"	
3.13E+05	2.00E-19	1.20E-19	"	
3.75E+05	1.50E-19	1.00E-19	"	
5.63E+05	1.00E-20	1.20E-21	"	
6.25E+05	3.55E-21	4.90E-22	"	

$He^{2+} + H \rightarrow He^+$

E(eV/amu)	$Q(cm^2)$	Error	Author	Year
1.50E+01	2.80E-16	1.60E-16	Fite	(1962)

$He^{2+} + H \rightarrow He^+$ (cont.)

E(eV/amu)	$\phi(cm^2)$	Error	Author	Year
6.60E+01	1.50E-16	1.20E-16	Fite	(1962)
1.37E+02	2.60E-16	1.50E-16	"	
2.63E+02	2.30E-16	8.00E-17	"	
3.70E+02	3.80E-16	1.30E-16	"	
5.00E+02	3.20E-17	9.00E-18	Nutt	(1978)
5.70E+02	3.40E-16	1.20E-16	Fite	(1962)
6.70E+02	8.40E-17	1.00E-17	Nutt	(1978)
8.30E+02	1.26E-16	1.50E-17	"	
8.63E+02	3.50E-16	8.00E-17	Fite	(1962)
1.00E+03	2.50E-16	2.30E-17	Nutt	(1978)
1.02E+03	4.10E-16		Fite	(1962)
1.17E+03	2.81E-16	3.30E-17	Nutt	(1978)
1.27E+03	4.70E-16	8.00E-17	Fite	(1962)
1.33E+03	3.62E-16	3.50E-17	Nutt	(1978)
1.51E+03	5.80E-16	1.10E-16	Fite	(1962)
1.67E+03	4.88E-16	5.60E-17	Nutt	(1978)
1.75E+03	2.70E-16	8.00E-17	Bayfield	(1975)
1.92E+03	6.50E-16	9.00E-17	Fite	(1962)
2.00E+03	6.00E-16	9.00E-17	Shah	(1978)
2.00E+03	5.88E-16	4.50E-17	Nutt	(1978)
2.24E+03	7.80E-16	1.00E-16	Fite	(1962)
2.25E+03	6.00E-16	1.80E-16	Bayfield	(1975)
2.33E+03	6.98E-16	5.00E-17	Nutt	(1978)
2.33E+03	6.90E-16	1.00E-16	Shah	(1978)
2.50E+03	7.10E-16	2.20E-16	Bayfield	(1975)
2.58E+03	9.80E-16	1.00E-16	Fite	(1962)
2.67E+03	7.40E-16	1.10E-16	Shah	(1978)
2.67E+03	7.02E-16	6.30E-17	Nutt	(1978)
2.87E+03	1.00E-15	1.00E-16	Fite	(1962)
3.00E+03	8.00E-16	1.20E-16	Shah	(1978)
3.00E+03	8.05E-16	1.32E-16	Nutt	(1978)
3.00E+03	9.60E-16	2.90E-16	Bayfield	(1975)
3.20E+03	1.03E-15	3.10E-16	"	
3.28E+03	1.01E-15	1.10E-16	Fite	(1962)
3.30E+03	9.15E-16	1.40E-16	Shah	(1978)
3.63E+03	1.18E-15	3.50E-16	Bayfield	(1975)
3.75E+03	1.17E-15	3.50E-16	"	
3.87E+03	1.30E-15	1.00E-16	Fite	(1962)
4.00E+03	9.85E-16	1.50E-16	Shah	(1978)
4.43E+03	1.54E-15	1.30E-16	Fite	(1962)
4.67E+03	1.08E-15	1.60E-16	Shah	(1978)
4.73E+03	1.63E-15	4.90E-16	Bayfield	(1975)
5.00E+03	1.72E-15	5.20E-16	"	
5.30E+03	1.50E-15	9.00E-17	Fite	(1962)
5.33E+03	1.13E-15	1.70E-16	Shah	(1978)
5.50E+03	1.84E-15	5.50E-16	Bayfield	(1975)
5.93E+03	1.48E-15	1.30E-16	Fite	(1962)
6.00E+03	1.16E-15	1.70E-16	Shah	(1978)
6.25E+03	1.90E-15	5.70E-16	Bayfield	(1975)
6.67E+03	1.22E-15	1.80E-16	Shah	(1978)
6.73E+03	1.17E-15	1.40E-16	Olson	(1977)
6.83E+03	1.66E-15	1.30E-16	Fite	(1962)
7.13E+03	1.15E-15	1.70E-16	Shah	(1978)
8.00E+03	1.20E-15	1.80E-16	"	
8.50E+03	1.18E-15	1.50E-16	Olson	(1977)
8.67E+03	1.23E-15	1.80E-16	Shah	(1978)
8.73E+03	1.66E-15	1.40E-16	Fite	(1962)
8.75E+03	1.88E-15	5.60E-16	Bayfield	(1975)
9.13E+03	1.24E-15	1.90E-16	Shah	(1978)
9.53E+03	1.88E-15	3.00E-16	Fite	(1962)
1.00E+04	1.22E-15	1.80E-16	Shah	(1978)
1.01E+04	1.29E-15	1.60E-16	Olson	(1977)
1.09E+04	1.60E-15	1.40E-16	Fite	(1962)
1.12E+04	1.25E-15	1.90E-16	Shah	(1978)
1.15E+04	1.88E-15	5.60E-16	Bayfield	(1975)
1.16E+04	1.20E-15	1.50E-16	Olson	(1977)
1.19E+04	1.56E-15	1.80E-16	Fite	(1962)
1.20E+04	1.66E-15	1.60E-16	"	
1.25E+04	1.23E-15	1.80E-16	Shah	(1978)

Table 8. (continued)

$H^+ + H_2 \rightarrow H$ (cont.)

E(eV/amu)	Q(cm^2)	Error	Author	Year
3.50E+04	2.71E-16		Schwirzke	(1960)
3.50E+04	2.84E-16		Chambers	(1965)
3.50E+04	3.38E-16		Afrosimov	(1969)
3.50E+04	3.25E-16		de-Heer	(1966)
3.60E+04	3.09E-16		Williams	(1966)
3.67E+04	2.60E-16		Fogel'	(1955)
3.87E+04	2.78E-16		Curran	(1959)
4.00E+04	2.65E-16		Afrosimov	(1969)
4.00E+04	5.16E-16		Gordeev	(1964)
4.00E+04	2.22E-16		Schwirzke	(1960)
4.00E+04	2.55E-16		de-Heer	(1966)
4.00E+04	2.26E-16		Chambers	(1965)
4.00E+04	2.65E-16		Stier	(1956)
4.00E+04	2.64E-16		Williams	(1966)
4.26E+04	2.36E-16		Curran	(1959)
4.45E+04	1.83E-16		Ribe	(1951)
4.50E+04	1.88E-16		Chambers	(1965)
4.50E+04	1.67E-16		Schwirzke	(1960)
4.50E+04	2.13E-16		Afrosimov	(1969)
4.60E+04	2.14E-16		Williams	(1966)
4.69E+04	2.09E-16		Curran	(1959)
4.83E+04	1.53E-16		Ribe	(1951)
4.87E+04	1.41E-16		"	
5.00E+04	1.34E-16		Schwirzke	(1960)
5.00E+04	1.78E-16		Barnett	(1958)
5.00E+04	1.62E-16		Afrosimov	(1969)
5.00E+04	1.76E-16		Stier	(1956)
5.00E+04	1.78E-16		de-Heer	(1966)
5.00E+04	1.41E-16		Chambers	(1965)
5.00E+04	9.79E-17		Dasequelles	(1966)
5.00E+04	1.70E-16		Williams	(1966)
5.13E+04	1.71E-16		Curran	(1959)
5.39E+04	1.15E-16		Ribe	(1951)
5.50E+04	1.26E-16		Chambers	(1965)
5.50E+04	9.71E-17		Schwirzke	(1960)
5.69E+04	1.47E-16		Curran	(1959)
6.00E+04	1.19E-16		Stier	(1956)
6.00E+04	1.21E-16		de-Heer	(1966)
6.00E+04	7.02E-17		Schwirzke	(1960)
6.25E+04	7.52E-17		Ribe	(1951)
7.00E+04	8.30E-17		de-Heer	(1966)
7.00E+04	4.42E-17		Dasequelles	(1966)
7.00E+04	7.81E-17		Stier	(1956)
7.29E+04	5.50E-17		Ribe	(1951)
8.00E+04	6.10E-17		de-Heer	(1966)
8.00E+04	5.20E-17		Stier	(1956)
8.11E+04	3.54E-17		Ribe	(1951)
8.88E+04	2.72E-17		"	
9.00E+04	4.70E-17		de-Heer	(1966)
1.00E+05	3.30E-17		"	
1.00E+05	2.49E-17		Stier	(1956)
1.00E+05	2.86E-17		Toburen	(1968)
1.00E+05	2.31E-17		Barnett	(1958)
1.03E+05	1.68E-17		Ribe	(1951)
1.09E+05	1.47E-17		"	
1.10E+05	1.70E-17		de-Heer	(1966)
1.20E+05	9.70E-18		Ribe	(1951)
1.20E+05	1.20E-17		de-Heer	(1966)
1.20E+05	1.31E-17		Stier	(1956)
1.28E+05	8.10E-18		Ribe	(1951)
1.30E+05	1.10E-17		de-Heer	(1966)
1.40E+05	6.00E-18		"	
1.40E+05	7.46E-18		Stier	(1956)
1.49E+05	4.58E-18		Ribe	(1951)
1.50E+05	6.92E-18		Barnett	(1958)
1.60E+05	4.18E-18		Stier	(1956)
1.80E+05	2.74E-18		"	
2.00E+05	1.75E-18		Barnett	(1958)
2.00E+05	1.74E-18		Stier	(1956)

$H^+ + H_2 \rightarrow H$ (cont.)

E(eV/amu)	Q(cm^2)	Error	Author	Year
2.50E+05	1.54E-19		Barnett	(1958)
2.50E+05	3.19E-19	3.00E-20	Hvelplund	(1982)
3.00E+05	2.42E-19		Toburen	(1968)
3.50E+05	9.72E-20		Barnett	(1958)
4.00E+05	4.03E-20	1.80E-21	Hvelplund	(1982)
4.25E+05	2.82E-20		Barnett	(1958)
4.40E+05	4.00E-20		Williams	(1969)
4.40E+05	3.60E-20		Welsh	(1967)
5.00E+05	2.00E-20		Williams	(1969)
5.00E+05	1.24E-20		Barnett	(1958)
5.00E+05	1.48E-20	6.00E-22	Hvelplund	(1982)
5.50E+05	1.11E-20		Toburen	(1968)
6.00E+05	7.60E-21		Williams	(1969)
6.00E+05	5.55E-21	2.30E-22	Hvelplund	(1982)
6.54E+05	4.00E-21		Welsh	(1967)
7.00E+05	3.60E-21		Williams	(1969)
7.00E+05	2.31E-21		Barnett	(1958)
8.00E+05	1.90E-21		Williams	(1969)
8.00E+05	1.56E-21		Toburen	(1968)
8.51E+05	1.10E-21		Welsh	(1967)
8.80E+05	9.20E-22		Williams	(1969)
9.00E+05	7.27E-22		Barnett	(1958)
1.00E+06	4.00E-22		Williams	(1969)
1.00E+06	4.74E-22		Toburen	(1968)
1.00E+06	4.09E-22		Barnett	(1958)
1.04E+06	5.80E-22		Schryber	(1967)
1.06E+06	3.50E-22		Welsh	(1967)
1.25E+06	9.60E-23		Williams	(1969)
1.25E+06	1.25E-22		Toburen	(1968)
1.43E+06	7.50E-23		Schryber	(1967)
1.50E+06	1.90E-23		Williams	(1969)
1.50E+06	5.18E-23		Toburen	(1968)
1.75E+06	8.40E-24		Williams	(1969)
1.75E+06	1.69E-23		Toburen	(1968)
2.00E+06	2.30E-24		Williams	(1969)
2.05E+06	1.70E-23		Schryber	(1967)
2.45E+06	6.00E-24		Welsh	(1967)
2.56E+06	4.10E-24		Schryber	(1967)
3.28E+06	1.70E-24		"	

$He^+ + H_2 \rightarrow He$

E(eV/amu)	Q(cm^2)	Error	Author	Year
2.50E+01	1.19E-16		Stedeford	(1955)
5.00E+01	1.42E-16		"	
1.00E+02	1.42E-16		"	
2.25E+02	1.26E-16		"	
2.50E+02	2.00E-16		Moran	(1973)
2.88E+02	1.94E-16		"	
3.25E+02	2.03E-16		"	
3.75E+02	2.05E-16		"	
4.00E+02	8.31E-17		Stedeford	(1955)
4.25E+02	2.05E-16		Moran	(1973)
4.75E+02	1.94E-16		"	
5.00E+02	5.32E-17		Stedeford	(1955)
5.25E+02	1.77E-16		Moran	(1973)
5.75E+02	1.82E-16		"	
6.25E+02	7.00E-17		Stedeford	(1955)
6.25E+02	1.79E-16		Moran	(1973)
6.75E+02	1.84E-16		"	
7.50E+02	1.93E-16		"	
1.18E+03	6.96E-17		Stedeford	(1955)
2.00E+03	7.53E-17		Barnett	(1958)
2.50E+03	1.12E-16		Stedeford	(1955)
2.50E+03	1.23E-16		de-Heer	(1966)
2.50E+03	1.18E-16	2.50E-18	Gilbody	(1973)
3.00E+03	1.07E-16		Barnett	(1958)

Table 8. (continued)

$H^+ + H_2 \rightarrow H$					$H^+ + H_2 \rightarrow H$ (cont.)				
eV/amu	$Q(cm^2)$	Error	Author	Year	E(eV/amu)	$Q(cm^2)$	Error	Author	Year
5.00E+01	2.26E-17		Cramer	(1961)	1.00E+04	8.21E-16		Williams	(1966)
5.50E+01	4.52E-17		"		1.03E+04	7.62E-16		Curran	(1959)
8.00E+01	3.96E-17		"		1.13E+04	7.44E-16		"	
1.00E+02	4.33E-17		"		1.20E+04	7.94E-16		Stier	(1956)
1.50E+02	4.98E-17		"		1.20E+04	7.06E-16		Williams	(1966)
2.00E+02	5.63E-17		"		1.23E+04	8.10E-16		Fogel'	(1955)
2.30E+02	1.10E-16		Stedeford	(1955)	1.26E+04	7.10E-16		Curran	(1959)
2.50E+02	6.48E-17		Cramer	(1961)	1.30E+04	9.66E-16		Gordeev	(1964)
3.00E+02	7.61E-17		"		1.35E+04	6.84E-16		Curran	(1959)
3.90E+02	2.30E-16		Stedeford	(1955)	1.40E+04	6.60E-16		Stedeford	(1955)
4.00E+02	1.18E-16		Cramer	(1961)	1.40E+04	6.50E-16		"	
5.00E+02	1.65E-16		Abbe	(1964)	1.47E+04	6.24E-16		Chambers	(1965)
8.90E+02	4.90E-16		Stedeford	(1955)	1.50E+04	9.57E-16		Gordeev	(1964)
1.00E+03	5.50E-16		Chambers	(1965)	1.50E+04	8.20E-16		Hollricher	(1965)
1.00E+03	2.27E-16		Abbe	(1964)	1.50E+04	7.61E-16		Afrosimov	(1969)
1.00E+03	6.24E-16		Gordeev	(1964)	1.50E+04	6.72E-16		de-Heer	(1966)
1.53E+03	6.74E-16		Hollricher	(1965)	1.50E+04	6.76E-16		Schwirzke	(1960)
1.60E+03	7.10E-16		Stedeford	(1955)	1.50E+04	6.32E-16		Chambers	(1965)
2.00E+03	1.12E-15		Gordeev	(1964)	1.50E+04	6.84E-16		Williams	(1966)
2.00E+03	4.28E-16		Abbe	(1964)	1.60E+04	6.79E-16		Stier	(1956)
2.00E+03	7.37E-16		Chambers	(1965)	1.66E+04	6.50E-16		Fogel'	(1955)
2.00E+03	7.34E-16		Williams	(1966)	1.67E+04	6.19E-16		Curran	(1959)
2.13E+03	7.24E-16		Curran	(1959)	1.70E+04	9.41E-16		Gordeev	(1964)
2.30E+03	8.80E-16		Stedeford	(1955)	1.80E+04	6.00E-16		Stedeford	(1955)
2.70E+03	7.90E-16		"		1.80E+04	5.88E-16		Williams	(1966)
2.72E+03	7.48E-16		Curran	(1959)	1.90E+04	5.60E-16		Stedeford	(1955)
2.80E+03	7.50E-16		Stedeford	(1955)	1.97E+04	5.46E-16		Curran	(1959)
2.80E+03	7.81E-16		Chambers	(1965)	2.00E+04	5.60E-16		de-Heer	(1966)
3.00E+03	8.40E-16		Williams	(1966)	2.00E+04	5.23E-16		Chambers	(1965)
3.05E+03	9.14E-16		Hollricher	(1965)	2.00E+04	5.43E-16		Schwirzke	(1960)
3.38E+03	7.70E-16		Curran	(1959)	2.00E+04	3.84E-16		Barnett	(1958)
3.50E+03	7.97E-16		Chambers	(1965)	2.00E+04	8.40E-16		Gordeev	(1964)
4.00E+03	7.69E-16		Stier	(1956)	2.00E+04	6.83E-16		Hollricher	(1965)
4.00E+03	1.00E-15		Gordeev	(1964)	2.00E+04	5.89E-16		Stier	(1956)
4.00E+03	8.37E-16		Williams	(1966)	2.00E+04	6.30E-16		Afrosimov	(1969)
4.04E+03	7.88E-16		Curran	(1959)	2.00E+04	5.76E-16		Williams	(1966)
4.40E+03	8.20E-16		Stedeford	(1955)	2.08E+04	5.20E-16		Fogel'	(1955)
4.40E+03	8.10E-16		"		2.30E+04	5.10E-16		Stedeford	(1955)
4.90E+03	7.92E-16		Chambers	(1965)	2.30E+04	4.50E-16		"	
5.00E+03	9.24E-16		Afrosimov	(1969)	2.32E+04	4.78E-16		Curran	(1959)
5.00E+03	7.96E-16		Curran	(1959)	2.50E+04	5.45E-16		Hollricher	(1965)
5.00E+03	8.44E-16		Williams	(1966)	2.50E+04	4.78E-16		de-Heer	(1966)
5.78E+03	8.10E-16		Curran	(1959)	2.50E+04	4.23E-16		Schwirzke	(1960)
5.80E+03	8.27E-16		Chambers	(1965)	2.50E+04	7.73E-16		Gordeev	(1964)
6.00E+03	8.06E-16		Stier	(1956)	2.50E+04	5.12E-16		Stier	(1956)
6.00E+03	1.05E-15		Gordeev	(1964)	2.50E+04	5.15E-16		Afrosimov	(1969)
6.00E+03	8.17E-16		Williams	(1966)	2.50E+04	4.43E-16		Chambers	(1965)
6.20E+03	8.40E-16		Stedeford	(1955)	2.54E+04	4.50E-16		Fogel'	(1955)
6.40E+03	8.70E-16		"		2.60E+04	4.62E-16		Williams	(1966)
6.89E+03	7.93E-16		Curran	(1959)	2.66E+04	4.18E-16		Curran	(1959)
7.00E+03	8.49E-16		Williams	(1966)	2.70E+04	3.90E-16		Stedeford	(1955)
7.36E+03	1.00E-15		Hollricher	(1965)	2.80E+04	4.20E-16		"	
7.70E+03	8.02E-16		Chambers	(1965)	2.97E+04	3.60E-16		Fogel'	(1955)
7.79E+03	7.94E-16		Curran	(1959)	3.00E+04	2.40E-16		Desequelles	(1966)
8.00E+03	8.45E-16		Stier	(1956)	3.00E+04	4.11E-16		Afrosimov	(1969)
8.00E+03	8.56E-16		Williams	(1966)	3.00E+04	4.45E-16		Hollricher	(1965)
8.60E+03	7.89E-16		Chambers	(1965)	3.00E+04	1.68E-16		Chambers	(1965)
8.96E+03	7.86E-16		Curran	(1959)	3.00E+04	3.40E-16		Schwirzke	(1960)
9.00E+03	8.55E-16		Williams	(1966)	3.00E+04	3.97E-16		de-Heer	(1966)
9.10E+03	8.10E-16		Stedeford	(1955)	3.00E+04	4.31E-16		Stier	(1956)
9.20E+03	8.00E-16		"		3.00E+04	6.63E-16		Gordeev	(1964)
9.30E+03	9.15E-16		Schwirzke	(1960)	3.00E+04	3.82E-16		Williams	(1966)
9.74E+03	9.69E-16		Hollricher	(1965)	3.04E+04	3.62E-16		Curran	(1959)
1.00E+04	8.19E-16		Stier	(1956)	3.20E+04	2.60E-16		Stedeford	(1955)
1.00E+04	1.05E-15		Gordeev	(1964)	3.20E+04	2.80E-16		"	
1.00E+04	8.32E-16		Schwirzke	(1960)	3.30E+04	3.10E-16		Fogel'	(1955)
1.00E+04	7.80E-16		Chambers	(1965)	3.40E+04	3.04E-16		Ribe	(1951)
1.00E+04	8.03E-16		de-Heer	(1966)	3.47E+04	3.16E-16		Curran	(1959)
1.00E+04	8.86E-16		Afrosimov	(1969)	3.50E+04	6.11E-16		Gordeev	(1964)
								"	

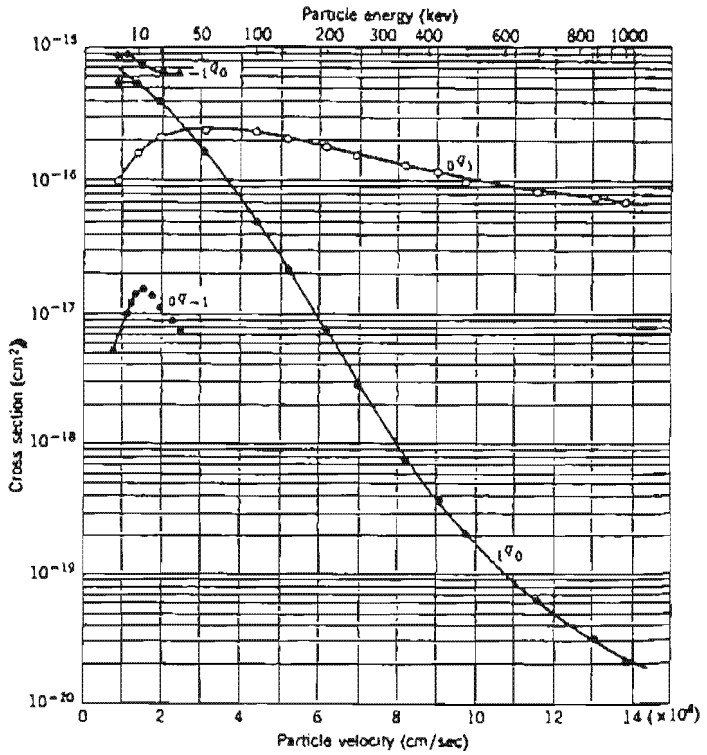

Figure 34. Charge transfer cross sections for impacting protons on N (curve 1^{q_0}) [from McDaniel (1964)]. The other curves give the charge transfer cross sections for impacting H atoms (curves 0^{q_1} and 0^{q-1}) and for impacting negative H ions (curve -1^{q_0}) on N.

Table 8). The program linearly interpolates to determine the charge exchange cross section for any energy between 0.17 eV and 600 keV. A very high accuracy can be obtained because of the use of many data.

Figure 33 shows the charge exchange and ionization cross sections for collisions between protons and atomic H. Charge transfer prevails below 100 keV but then quickly decreases so that, for higher energies, electron production becomes the only important process.

For He, the computer code also interpolates linearly between measured values given by Bransden et al. (1954) up to 500 keV. For higher energies, the data are extrapolated. For high energies, the charge exchange cross section becomes negligible.

The same comments apply to N. The data are taken from McDaniel et al. (1962) from 5 keV to 1 MeV and are illustrated in Fig. 34. They were fitted by a decreasing exponential to obtain an analytic function:

$$\ln \sigma(E_\mathrm{p}) = -4.018 + 4.8989 \exp(-E_\mathrm{p}/377683)\,. \tag{2.57}$$

Generally, the process of resonance charge exchange occurs most readily between an ion and its parent atom. However, for certain ion-neutral pairs, there occurs an

accidental resonance in ionization energies, permitting charge exchange to proceed rapidly at thermal energies. The most important accidentally resonant charge exchange process in the upper atmosphere involves atomic O and H ions according to the relation

$$O + H^+ \rightarrow O^+ + H\,.$$

From beam experiments, the value

$$\sigma(E_p) = 2\,(3.47 - 0.20 \log E_p)^2 \times 10^{-16} \tag{2.58}$$

has been obtained over the energy range 50 eV to 10 keV. For energies higher than 500 keV, charge exchange becomes negligible and ionization prevails. Between 10 and 500 keV, interpolated values are used.

Proton-ion collisions

The ionization cross sections of high energy protons (> 600 keV) are the same as the ionization cross sections by electrons when they have the same velocity. The Coulomb cross section is only prevalent for collisions with ambient electrons and for low proton energies.

Coulomb interaction Equation (2.50) gives the average Coulomb cross section for two charged particles. It is applicable to high energy protons impacting on ions:

$$\sigma(E_p) = \frac{2\pi}{(4\pi\epsilon_0)^2} \left[\frac{m_p + m_i}{m_i} \frac{Z_p Z_i e^2}{2E_p}\right]^2 \ln\Lambda\,. \tag{2.59}$$

This elastic collision cross section is very important for collisions between energetic protons (or any other ions) impacting on electrons, because of the small mass of the electron ($m_i = m_e = m_p/1832$). The Coulomb collisions of ring current ions with plasmaspheric electrons are found to be one of the major loss mechanisms for ring current ions, together with charge exchange (Fok et al. 1993, Kozyra et al. 1987, Sheldon & Hamilton 1993, Noël & Prölss 1993). Note also that this cross section varies with Z_i^2, i.e. it is more important for highly charged ions than for singly charged ones.

Ionization of ions by proton impact McDaniel et al. (1962) have shown that the ionization cross section by proton impact corresponds to the ionization cross section by electron impact when the velocities of the projectiles are the same and when the energy of the electron is above about 300 eV (i.e. 600 keV for the proton,

since $E_p = 1836\,E_e$). The ionization cross section of ions for high energy protons is therefore given by the analytic function of Lotz (1966) [cf. Eq. (2.47)]:

$$\sigma(E_p) = \xi a \frac{\ln(E_p/1836/\bar{I})}{\bar{I}E_p/1836}. \tag{2.60}$$

The computer code CROSS computes the ionization cross section for ions of He, C, N, O, N_2, O_2 and Ne in different ionization states.

2.5.4 Software implementation

In order to write a program giving the cross sections for collisions of electrons or protons with the main atmospheric constituents as a function of the kinetic energy of the incident particle, we have scanned the literature. To find recent values of the different cross sections, the bibliographic data base GAPHYOR (Humbert 1993, Delcroix 1992) has been very useful. For each possible collision process, GAPHYOR gives the references of books and papers dealing with this subject.

The different atmospheric components which are considered in our program are essentially atomic and molecular H, He, O and N. For electron collision cross sections, all the results are valid for energies higher than 500 eV. For O, the proton cross sections are a little overestimated between 10 and 500 keV due to interpolations. The collision cross sections of protons impacting on O_2 molecules may be underestimated below 100 keV because charge exchange has been neglected for O_2. For all other atoms and molecules, the cross sections are the best currently available values at energies above 500 eV.

For proton-ion collisions the cross sections are only valid for energies higher than 200 keV for the reasons given above. However, the cross section for collisions between energetic protons and electrons is correct because the Coulomb interaction prevails.

It is also important to note that the experimental values are generally measured below 100 keV for electrons. Because these energies are much larger than the excitation and ionization level, the cross sections are fitted with analytic functions based on the Bethe-Born approximation and extrapolated for higher energies. When the cross sections are obtained from interpolated measurements, the program also extrapolates for higher energies than given in the tables.

We illustrate the results obtained with CROSS in Table 9, which shows the values used by Hassitt (1964) compared with the values found by CROSS at 500 keV and at 1 MeV. At 500 keV, the values for neutral constituents are similar, but at 1 MeV the values obtained with CROSS are much higher because the Coulomb cross section between protons and electrons decreases as E^{-2}. The ion collision cross sections are lower, due to the higher ionization threshold of ions compared to neutral atoms.

Table 9. Values of the total cross section for collisions between energetic protons and atmospheric particles divided by the total (Coulomb) cross section for collisions between energetic protons and electrons. The values used by Hassitt (1964) are compared with the values found by the program CROSS at 500 keV and at 1 MeV.

Species	Hassitt	CROSS 500 keV	CROSS 1 MeV
e^-	1.0	1.0	1.0
O_2	7.16	7.94	19.0
N_2	6.36	7.71	17.8
O	3.58	3.43	7.9
N	3.2	3.43	7.8
He	1.01	1.18	2.8
H	0.52	1.10	2.3
O_2^+	6.72	2.87	6.51
N_2^+	6.32	2.86	6.49
O^+	3.14	1.43	3.0
He^+	0.50	0.19	0.50

CROSS has been added as a subroutine to our copy of Hassitt's software. The choice between the original energy independent cross sections and CROSS is made with the NAMELIST parameter CROSS.

2.5.5 Application to the density profiles through the SAA

Figures 35–36 represent the average number density profile through the SAA obtained with MSISE-90, IRI-90 and CA for the summer solstice and local midnight, for conditions of low and high solar activity, respectively. The averages were made first with Hassitt's cross sections as weight factors, dividing the cross sections by 100 for normalisation. Then, the cross sections obtained with CROSS were used, normalised by dividing by 10^{12}, for four proton energies: 0.1, 1, 10 and 100 MeV.

The first feature to note is that the five curves in each graph are almost identical except for a shift towards lower average density for higher energy. The main difference besides this shift is that for the lowest energy and for Hassitt's cross sections the density curve is steeper above 1000 km than the other curves for higher energies. This effect is due to the increased importance of the Coulomb cross section at lower energies.

The dependence of n_s on energy strongly influences the shell height H_s. Figures 37–38 show H_s as a function of altitude for the density profiles in Figs. 35–36.

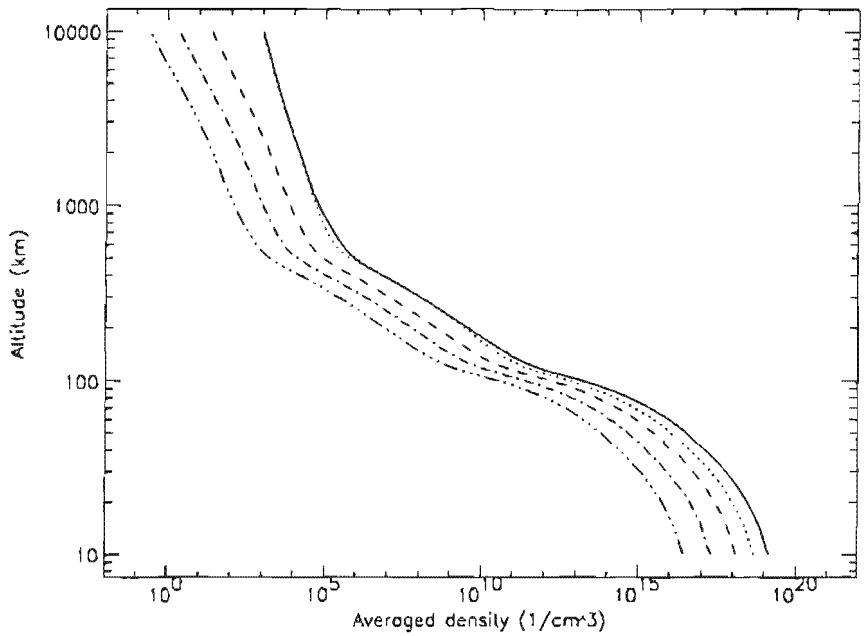

Figure 35. Averaged number density profiles in the SAA obtained with MSISE-90, IRI-90 and CA for the summer solstice, midnight L.T., for low solar activity. The solid line was obtained with Hassitt's cross section values, the other lines with the CROSS values for four energies (in MeV): 0.1 (dotted), 1 (dashed), 10 (dot-dashed), 100 (triple-dot-dashed).

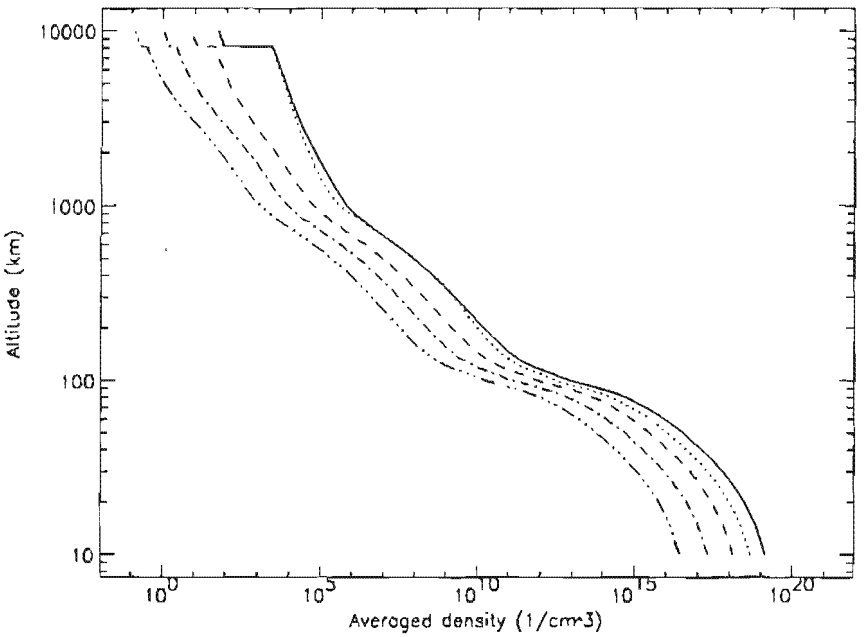

Figure 36. Averaged number density profiles in the SAA obtained with MSISE-90, IRI-90 and CA for the summer solstice, midnight L.T., for high solar activity. The line styles have the same meaning as in Fig. 35.

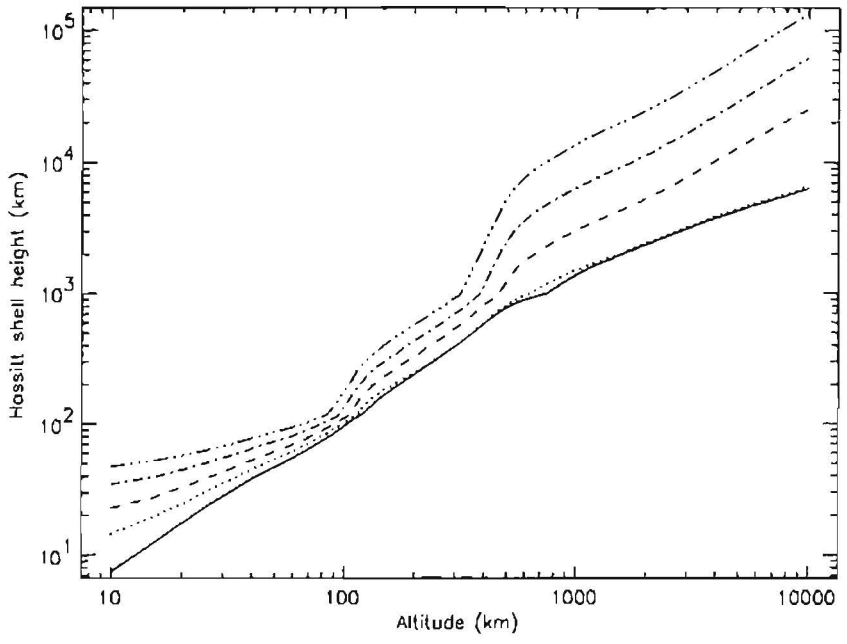

Figure 37. Hassitt shell height as a function of altitude for the density profiles in Fig. 35

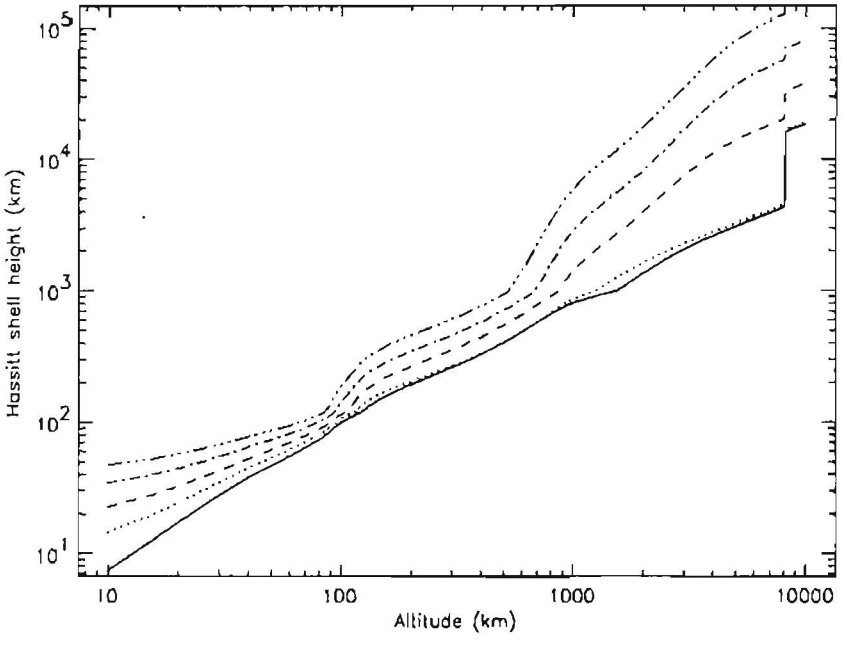

Figure 38. Hassitt shell height as a function of altitude for the density profiles in Fig. 36

Chapter 3

Application of the drift shell averaged density

In this chapter, we report on results obtained the software described in Chapter 2. In Sect. 3.1 we show the distribution of several parameters resulting from the calculation over the world map at constant altitude. In Sect. 3.2 we demonstrate the usefulness of the drift shell averaged density n_s by applying it to the proton flux distribution given by the AP-8 models.

3.1 Distribution of parameters

As a first application, we ran the software for a grid of points at altitude 1000 km. First, we calculated the (B, L) coordinates of each point—for pitch angle 90°—with BLXTRA. The resulting (B, L) were then used as input to the shell averaging software, producing values of n_s for each point in the grid. We also stored the minimum altitude reached on each drift shell, denoted by $h_{\min}$, and the local averaged number density in these points, denoted by $n_{\min}$.

Figure 39 shows the distribution of $\log n_s$ over the world map. The white filling indicates that the drift shell intersects the Earth's surface, so that there can be no trapped particles on this shell. Apparently, at 1000 km, n_s is defined only in a region around the SAA and in a narrow band at high latitude. At lower altitudes, these regions become gradually smaller, while they increase at higher altitudes.

The distribution of n_s has a broad minimum coinciding with the heart of the SAA. This is consistent with the fact that the geomagnetic field distribution shows a depression in the region of the SAA. Trapped particles passing through this region will not move closer to the Earth elsewhere on their longitudinal drift path. Consequently, the atmospheric density they encounter here is the maximum density they

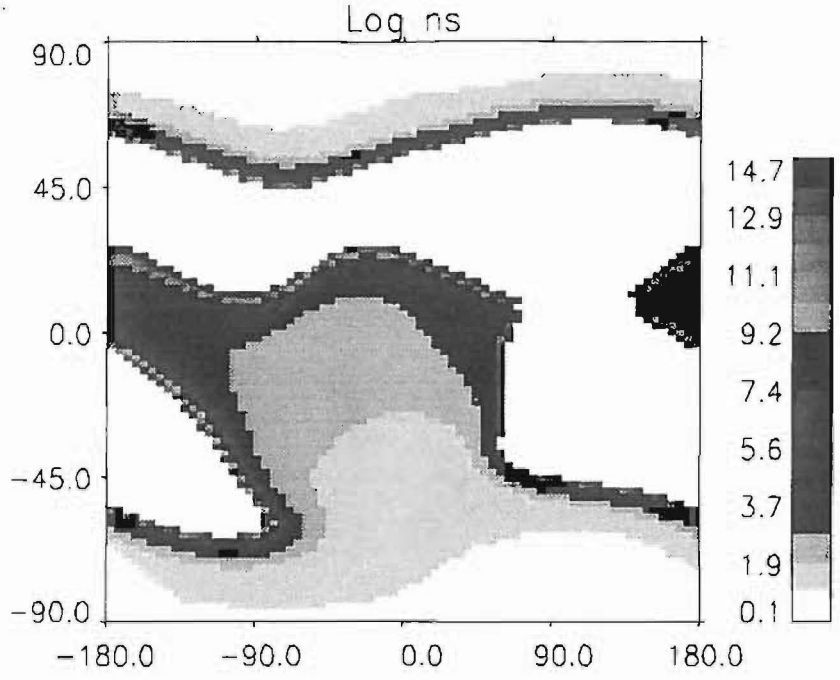

Figure 39. Distribution of $\log n_s$ over the world map at 1000 km

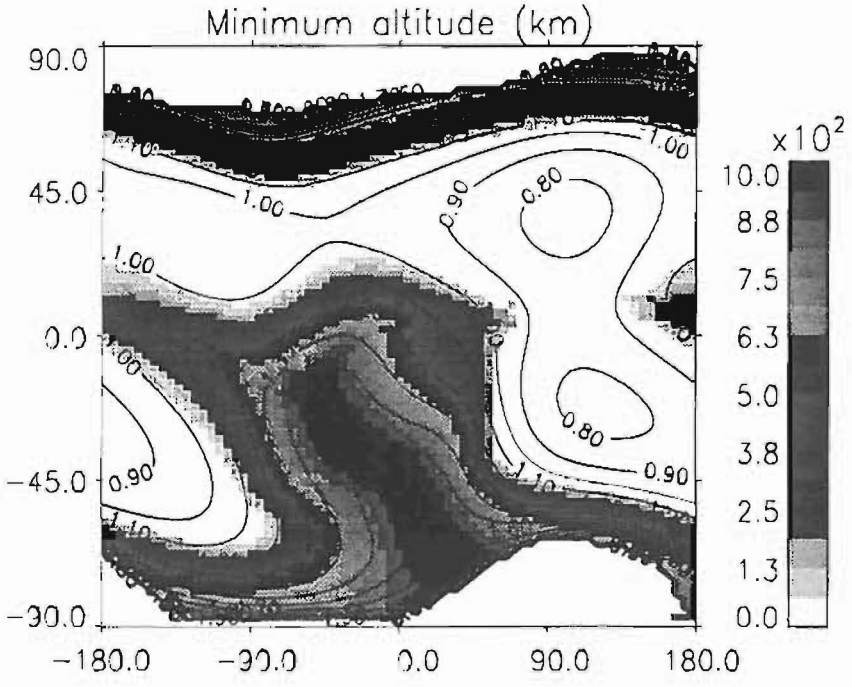

Figure 40. Distribution of h_{min} over the world map at 1000 km. The solid lines represent constant values of the ratio B_c/B.

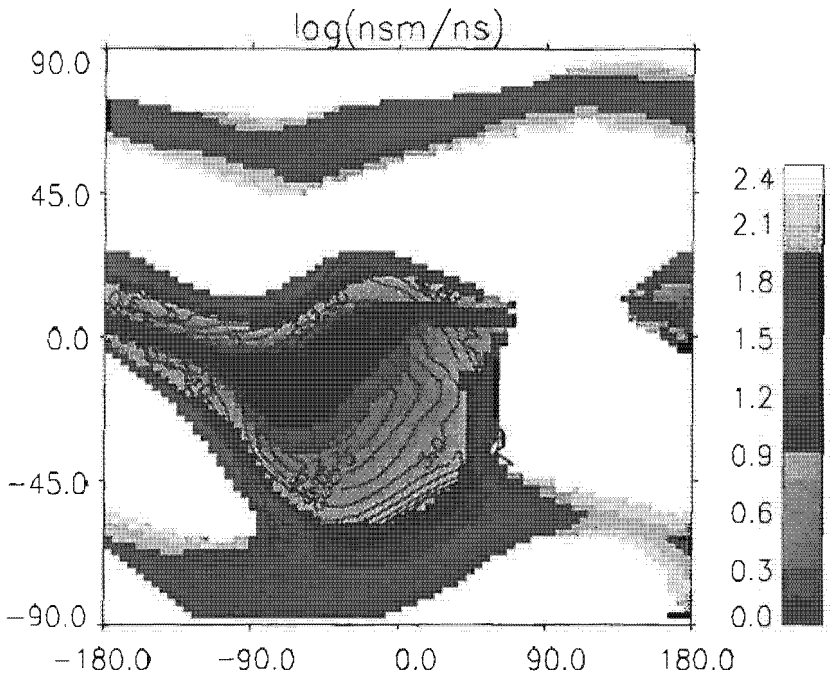

Figure 41. Distribution of the ratio n_{min}/n_s over the world map at 1000 km. The solid lines are lines of constant AP-8 MIN flux above 10 MeV.

see on their drift path. The minimum altitude on the drift shells associated with the grid points at 1000 km is shown in Fig. 40. h_{min} indeed reaches its maximum around the centre of the SAA.

In Fig. 40 we superimposed the contour lines of constant B_c/B, with $B_c = B_0 0.67 L^{3.452}$. When the ratio $B_c/B > 1$ the corresponding point is above the cut-off defined by B_c and vice versa. The contour lines correspond reasonably well with the borders of regions of constant h_{min}.

Figure 41 shows the distribution of the ratio n_{min}/n_s over the world map. The solid lines are lines of constant AP-8 MIN flux above 10 MeV. The lines of constant flux correspond to borders of regions of constant n_{min}/n_s, indicating that this ratio provides a good description of the flux distribution in the SAA.

3.2 Application to AP-8

We calculated the drift shell averaged density n_s for the AP-8 grid points represented in Fig. 2 with Hassitt's (1965b) software, updated as described in Chapter 2. Figure 42 shows the dependence of these proton fluxes on n_s for $L = 1.2$ and $L = 1.5$. It can be seen that for both the solar maximum (MAX) and solar minimum (MIN) fluxes, the curves for the respective L values virtually coincide (this is also the case

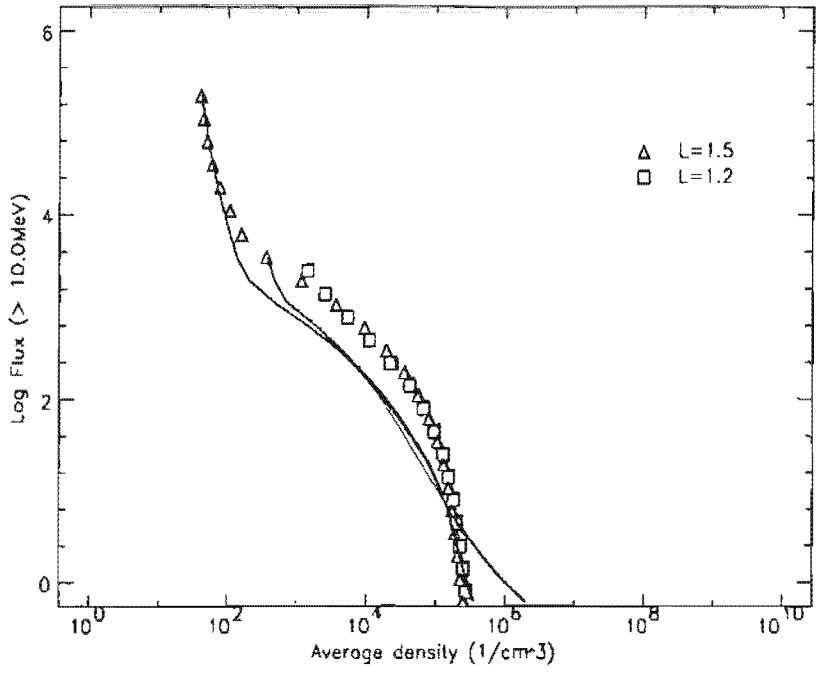

Figure 42. Integral AP-8 MIN/MAX proton flux above 10 MeV as a function of the drift shell average of the atmospheric density for low L-values. The symbols and lines have the same meaning as in Fig. 2.

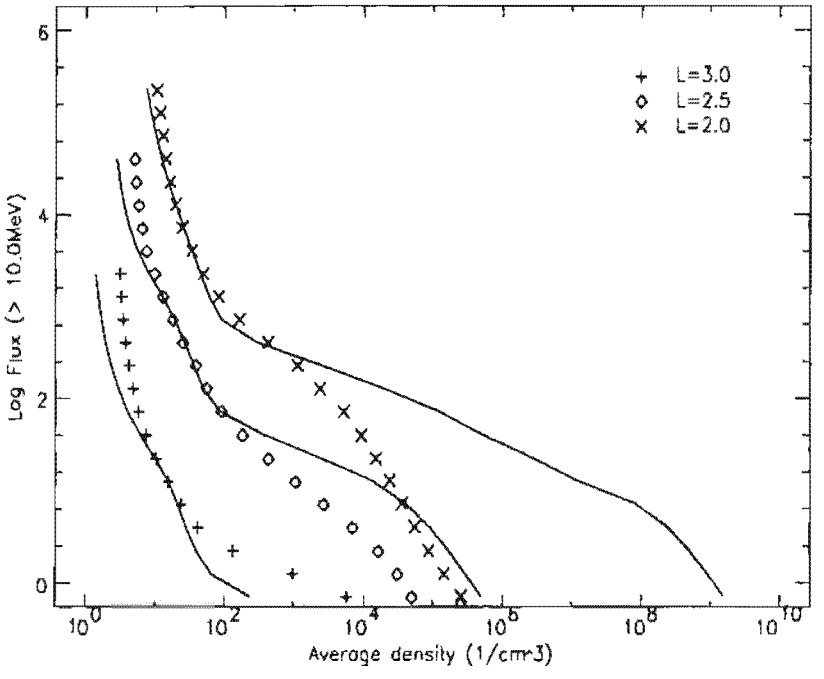

Figure 43. Integral AP-8 MIN/MAX proton flux above 10 MeV as a function of the drift shell average of the atmospheric density for high L-values. The symbols and lines have the same meaning as in Fig. 2.

for intermediate values of L up to $L \simeq 1.7$, which are not shown in Fig. 42).

It thus seems that for low L-values the drift shell averaged density n_s is very well suited to represent the trapped particle distribution, as its eliminates the dependence of the flux on L.

The two curves for solar minimum in Fig. 42 diverge somewhat for the highest values of n_s. This may be due to inaccuracies in the AP-8 MIN model for very low altitudes. In Fig. 4, it can be seen that the lowest invariant altitude in AP-8 MIN displays some irregularity around $L = 1.2$ and especially for $L \geq 2.0$, where it fluctuates strongly.

Since we used extensive atmospheric and ionospheric models for the calculation of n_s, we expected the respective curves for solar minimum and maximum in Fig. 42 to be closer together, although they do overlap for the highest densities. Again, we need to re-investigate the solar minimum data, since AP-8 MIN resulted from the combination of different data sets.

For values of $L > 1.7$, the AP-8 flux vs. n_s curves, shown in Fig. 43, no longer coincide. From this we conclude that two different populations can be distinguished in the AP-8 models. Below $L \leq 1.7$ (the limiting value for L depends on the particle energy), the trapped particle flux is governed by the vertical distribution of the atmospheric density. At higher L values, the proton flux already reaches negligible values some distance above the atmospheric cut-off height. The value $L \simeq 1.7$ corresponds to the location of the maximum in the proton flux distribution for $E = 10\,\mathrm{MeV}$. This explains the lowering of the curves in Fig. 43 corresponding to progressively higher L values.

3.3 Concluding remarks

On the basis of our analysis of the AP-8 flux distribution, it appears that the drift shell averaged density n_s is very effective in organising fluxes for the lowest L values, and may therefore be considered a good candidate to replace L as a coordinate for the low-altitude environment.

It should be kept in mind that the AP-8 models are smoothed and extrapolated averages of a number of data sets, so that it would be preferable to look at original data sets, old or new, which have a better resolution at low altitudes. To this effect, we have started to re-analyse the AZUR proton data. The AZUR satellite (Hovestadt et al. 1972) operated from November 1969 to June 1970 in a polar orbit with perigee 383 km, apogee 3145 km and inclination 103°. It measured proton fluxes along two pitch angles, 90° and 45°, in six energy channels between 1.5 MeV and 104 MeV. The low-altitude part of AP-8 MAX is based on the AZUR proton data set.

References

Allen, C.W.: 1985, *Astrophysical Quantities*, The Athlone Press

Anderson, A.D., Francis, W.E.: 1964, *A semitheoretical model for atmospheric properties from 90 to 10,000 km*, Lockheed Missiles and Space Company 6-74-64-19

Angerami, J.J., Thomas, J.O.: 1964, *The Distribution of Electrons and Ions in the Earth's Exosphere*, J. Geophys. Res. **69**, 4537–4560

Bailey, D.K.: 1959, *Abnormal ionization in the lower ionosphere associated with cosmic-ray flux enhancements*, Proc. IRE **47**, 255–266

Banks, P.M., Kockarts, G.: 1973, *Aeronomy*, Academic Press, New York, pp. 785

Bethe, H.: 1930, *Zur Theorie des durchgangs schneller Korpuskularstrahler durch Materie*, Ann. Phys. **5**, 325–400

Bilitza, D.: 1990, *International Reference Ionosphere 1990*, NSSDC/WDC-A-R&S 90-22

Bransden, B.H., Dalgarno, A., King, N.M.: 1954, *Electron Capture-IV: Capture from Helium Atoms by Fast Protons*, Proc. Phys. Soc. London **A67**, 1075–1089

Cain, J.C., Hendricks, S.J., Langel, R.A., Hudson, W.V.: 1967, *A Proposed Model for the International Geomagnetic Reference Field-1965*, J. Geomag. Geoelectr. **19**, 335–355

Carpenter, D.L., Anderson, R.R.: 1992, *An ISEE/Whistler Model of Equatorial Electron Density in the Magnetosphere*, J. Geophys. Res. **97**, 1097–1108

Chiu, Y.T., Luhmann, J.G., Ching, B.K., Boucher, D.J.: 1978, *An Equilibrium Model of Plasmaspheric Composition and Density*, The Aerospace Corporation, Los Angeles, SSL-78(3960-04)-3

Daly, E.J., Evans, H.D.R.: 1993, *Problems in Radiation Environment Models at Low Altitudes*, Memorandum ESA/ESTEC/WMA/93-067/ED

Delcroix, J.-L.: 1992, *Base de données GAPHYOR, Atomes, molécules, gaz neutres et ionisés*, Centre National de la Recherche Scientifique, Vol. 15, Tomes 1 et 2

Fok, M.C., Kozyra, J.U., Nagy, A.F., Rasmussen, C.E., Khazanov, G.V.: 1993, *Decay of Equatorial Ring Current Ions and Associated Aeronomical Consequences*, J. Geophys. Res. **98**, 19381–19393

Green, A.E.S., Barth, C.A.: 1965, *Calculations of Ultraviolet Molecular Nitrogen Emissions from the Aurora*, J. Geophys. Res. **70**, 1083–1092

Green, A.E.S., Dutta, S.K.: 1967, *Semi-empirical Cross Sections for Electron Impacts*, J. Geophys. Res. **72**, 3933–3941

Hassitt, A.: 1964, *An average atmosphere for particles trapped in the Earth's magnetic field*, University of California at San Diego

Hassitt, A.: 1965a, *The Drift Velocity of Trapped Particles*, J. Geophys. Res. **70**, 535–540

Hassitt, A.: 1965b, *Average Effect of the Atmosphere on Trapped Protons*, J. Geophys. Res. **70**, 5385–5394

Hedin, A.E.: 1991, *Extension of the MSIS thermosphere model into the middle and lower atmosphere*, J. Geophys. Res. **96**, 1159-1172

Hedin, A.E.: 1983, *A revised thermospheric model based on mass spectrometer and incoherent scatter data, MSIS-83*, J. Geophys. Res. **88**, 10170–10188

Hedin, A.E.: 1987, *MSISE-90 thermospheric model*, J. Geophys. Res. **92**, 4649–4662

Hedin, A.E., Salah, J.E., Evans, J.V., Reber, C.A., Newton, G.P., Spencer, N.W., Kayser, D.C., Alcaydé, D., Bauer, P., Cogger, L., McClure, J.P.: 1977a, *A Global Thermospheric Model Based on Mass Spectrometer and Incoherent Scatter Data MSIS 1. N_2 Density and Temperature*, J. Geophys. Res. **82**, 2139–2147

Hedin, A.E., Reber, C.A., Newton, G.P., Spencer, N.W., Brinton, H.C., Mayr, H.G., Potter, W.E.: 1977b, *A global Thermospheric Model Based on Mass Spectrometer and Incoherent Scatter Data MSIS 2. Composition*, J. Geophys. Res. **82**, 2148–2156

Hovestadt, D., Achtermann, E., Ebel, B., Haüsler, B., Pachmann, G.: 1972, *New observations of the proton population of the radiation belt between 1.5 and 104 MeV*, Earth's Magnetospheric Processes, B.M. McCormac (ed.), D. Reidel Publishing Company, Dordrecht, Holland, 115–119

Humbert, D.: 1993, *Manuel d'utilisation GAPHYOR*, Université Paris-Sud, Orsay, France

Jensen, D.C., Cain, J.C.: 1962, *An Interim Geomagnetic Field*, J. Geophys. Res. **67**, 3568

Jusick, A.T., Watson, C.E., Peterson, L.R., Green, A.E.S.: 1967, *Electron Impact Cross Sections for atmospheric Species, 1. Helium*, J. Geophys. Res. **72**, 3943–3951

Kamiyama, H.: 1966, *Ionization and excitation by precipitating electrons*, Rep. Ionos. Space Res. Japan **20**, 171–187

Kozyra, J.U., Shelley, E.G., Comfort, R.H., Brace, L.H., Cravens, T.E., Nagy, A.F.: 1987, *The Role of Ring Current O^+ in the Formation of Stable Auroral Red Arcs*, J. Geophys. Res. **92**, 7487–7502

Lemaire, J.: 1989, *Plasma distribution models in a rotating magnetic dipole and refilling of plasmaspheric flux tubes*, Phys. Fluids **B1**, 1519–1525

Lenchek, A.M., Singer, S.F.: 1962, *Geomagnetically trapped protons from cosmic-ray albedo neutrons*, J. Geophys. Res. **67**, 1263–1287

Lew, J.S.: 1961, *Drift rate in a dipole field*, J. Geophys. Res. **66**, 2681–2865

Lotz, W.: 1966, *Electron-impact ionization cross-sections and ionization rate coefficients for atoms and ions*, Astroph. J. Suppl. Series **128**, 207–239

McDaniel, E.W.: 1964, *Collision phenomena in ionized gases*, John Wiley & Sons Editions, U.S.A., pp. 775

McDaniel, E.W., Hooper, J.W., Martin, D.W., Harmer, D.S.: 1962, Proceedings of Fifth International Conference on Ionization Phenomena in Gases, Munich, North Holland, Amsterdam, Vol. 1, 60

McIlwain, C.E.: 1961, *Coordinates for Mapping the Distribution of Magnetically Trapped Particles*, J. Geophys. Res. **66**, 3681–3691

Newkirk, L.L., Walt, M.: 1964, *Longitudinal drift velocity of geomagnetically trapped particles*, J. Geophys. Res. **69**, 1759–1763

Noël, S., Prölss, G.W.: 1993, *Heating and Radiation Production by Neutralized Ring Current Particles*, J. Geophys. Res. **98**, 17317–17325

Pfitzer, K.A.: 1990, *Radiation Dose to Man and Hardware as a Function of Atmospheric Density in the 28.5 Degree Space Station Orbit*, MDSSC Report No. H5387 Rev A

Ray, E.C.: 1960, *On the Theory of Protons Trapped in the Earth's Magnetic Field*, J. Geophys. Res. **65**, 1125–1134

Rees, M.H.: 1963, *Auroral ionization and excitation by incident energetic electrons*, Planet. Space Sci. **11**, 1209–1218

Roederer, J.G.: 1970, *Dynamics of Geomagnetically Trapped Radiation*, Springer-Verlag

Rossi, B., Olbert, S.: 1981, *Introduction to the Physics of Space*, McGraw-Hill Company

Rudd, M.E., Kim, Y.-K., Madison, D.H., Gallagher, J.W.: 1985, *Electron production in proton collisions: total cross sections*, Rev. Mod. Phys. **57**, 965–994

Rycroft, M.J., Jones, I.R.: 1985, *Modelling the plasmasphere for the International Reference Ionosphere*, Adv. Space Res. **5**, 21–27

Rycroft, M.J., Jones, I.R.: 1987, *A suggested model for the IRI plasmaspheric distribution*, Adv. Space Res. **7**, 13–22

Sawyer, D.M., Vette, J.I.: 1976, *AP-8 Trapped Proton Environment for Solar Maximum and Solar Minimum*, NSSDC/WDC-A-R&S 76-06

Sheldon, R.B., Hamilton, D.C.: 1993, *Ion Transport and Loss in the Earth's Quiet Ring Current 1. Data and Standard Model*, J. Geophys. Res. **98**, 13491–13508

Tawara, H., Kato, T., Nakai, Y.: 1985, *Electron Capture and Loss*, Atomic Data and Nuclear Data Tables **32**, 249–270

Vette, J.I.: 1991, *The AE-8 Trapped Electron Model Environment*, NSSDC/WDC-A-R&S 91-24

Wilson, G.R.: 1992, *Semikinetic modeling of the outflow of ionospheric plasma through the topside collisional to collisionless transition region*, J. Geophys. Res. **97**, 551–565